EEG analysis of naturalistic viewing: From connectivity analysis to reliable extraction of neural components

A Thesis Submitted for the Degree of Doctor of Philosophy in Computer Science

Iffah Syafiqah Suhaili

Supervisor:

Dr. Juhász Zoltán

DOI:10.18136/PE.2026.1006

Department of Electrical Engineering and Information Systems

Doctoral School of Information Science and Technology

University of Pannonia

Veszprém, Hungary

2026

EEG analysis of naturalistic viewing: From connectivity analysis to reliable extraction of neural components

The thesis was prepared for the award of a doctoral degree (PhD) within the framework of the Doctoral School of Information Science and Technology at University of Pannonia

in the discipline of Computer Sciences

Written by **Iffah Syafiqah Suhaili**

Supervisor: **Dr. Juhász Zoltán**

I recommend the dissertation for acceptance: yes / no.

…….
supervisor

I recommend the dissertation for peer review.

…….
chair of the DDHC

The PhD-candidate has achieved ……. % at the public debate.

The composition of the Final Examination Committee:

chair: ……

reviewers: ……

members: ……

Veszprém, …….

…….
chair of the committee

Qualification of degree: …….

Veszprém, …….

…….
chair of the UDHC

Acknowledgment

Alhamdulillah. All praise due to the Almighty, for the strength, clarity and quiet persistence that carried me through the many unexpected turns of this doctoral journey.

First and foremost, I would like to express my sincere gratitude to my supervisor, Dr. Juhász Zoltán, for his exceptional academic expertise, unwavering support and steady wisdom, throughout the entirety of my work. From the earliest stages of shaping my research proposal to the final submission of this thesis, his guidance has been instrumental in my academic growth. His guidance was never limited to technical advice; it extended to perspective, encouragement and the kind of mentorship that strengthens both skill and character. Our discussions grounded me when I felt overwhelmed, challenged me when I needed direction and reminded me that setbacks are an inherent part of meaningful research. I am profoundly grateful for the trust he placed in me and for the opportunities he opened along the way. I would also like to thank Prof. Nagy Zoltán, whose expertise, thoughtful feedback and consistent involvement have supported this research. His insights and time has improved the scientific quality of this work, and I am sincerely thankful for his contribution.

My heartfelt thanks to Prof. Hangos Katalin, Prof. Hartung Ferenc, Prof. Ágnes Vathy-Fogarassy, Dr. Dulai Tibor and Dr. Görbe Péter from the doctoral school for their support and assistance during each semester report. I am equally thankful to my lecturers, Dr. Bari Ferenc, Prof. Kósa István, Prof. István Vassányi, Prof. Tibor Nyári for generously sharing their knowledge to me. I would also like to express my appreciation to all the staff of the Faculty of Information Technology, especially, Lényi Szilvia, Dr. Fodor Attila, Ujvári Orsolya, Prof. Lányi Cecília, Dr. Süle Zoltán, Dr. Szűcs Veronika, Gazdag-Kéri Renáta, and Nagy Róbert, as well as the International Office of the University of Pannonia, for their invaluable academic and administrative support.

I am grateful to the Hungarian government and the Stipendium Hungaricum Scholarship for supporting my studies in Hungary over the past four years. I also wish to thank the University Research Scholarship Programme (EKOP, 2024-2.1.1-EKOP-2024-00025/58), the Faridah Awang Scholarship Programs: Wook Ismail Merit Scholarship and the Santha Kalman Foundation, for their financial support to my research. I would also like to thank the Embassy of Malaysia in Hungary for their assistance and support during my time abroad. To all the participants who generously gave their time to take part in my research, thank you. Your willingness, patience and cooperation made this research possible.

To my family – my mother, Luluk Mufidah, my father, Suhaili Zakaria, my brothers, my grandparents and relatives – thank you for your endless prayers, patience and belief in my path. Your support has been my pillar of strength, especially during the most challenging phases of this journey. This achievement is as much yours as it is mine.

My heartfelt thanks also go to my lab mates, colleagues and friends – Zeyu Wang, Jinat Ara, Maulana Fariz, Tóth Bálint, Emeralda Erna, Nadhirah Syafiqah, Nazirah Mahmud, Amalina Rusli, Dr. Mohamed Issa, Hanas Hanafi and Hanan Namrouti – for being my support system in ways both big and small, for the conversations, the encouragement and the understanding during the highs and lows of this journey. You have made even the most difficult days more bearable. To my long-distance friends back in Malaysia, thank you for keeping me close with your stories, laughter and constant support. Even from afar, you made me feel connected and never alone.

Lastly, I would like to thank myself for not giving up, for showing up even when it was hard. For learning, unlearning and growing through every phase of this journey.

Iffah Syafiqah, 2026

Abstract

Aesthetic perception engages a distributed set of perceptual, cognitive and affective processes that unfold rapidly during visual exploration. Understanding how the brain coordinates these processes requires methods capable of capturing fast oscillatory dynamics and large-scale interactions between neural populations. Electroencephalography (EEG), with its millisecond temporal resolution, provides a powerful tool for studying these mechanisms, but its interpretation is complicated by volume conduction, source mixing and the presence of eye-movement-related activity during naturalistic viewing. This thesis addresses these challenges by investigating oscillatory connectivity during aesthetic perception and by establishing methodological foundations for the reliable use of Independent Component Analysis (ICA) in naturalistic EEG research.

The work addresses three major gaps: (i) the limited application of robust, zero-lag-insensitive connectivity metrics to aesthetic perception, (ii) the lack of physiological characterisation of fixation-locked neural activity during free-viewing and (iii) the absence of systematic validation of ICA preprocessing pipelines for extracting meaningful neural components.

In the first empirical study, high-density EEG was used to examine how abstract and figurative paintings modulate oscillatory connectivity. Time-resolves connectivity was quantified using the debiased weighted Phase-Lag Index (dwPLI), a measure designed to minimise spurious connections arising from volume conduction. The results revealed distinct style-specific network configurations happen as early as 100 ms and persisting through 300-500 ms across delta, theta, alpha, beta and gamma frequency bands. These findings demonstrate that aesthetic perception is supported by rapid and sustained reorganisation of functional networks, and that artistic style shapes inter-regional communication from early perceptual analysis through later integrative stages.

The second study focuses on fixation-locked neural dynamics during free-viewing. By synchronising EEG with high-precision eye-tracking data, strong fixation-evoked lambda responses were identified across participants. These components were validated through three criteria: (i) waveform morphology consistent with acknowledged lambda responses, (ii) peak latencies matching established physiological ranges for saccade-onset and saccade-offset responses and (iii) ground-truth matching between ICA-detected peaks and eye-tracker-derived saccade events. This provides strong evidence that ICA can isolate meaningful neural components even in data containing frequent eye movements and in naturalistic settings.

A systematic exploration of preprocessing parameters further shows that ICA reliability depends critically on specific combinations of high-pass filtering, low-pass filtering and other preprocessing settings. Within optimal parameter ranges, ICA consistently extracts lambda-related components with stable topographies and reproducible temporal structure. Outside these ranges, decomposition quality degrades substantially. These results provide the evidence-based guidelines for preprocessing pipelines tailored to naturalistic EEG settings.

Collectively, the findings advance theoretical understanding of aesthetic perception as a dynamic, network-level process and establish a methodological roadmap for future component-space connectivity research. The thesis demonstrates that combining oscillatory connectivity, fixation-locked analysis and validated ICA pipelines enables a more precise characterisation of how the brain organises information during real-world visual experience.

Összefoglaló

Az esztétikai észlelés a perceptuális, kognitív és affektív folyamatok kiterjedt agyi hálózatát aktiválja, amelyek a vizuális feltárás során gyorsan bontakoznak ki. Annak megértése, hogy az agy miként hangolja össze ezeket a folyamatokat, olyan módszereket igényel, amelyek képesek megragadni a gyors oszcillációs dinamikát és a nagyléptékű neurális populációk közötti kölcsönhatásokat. Az elektroenkefalográfia (EEG) milliszekundumos időbeli felbontásával hatékony eszközt kínál e mechanizmusok vizsgálatához, értelmezését azonban megnehezíti a térfogati vezetés, a forráskeveredés, valamint a természetes nézés közben fellépő szemmozgás-eredetű aktivitások jelenléte. A disszertáció ezeket a kihívásokat úgy közelíti meg, hogy vizsgálja az oszcillációs konnektivitást az esztétikai észlelés során, valamint módszertani alapokat teremt az Independent Component Analysis (ICA) megbízható alkalmazásához természetes nézési helyzetekben rögzített EEG adatokon.

A kutatási munka három fontos problématerületet céloz meg: (i) a robusztus, zéró-késleltetésre kevéssé érzékeny konnektivitási metrikák alkalmazásának hiányát az esztétikai észlelés kutatásában, (ii) a fixációhoz kötött neurális aktivitás fiziológiai jellemzésének hiányát szabad nézés során, valamint (iii) az ICA-alapú előfeldolgozási pipeline szisztematikus validációjának hiányát a fiziológiai jelentéssel bíró agyi eredetű független komponensek kinyerése során.

Az első empirikus vizsgálatban nagyfelbontású EEG-t alkalmaztunk annak feltárására, hogy az absztrakt és figuratív festmények miként modulálják az oszcillációs konnektivitást. Az agyi kapcsolatokat a térfogati vezetésből eredő téves kapcsolatok minimalizálására tervezett, torzításmentes súlyozott fáziskésés-indexszel (debiased weighted Phase Lag Index, dwPLI) kvantifikáltuk. Az eredmények azt mutatták, hogy a stílusfüggő hálózati konfigurációk már 100 ms körül megjelennek, és 300–500 ms között is fennmaradnak a delta, théta, alfa, béta és gamma frekvenciasávokban. Ezek az eredmények azt jelzik, hogy az esztétikai észlelés gyors és tartós funkcionális hálózati átrendeződésen alapul, és hogy a művészeti stílus már a korai perceptuális feldolgozástól kezdve befolyásolja az agyterületek közötti kommunikációt.

A második vizsgálat a fixációhoz kötött idegi dinamikára összpontosít szabad nézés során. Az EEG és a nagy pontosságú szemkövetés szinkronizálásával erőteljes lambda-válaszokat azonosítottunk a résztvevők körében. Ezeket a komponenseket három kritérium alapján validáltuk: (i) hullámforma-morfológiájuk megfelelt a szakirodalomban leírt lambda-válaszoknak, (ii) csúcs-latenciáik illeszkedtek a szakkádkezdethez és szakkádvéghez kapcsolódó fiziológiai tartományokhoz, valamint (iii) az ICA által detektált csúcsok időben pontosan egyeztek a szemkövető által mért szakkád eseményekkel. Ez erős bizonyítékot szolgáltat arra, hogy az ICA képes jelentéssel bíró neurális komponensek elkülönítésére még gyakori szemmozgásokat tartalmazó, természetes nézési helyzetekben rögzített adatokban is.

Az előfeldolgozási paraméterek szisztematikus feltárása továbbá azt mutatja, hogy az ICA megbízhatósága kritikus módon függ a magas- és aluláteresztő szűrés, valamint további előfeldolgozási paraméterek specifikus kombinációitól. Az optimális paramétertartományokon belül az ICA következetesen stabil topográfiájú és reprodukálható időbeli szerkezetű, lambda-válaszhoz kapcsolódó komponenseket nyer ki. E tartományokon kívül a dekompozíció minősége jelentősen romlik. Az eredmények bizonyítékokon alapuló iránymutatást nyújtanak a természetes nézési helyzetekhez igazított EEG-előfeldolgozási pipeline kialakításához.

Összességében az eredmények előmozdítják az esztétikai észlelés dinamikus, hálózati szintű folyamatként való elméleti megértését, és módszertani útmutatót kínálnak a jövőbeli komponens-alapú konnektivitási kutatásokhoz. A disszertáció bemutatja, hogy az oszcillációs konnektivitás, a fixációhoz kötött elemzés és a validált ICA-pipeline kombinációja pontosabb információkat szolgáltat arról, miként szervezi az agy az információfeldolgozást valós vizuális élmények során.

List of figures

List of tables

List of abbreviations

BEM	Boundary Element Methods
CHS	Calinski-Harabasz Score
CWT	Continuous Wavelet Transform
DBS	Davies-Bouldin Score
DFT	Discrete Fourier Transform
DIPFIT	Dipole Fitting
DTI	Diffusion Tensor Imaging
dwPLI	debiased weighted Phase-Lag Index
EEG	Electroencephalography
EOG	Electrooculography
EPSP	Excitatory Postsynaptic Potential
ERN	Error-Related Negativity
ERP	Event-Related Potential
ERSP	Event-Related Spectral Perturbation
FEM	Finite Element Methods
FFT	Fast Fourier Transform
fMRI	Functional Magnetic Resonance Imaging
FRP	Fixation-Related Potential
fs	Frequency sampling rate
GUI	Graphical User Interface
HCA	Hierarchical Cluster Analysis
HEOG	Horizontal EOG
HP	High-pass cut-off
IC	Independent Component
ICA	Independent Component Analysis
IPSP	Inhibitory Postsynaptic Potential
JADE	Joint Approximate Diagonalization of Eigenmatrices
LP	Low-pass cut-off
LPP	Late Positive Potential
MEG	Magnetoencephalography
MNE	Minimum Norm Estimate
MRI	Magnetic Resonance Imaging
PANAS	Positive and Negative Affect Schedule
PCA	Principal Component Analysis
PLI	Phase-Lag Index
PLV	Phase Locking Value
SD	Standard Deviation
SI	Similarity Index
SVD	Singular Value Decomposition
V1	Primary Visual Cortex
VEOG	Vertical EOG
wPLI	weighted Phase-Lag Index

Table of contents

1. INTRODUCTION

1.1 Background and motivation

1.1.1 Neuroaesthetics and the motivation for studying aesthetic perception

Neuroaesthetics is an interdisciplinary field that investigates the neural mechanisms underlying aesthetic perception, evaluation and experience [1], [2], [3], [4]. Research in this area aims to understand how the brain integrates perceptual, cognitive and affective processes when individuals engage with artworks or other visually complex stimuli. Aesthetic experience is not limited to the appreciation of beauty, but it also encompasses the broader set of processes through which viewers interpret visual information, extract meaning and form evaluative judgements [5], [6]. Because these processes draw on perception, memory, semantic knowledge and affective evaluation, they unfold in a sequence that moves from early visual analysis to higher-order interpretation and appraisal. Consistent with this view, studies using behavioural measures, eye-tracking and neuroimaging support this multi-stage architecture, showing that aesthetic perception engages distributed networks spanning occipital, parietal, frontal and limbic regions [2], [7], [8].

A key challenge in neuroaesthetics is that many of the processes involved in aesthetic perception unfold rapidly, often within the first few hundred milliseconds of viewing an artwork. Understanding these early stages requires investigating the temporal organisation of neural activity and the mechanisms through which distributed neural populations coordinate their responses. One such mechanism is neural oscillations which will be introduced in the next section.

1.1.2 Neural oscillations as mechanisms of cognitive function

Understanding how the brain coordinates information across distributed regions during perception, memory, decision-making and other higher-order functions remains a central challenge in neuroscience. Neural oscillations, which is the rhythmic fluctuations in neuronal excitability, provide a fundamental mechanism for this coordination [9], [10]. By regulating the timing of neuronal firing, oscillations shape communication between distant regions and create windows of enhanced or suppressed excitability that structure information flow across the cortex [11], [12], [13].

Different frequency bands have been associated with distinct cognitive processing i.e. theta rhythms with memory encoding [14], [15], alpha rhythms with attentional control [16] and sensory inhibition [17], beta rhythms with sensorimotor integration [18] and gamma rhythms with perceptual binding [19]. Importantly, these oscillatory processes unfold dynamically, forming transient networks that reflect moment-to-moment changes in cognitive demands, such as memory formation, decision-making and attention [20], [21], [22]. Oscillatory interactions can occur both within frequency bands (e.g. phase synchronisation between two theta rhythms) and across frequency bands (e.g. coupling between alpha and theta rhythms). These cross-frequency relationships have been proposed as mechanisms for integrating information across spatial and temporal scales, supporting complex cognitive functions that require coordination between distributed neural systems.

Because oscillatory processes unfold rapidly and are not necessarily time-locked to external events, they often remain invisible in traditional event-related analyses. Capturing these dynamics requires methods that can resolve fast temporal changes and quantify interactions between neural populations.

1.1.3 EEG as a tool for capturing brain dynamics

Electroencephalography (EEG) offers unique advantages to study these dynamics because it records neural activity with millisecond precision and can reveal how oscillatory activity changes on behaviourally relevant timescales [23], [24]. When combined with appropriate analysis methods, EEG can reveal large-scale interactions across frequency bands such as theta, alpha and beta rhythms and link these patterns to cognitive processes including memory encoding, decision-making and perceptual evaluation [14], [25], [26]. Source-level analyses

further show that oscillatory networks reorganise depending on task demands and can predict behavioural outcomes, with different frequencies and cortical regions contributing in specific ways [27]. These findings highlight the potential of EEG to reveal the temporal structure of cognitive processes and the dynamic coordination of distributed neural systems.

Traditional EEG analyses, such as Event-Related Potential (ERP), have played a central role in characterising stimulus-evoked responses. ERPs isolate activity that is time-locked and phase-aligned across trials. However, because ERPs rely on averaging, they are less sensitive to ongoing, non-phase-locked oscillatory dynamics that support functional interactions between brain regions. Many forms of neural coordination such as transient synchronisation, rapid shifts in network configuration or cross-frequency coupling may therefore remain undetected in ERP-based approaches.

These limitations of ERP-based approaches point to a broader issue: interpreting EEG signals is inherently challenging. Scalp recordings reflect linear mixtures of multiple neural and non-neural sources, meaning that each electrode captures activity from several cortical generators as well as artefacts such as eye movements and muscle activity [28], [29]. This mixing complicates interpretation and can obscure the underlying neural processes. High density EEG and advanced inverse modelling approaches can partially mitigate spatial blurring by projecting sensor data into source space [30], [31], but some degree of mixing remains. As a result, careful preprocessing and method selection are essential for drawing valid conclusions about functional interactions from EEG data. These challenges motivate the need for analytical approaches that can better capture how neural activity is organised across space and time. Understanding these challenges is essential before considering how EEG can be used to study interactions between brain regions, which is the focus of the next section.

In the context of this thesis, Chapter 2 provides the theoretical and methodological background necessary for understanding these challenges, including the origins of EEG signals, the physics of volume conduction, the principles of connectivity metrics and the rationale for source and component separation.

1.1.4 Challenges in interpreting EEG signals

Traditional EEG analyses often treat electrode signals as if they directly reflect underlying neural sources. In reality, the scalp electric field generated by a single cortical source spreads across multiple electrodes, and each electrode receives contributions from many sources. This phenomenon, known as volume conduction, can create the appearance of coordinated activity even when no true interaction exists [28], [32]. Because of this, analyses that rely on instantaneous relationships between signals such as simple correlations or zero-lag synchrony can be misleading [33], [34]. These issues have important implications for studies that aim to understand how brain regions interact. If the signals being compared are mixtures of multiple sources, then any apparent relationship may reflect shared mixing rather than genuine communication.

These limitations have motivated the development of approaches that focus on patterns of coordinated activity rather than raw sensor signals. This conceptual shift has led to increasing interest in functional connectivity, a broad term referring to statistical relationships between neural signals that may reflect coordinated processing across regions.

1.1.5 Functional connectivity as a window into neural interactions

The brain operates as a network, with cognitive functions emerging from interactions between distributed regions rather than isolated activity in single areas [35], [36]. Functional connectivity provides a conceptual framework for studying these interactions by examining how neural signals vary or synchronise over time [37]. When applied carefully, connectivity analyses can reveal how networks form, dissolve and reorganise in response to changing task demands.

In the context of aesthetic perception, connectivity approaches offer the potential to uncover how visual, emotional and semantic processes are integrated when viewing different artistic styles [38]. While many EEG studies of aesthetic experience focus on ERPs or spectral

power [39], [40], [41], [42], [43], far fewer examine how distributed networks support aesthetic judgement. This gap limits our understanding of the dynamic processes underlying art perception. Functional connectivity therefore provides a conceptual framework for studying how distributed neural populations coordinate during cognitive tasks [37]. However, its interpretability still depends on the quality of the underlying signals. Because EEG sensors capture mixtures of multiple sources, understanding interactions between regions also requires approaches that can separate overlapping activity [44], [45].

1.1.6 The role of source separation

A second conceptual challenge arises from the fact that EEG signals are mixtures of multiple neural sources. When signals overlap, it becomes difficult to determine whether observed patterns reflect true neural interactions or simply shared mixing. To address this problem, three broad categories of source-separation approaches have been developed in EEG research [46]. First, simple spatial filters aim to reduce correlations between neighbouring scalp channels by sharpening the spatial resolution of the EEG signal. Examples include the surface Laplacian [47], which make the signal more local and therefore less affected by widespread volume conduction. Second, more complex spatial filters use realistic head models to estimate activity within specific cortical regions or networks. Methods such as minimum norm estimates (MNE) [48], Beamforming [49] or dipole fitting (DIPFIT) [50] fall into this category and attempt to reconstruct the underlying neural sources more directly. Third, blind source-separation methods seek to unmix the EEG signals into statistically distinct components without relying on anatomical models.

One widely used approach in the third category is Independent Component Analysis (ICA), which attempts to separate EEG signals into statistically independent components [44], [51]. Importantly, ICA does not recover true anatomical sources, but rather, it identifies components that behave as if they arise from independent processes under specific statistical assumptions. ICA's practical strengths in EEG research include effective isolation of common artefacts, extraction of physiologically meaningful neural sources and improved precision for subsequent analyses such as connectivity and source-localisation [45], [52]. Applied carefully, ICA can reduce false inflation of synchrony by recovering representations that are closer to single sources than scalp electrodes. It can serve as a possible practical alternative to inverse modelling when combined with DIPFIT or spatial projection to cortical regions [53], [54], although the resulting components should still be interpreted as models of underlying sources rather than direct measurement of them.

Although ICA is commonly used to remove artefacts, it can also isolate neural components that reflect meaningful cognitive processes [45], [52]. However, the reliability of ICA depends on preprocessing choices, data quality and algorithm parameters [52], [55], and its performance for extracting cognitive components has not been systematically evaluated. These considerations illustrate why source separation is increasingly viewed as an important complement to, for example, connectivity-based approaches. By improving the separability of neural signals, methods such as ICA can enhance the interpretability of EEG data and support more reliable inferences about neural interactions.

This motivates one of the aims for the thesis: to assess how reliably ICA can extract a well-defined cognitive component under different preprocessing conditions which is addressed more in Chapter 4. To contextualise these methodological developments, the next section offers a brief historical perspective on neural oscillations.

1.1.7 A brief historical perspective

The study of neural oscillations has changed considerably over the past century. The field began in 1924, when Hans Berger recorded the first human electroencephalogram and identified the 8-12 Hz alpha rhythm over posterior scalp regions [56]. His work demonstrated that rhythmic electrical activity could be measured non-invasively, laying the foundation for systematic study of brain rhythms. Early research focused mainly on describing different frequency bands (e.g. delta, theta, alpha and beta) and relating them to behavioural states such as wakefulness and

sleep [57]. Although important, this work was largely descriptive and offered limited insight into how oscillations contribute to cognition.

In the 1980s and 1990s, improved recording and analysis techniques allowed researchers to explore the functional significance of oscillations. Rather than focusing solely on where rhythms appeared on the scalp, studies began examining how oscillatory patterns changed during different tasks and mental states, showing a shift toward a more functional interpretation [19], [58]. In the early 2000s, research increasingly focused on how oscillations support communication between brain regions. Studies showed that phase synchronisation between distant areas can facilitate information transfer and large-scale integration [59]. The communication-through-coherence framework formalised this idea, proposing that aligned oscillatory phases create favourable conditions for effective neural communication [11], [12].

Over the past decade, oscillatory research has converged with the broader field of network neuroscience. This perspective views the brain as a dynamic system whose connectivity patterns reorganise with task demands [60], [61]. Advances in graph-theory analysis, time-resolved connectivity methods and machine learning have made it possible to study how oscillatory networks form, dissolve and reconfigure across different timescales [62], [63]. Rather than focusing on individual rhythms, recent work emphasises how distributed patterns of connectivity support flexible, task-dependent organisation [27], [64].

This historical development, from early descriptive observations to dynamic network analyses, provides the conceptual foundation for the present thesis. Building on this context, the next section identifies the specific gaps in current research that motivate the work carried out in this thesis.

1.2 Research gaps

Despite substantial progress in oscillatory and connectivity research, several gaps remain that motivate the present work.

Gap 1: Limited application of robust connectivity methods to study aesthetic perception
While numerous studies have examined the neural correlates of aesthetic experience using EEG, most focus on ERPs or spectral power changes [39], [40], [41], [42], [43]. Few studies have investigated the dynamic functional connectivity networks that highlight aesthetic perception [38], [65], particularly the temporal progress of connectivity patterns during the processing of different artistic styles (abstract versus figurative art).

Moreover, when connectivity analyses are conducted, there is often insufficient attention to volume conduction mitigation. Although robust connectivity metrics have been developed to reduce spurious connectivity caused by volume conduction [33], [34], [66], their application to understanding the time-resolved, frequency-specific networks involved in aesthetic perception remains limited.

Gap 2: Limited physiological and methodological understanding of fixation-locked neural activity during naturalistic viewing
Fixation and saccades structure visual exploration, yet the neural responses time-locked to these events remain difficult to isolate and interpret in naturalistic settings. Most of what is known about fixation-locked activity comes from highly controlled paradigms, where visual input and eye movements are constrained. In contrast, during free viewing of complex stimuli such as artworks, fixations vary widely in duration, visual content and cognitive demands. It is therefore unclear which neural components reliably accompany fixations, what physiological processes they reflect and how they contribute to perceptual or aesthetic evaluation.

Moreover, fixation-related signals overlap with saccade-related activity, ongoing oscillations and stimulus-driven responses, making it challenging to extract meaningful neural markers. This gap limits our ability to understand how perception unfolds across rapid sequence of fixations that characterise real-world viewing.

Gap 3: Insufficient validation of ICA for extracting cognitive EEG components in naturalistic viewing

ICA is often applied as a routine processing step, primarily for artefact removal, but its ability to reliably extract cognitive components under different preprocessing choices remains insufficiently tested [53], [54]. In the broader ICA literature, preprocessing decisions including filtering parameters, referencing methods, channel interpolation strategies and artefact handling procedures [67], [68] are known to influence the statistical properties of the data. These choices can substantially alter the number, quality and interpretability of the resulting components, raising concerns about the reproducibility of ICA-derived neural signals.

Despite its widespread adoption, there is limited systematic evidence demonstrating how consistently ICA can recover meaningful cognitive activity across different datasets, tasks or preprocessing pipelines. This gap is especially pronounced in free-viewing EEG, where frequent saccades and fixation-locked responses introduce additional complexity and place greater demands on ICA performance. The lack of validation in such naturalistic settings limits confidence in ICA-based interpretations and highlights the need for rigorous evaluation of its reliability in capturing functionally relevant neural processes.

1.3 Research objectives

This thesis addresses the identified gaps through a sequence of linked objectives that together strengthen both the scientific and methodological foundations of EEG connectivity research in naturalistic cognitive paradigms.

Objective 1: Characterise functional connectivity dynamics in aesthetic perception
Investigate the temporal and spectral dynamics of functional connectivity networks during the perception of abstract and figurative paintings, using relevant connectivity metric.
Assumption: Aesthetic perception is not a single static process but unfolds across multiple temporal stages. Early viewing stage is expected to reflect perceptual and sensory analysis, whereas later viewing may involve more integrative, interpretative and evaluative processes. Different forms of visual content may therefore engage partially distinct patterns of large-scale neural coordination. Therefore, this objective aims to characterise how functional brain networks evolve across time and frequency during aesthetic perception.**Objective 2: Identify and characterise fixation-locked neural activity in naturalistic viewing**
Determine whether reliable fixation-locked neural responses can be extracted during free viewing of paintings and describe their temporal and spatial properties.
Assumption: Visual perception during natural viewing unfolds through a sequence of fixations and saccades, with each fixation providing an opportunity for new visual information to be processed. Meaningful neural activity associated with these fixation events should therefore be observable within the EEG signal when these features are carefully extracted. This objective aims to establish whether physiologically meaningful fixation-locked neural activity can be identified and characterised during naturalistic viewing.

Objective 3: Assess the stability of ICA decomposition for cognitive EEG components in naturalistic viewing
Systematically evaluate how preprocessing choices affect the stability and reproducibility of ICA-derived cognitive components.
Assumption: Reliable neural components should remain reasonably consistent across realistic preprocessing variations. If component-level interpretations are to be used in naturalistic EEG research, the robustness of the extraction procedure must first be established. This objective aims to identify preprocessing conditions that support reliable and reproducible extraction of meaningful neural activity.

Integration and future directions
Although these objectives address different methodological challenges, they are conceptually linked. Objective 1 characterises large-scale network dynamics during aesthetic perception. Objective 2 investigates whether meaningful fixation-locked neural activity can be identified during naturalistic viewing. Objective 3 evaluates the reliability of the component extraction procedures required to support such analyses. Together, these objectives provide a

methodological framework for studying cognitive processes in naturalistic EEG research and establish the foundations for future component-space investigations of functional connectivity.

1.4 Thesis organisation

This thesis is organised into seven chapters that build progressively from theoretical foundations to methodological contributions and broader implications.

Chapter 1 (Introduction) outlines the background and motivation for the thesis, the conceptual challenges in interpreting EEG signals, identify the key research gaps and the three research objectives that guide the work.

Chapter 2 (Conceptual and methodological foundations) provides the foundational concepts necessary for understanding this thesis. It describes the EEG signal generation and the neurophysiological basis of scalp-recorded electrical activity, the physics of head volume conduction and its implications for signal interpretation, oscillatory mechanisms in cognition and their functional significance, connectivity concepts and the pitfalls of sensor-space approach, and an introduction to ICA and inverse methods. This chapter establishes the theoretical motivation for the methodological choices made throughout the thesis.

Chapter 3 (Sensor-space connectivity analysis) presents the first empirical study, addressing Objective 1. It examines functional connectivity during aesthetic perception using a connectivity metric designed to mitigate volume-conduction effects. The chapter characterises how connectivity patterns evolve across time and frequency during the viewing of different artistic styles.

Chapter 4 (Fixation-locked activity and ICA reliability) addresses both Objective 2 and 3. The first part investigates whether reliable fixation-locked neural activity can be identified during naturalistic art viewing. The second part systematically evaluates how preprocessing choices influence the stability and reproducibility of ICA decompositions. Together, these analyses provide a methodological basis for interpreting fixation-related signals and for assessing the robustness of ICA in cognitive EEG research, especially in free-viewing settings.

Chapter 5 (General discussion), synthesises the findings from the empirical studies, discusses their theoretical and methodological implications and outlines best-practice recommendations for sensor-space and component-space analyses. It also considers how the results inform future research on oscillatory dynamics and connectivity in naturalistic cognitive paradigms.

Chapter 6 (Conclusion) summarises the main findings of the thesis work.

Chapter 7 (Contribution to science) provides a concise overview of the thesis's key scientific and contributions and list the publications from this work.

2. CONCEPTUAL AND METHODOLOGICAL FOUNDATIONS

2.1 Introduction to EEG

EEG is a non-invasive neuroimaging technique that measures electrical activity in the brain by recording voltage fluctuations from electrodes placed on the scalp [57]. Since its first application in humans by Hans Berger in 1929 [56], EEG has become one of the most widely used tools in neuroscience research and clinical practice. The primary advantage of EEG lies in its exceptional temporal resolution, with the ability to capture neural dynamics at the millisecond scale [69]. This makes EEG particularly valuable for studying rapid cognitive processes such as perception, attention and decision-making, where timing is critical.

Compared to other neuroimaging modalities, EEG offers distinct trade-offs. While functional magnetic resonance imaging (fMRI) provides superior spatial resolution by measuring blood oxygenation changes, it suffers from poor temporal resolution due to the sluggish hemodynamic response [70], [71]. Magnetoencephalography (MEG) shares EEG's excellent temporal resolution and offers better spatial precision by measuring magnetic fields generated by neural activity, but MEG systems are significantly more expensive and less portable [72], [73]. EEG's combination of high temporal resolution, relatively low cost and high portability makes it an attractive option for investigating the temporal dynamics of brain activity, particularly in naturalistic settings where other methods may be impractical. These trade-offs between EEG, MEG and fMRI are summarised in Table 1.

Table 1. The trade-offs between EEG, MEG and fMRI in terms of temporal resolution, spatial resolution, cost and portability.

Modality	Temporal resolution	Spatial resolution	Cost	Portability
EEG	Excellent	Low	Low	High
MEG	Excellent	Moderate-High	Very high	Low
fMRI	Poor	Very high	Very high	Very low

2.1.1 Neurophysiological origins of the EEG signal

To understand what EEG measures, it is necessary to investigate the neurophysiological processes that generate the signals recorded at the scalp. EEG primarily reflects the synchronous postsynaptic potentials of large populations of cortical pyramidal neurons [29], [74]. The basic neurophysiological mechanisms underlying this process are illustrated in Figure 1. When a neuron receives input at its synapses, it generates postsynaptic potentials [75] which is either excitatory or inhibitory (EPSP and IPSP) that cause the ionic currents to flow along the dendrites and through extracellular space [74]. Individual neurons produce electrical fields that are far too weak to be detected at the scalp. However, when thousands to millions of pyramidal cells are activated simultaneously and perpendicular to the cortical surface, their individual electric fields summate to produce a signal strong enough to be propagate through the brain tissue, cerebrospinal fluid, skull and scalp to be recorded by surface electrodes [29], [74], [76]. The pyramidal neurons' parallel arrangement with dendrites extending toward the cortical surface creates favourable conditions for field summation, making them the primary generators of scalp-recorded EEG [29].

The difference between near-field and far-field activity is important for understanding EEG signals. Near-field activity refers to electrical potentials recorded close to their source, where the signal is strong and spatially localised. In contrast, far-field potentials are recorded at a distance from the generating source. In the case of scalp EEG, this distance includes multiple layers of tissue with different electrical conductivities [29], [77]. As electrical signals propagate from cortical sources to the scalp, they undergo spatial blurring and attenuation. This means that the signal recorded at any single scalp electrode represents a mixture of activity from multiple underlying brain regions, with nearby sources contributing to more strongly than the distant ones [28], [29].

Approximately, 80% of the EEG signal originates from postsynaptic potentials, while action potentials contribute roughly 20% [74], [78]. This reflects that postsynaptic potentials last longer (tens of milliseconds) compared to the brief duration of action potentials (1-2

milliseconds), which allow greater temporal summation. Subcortical structures can also contribute to the scalp EEG, but their signals are generally weaker and more diffuse due to the greater distance and the radial orientation of many deep structures, which may produce closed-field configurations that do not project strongly to the scalp [29].

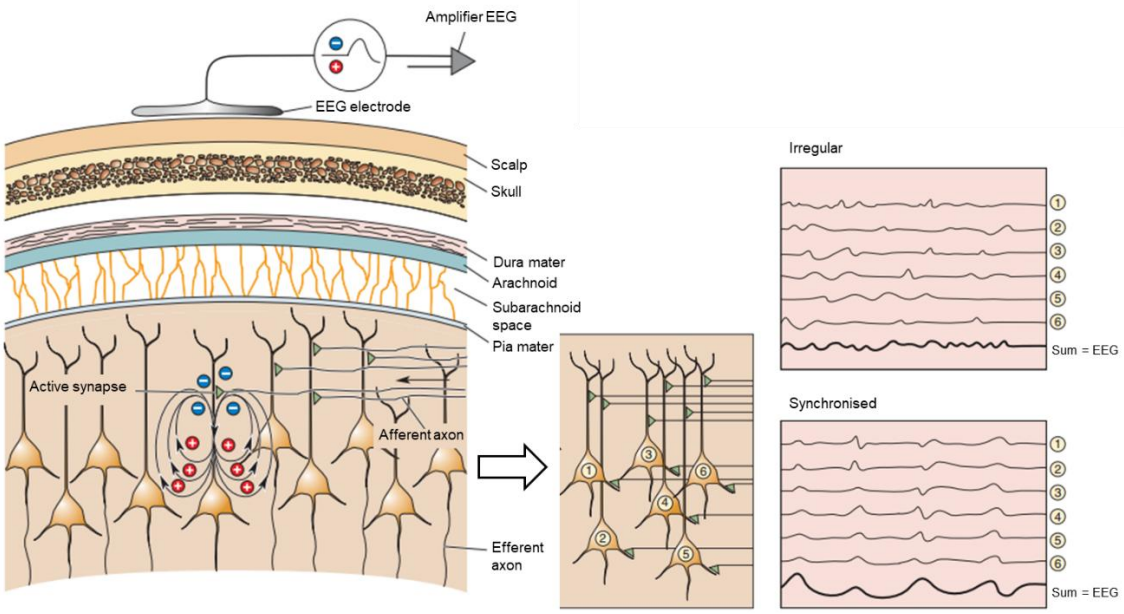

Figure 1. Generation and propagation of EEG signals. Synchronous postsynaptic potentials in cortical pyramidal neurons generate extracellular fields that propagate through brain tissues and is detected at the scalp by EEG electrodes. Signal amplitude depends on both voltage strength and the population synchrony. Adapted from [79].

2.1.2 The EEG forward and inverse problems

The relationship between brain sources and scalp recordings can be formalised through the concepts of the forward problem and the inverse problem [31]. The forward problem addresses the question: given a known configuration of neural sources in the brain, what electrical potentials will be measured at the scalp? This problem is relatively straightforward and has a unique solution. It can be modelled using volume conduction models that describe how electrical currents propagate through the head's various tissue layers (brain, cerebrospinal fluid, skull, scalp), each with different conductivity properties [29], [31]. Modern forward models often use realistic head geometries derived from structural Magnetic Resonance Imaging (MRI) scans and employ techniques such as boundary element methods (BEM) or finite element methods (FEM) to accurately simulate the physics of electrical propagation [31].

The inverse problem, in contrast, is far more challenging: given the recorded scalp potentials, can we determine the location, orientation and strength of the underlying neural sources? Unfortunately, this problem is mathematically ill-posed because there are infinitely many possible source configurations that could produce the same pattern of scalp recordings [31], [80]. This fundamental ambiguity arises from the fact that we typically have far fewer recording electrodes (e.g. 64-128 channels) than potential source locations in the brain (thousands to millions of possible source points). Additionally, scalp EEG is spatially blurred due to volume conduction. At the same time, different combinations of activity from multiple brain regions can produce similar scalp topographies.

Various approaches attempt to solve the inverse problem by providing additional assumptions, such as MNE (which assume sources with minimum overall energy), Beamformers (which use spatial filters to isolate activity from specific locations) or DIPFIT (which assumes a small number of equivalent current dipoles) [31], [80]. Each approach involves different trade-offs between spatial resolution, sensitivity to deep sources and computational complexity.

Because the inverse problem is not well-defined, any attempt to localise sources from scalp EEG must rely on additional constraints. These constraints may involve limiting possible locations of neural sources, assuming specific dipole configurations or using anatomical information to reduce the number of plausible solutions [31], [81].

2.1.3 ERPs and their limitations

ERPs represent one of the most established methods for analysing EEG data [77]. ERPs are voltage deflections in the EEG that are time-locked to specific sensory, cognitive or motor events. They are typically extracted by averaging EEG epochs across many trials of the same experimental condition, under the assumption that brain activity consistently related to the event will remain in the average while random background EEG activity will cancel out [77]. This averaging process, shown in Figure 2 reveals waveforms with characteristic positive and negative peaks that occur at specific latencies after stimulus onset. Well-known ERP components include the P300 (a positive deflection around 300 ms associated with attention and memory processes), the N400 (a negative component around 400 ms sensitive to semantic processing) and the error-related negativity (ERN, associated with error monitoring) [82]. These components have been extensively studied and provide valuable insights into the timing of cognitive processes.

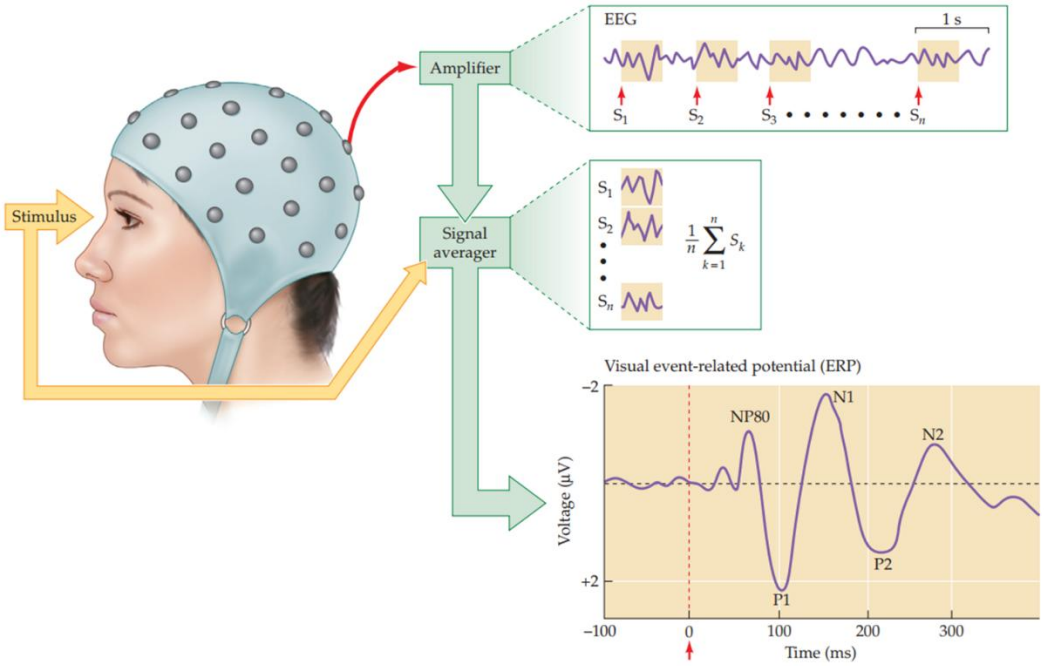

Figure 2. Event-related potentials and the averaging process. EEG epochs time-locked to the repeated stimulus (S1…Sn) are averaged to improve consistent, event-related activity while reducing unrelated background noise. The resulting averaged waveform reveals characteristic ERP components, such as early sensory peaks and later cognitive deflections. Adapted from [83].

However, ERPs have important limitations that motivate the analysis of neural oscillations. The averaging procedure used to extract ERPs is based on the assumption that the brain response is both time-locked and phase-locked to the stimulus event [84]. This means that ERPs primarily capture evoked activity (neural responses that are strictly synchronised to the stimulus). In contrast, induced activity oscillatory responses that are time-locked but not phase-locked is eliminated by the averaging process [19], [85]. This is problematic because a growing body of research suggests that induced oscillatory activity carries important information about cognitive processes and that the brain's response to events often involves changes in ongoing oscillations rather than simply additive evoked responses [84], [86].

Furthermore, ERP analysis treats the brain's response as a series of discrete, static voltage peaks (e.g. P300 or N170), which may not fully capture the dynamic, oscillatory nature of

neural communication [86]. Traditionally, ERPs have been interpreted within an additive framework, in which the stimulus evokes a new, time-locked and phase-locked neural response through averaging. In contrast, alternative views propose that ERPs may instead arise from the phase-resetting of ongoing neural oscillations, reflecting the fact that the brain is continuously active even before stimulus onset [87], [88]. Modern perspectives emphasise that neural processing relies heavily on rhythmic synchronisation across different frequency bands and that these oscillations play a crucial role in coordinating information processing across distributed brain networks [12]. To fully understand brain dynamics, methods that can characterise not just the averaged, phase-locked responses captured by ERPs, but also the time-varying oscillatory activity that reflects ongoing neural communication are needed.

2.2 Neural oscillations and temporal dynamics of the brain activity

2.2.1 Characteristics and origins of neural oscillations

Neural oscillations represent rhythmic fluctuations in the excitability of neuronal populations, manifesting as periodic changes in membrane potentials that can be recorded at various spatial scales, from single neurons to large-scale cortical networks [9], [10]. These oscillations are not merely epiphenomena of neural activity but constitute fundamental mechanisms through which the brain organises information processing, coordinates communication between distant regions and implements cognitive operations [10], [11], [12], [59]. At their core, neural oscillations reflect the synchronised activity of neuronal ensembles, where the temporal coordination of firing patterns creates measurable rhythmic fluctuations in local field potentials that propagate across the cortex [10], [59].

The derivation and quantification of oscillatory activity from electrophysiological signals require sophisticated mathematical approaches that decompose complex, non-stationary neural signals into their constituent frequency components. Traditionally, the Fourier transform serves as the foundational method for this decomposition, converting time-domain signals into the frequency domain by expressing the signal as a sum of sinusoidal components with different frequencies, amplitudes and phases. For a continuous signal $x(t)$, the Fourier transform is defined as:

$$X(f) = \int_{-\infty}^{\infty} x(t)\, e^{-i2\pi f t} dt \tag{1}$$

where $X(f)$ represents the frequency-domain representation, f denotes frequency and i is the imaginary unit [86].

In practice, EEG and MEG data are discrete, requiring the use of the discrete Fourier transform (DFT) or its computationally efficient implementation, the Fast Fourier Transform (FFT). Fourier analysis provides frequency information but assumes signal stationarity and cannot capture the time-varying nature of neural oscillations that characterise dynamic cognitive processes. Wavelet transforms address this limitation by providing simultaneous time-frequency localisation through the use of basis functions (wavelets) that are localised in both time and frequency domains [86], [89]. The continuous wavelet transform (CWT) [90] is defined as:

$$W(a,b) = \frac{1}{\sqrt{|a|}} \int_{-\infty}^{\infty} x(t)\, \psi^* \left(\frac{t-b}{a}\right) dt \tag{2}$$

where ψ is the mother wavelet, a is the scale parameter (inverse of frequency), b is the translation parameter (time shift) and $*$ denotes complex conjugation. To illustrate the diversity of mother wavelet shapes used in time-frequency analysis, Figure 3 presents several widely used wavelet families, including Daubechies, Morlet, Gaussian, Mexican Hat, Haar, Symlet, Coiflet and Meyer wavelets. Complex Morlet wavelets are particularly popular in neuroscience applications due to their optimal time-frequency resolution trade-off and their ability to extract both amplitude and phase information simultaneously [86]. Figure 4 illustrates a representative

Event-Related Spectral Perturbation (ERSP) computed using Morlet wavelets, demonstrating how spectral power evolves over time for a single EEG channel.

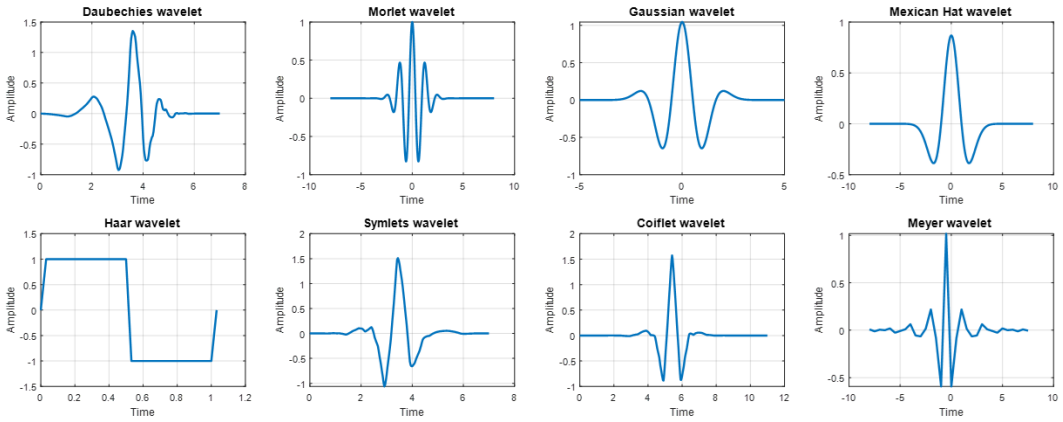

Figure 3. Examples of commonly used mother wavelets $\psi(t)$ from several wavelet families, including Daubechies, Morlet, Gaussian, Mexican Hat, Haar, Symlet, Coiflet, and Meyer wavelets. These functions illustrate the diversity of time-frequency localised basis functions used in continuous wavelet analysis.

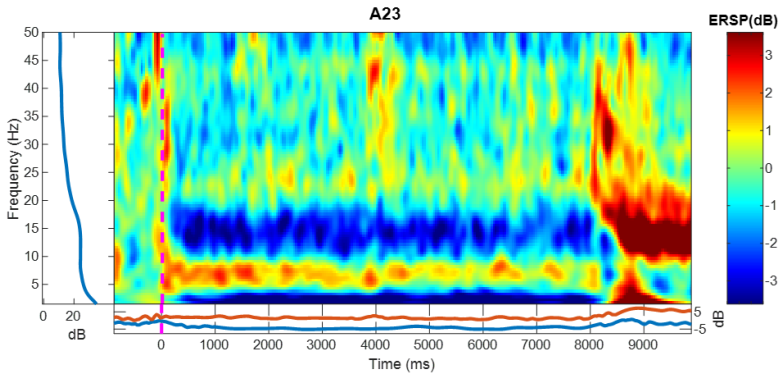

Figure 4. Example ERSP derived from Morlet wavelet analysis. The colour scale represents event-related power changes, where warm colours indicate increases and cool colours indicate decreases across time and frequency.

The Hilbert transform provides an alternative approach for extracting instantaneous amplitude and phase from band-pass filtered signals, offering a complementary perspective on oscillatory dynamics [86]. For a real-valued signal $x(t)$, the Hilbert transform $H[x(t)]$ is defined as:

$$H[x(t)] = \frac{1}{\pi}\int_{-\infty}^{\infty}\frac{x(\tau)}{t-\tau}d\tau \tag{3}$$

The analytic signal $z(t) = x(t) + iH[x(t)]$can then be expressed in polar form as $z(t) = A(t)e^{i\phi(t)}$, where $A(t)$ represents the instantaneous amplitude envelope and $\phi(t)$ represents the instantaneous phase [86]. A practical illustration of this extraction process is shown in Figure 5. This phase information is crucial for understanding how oscillations coordinate neural communication, as the phase of an oscillation determines the temporal windows during which neurons are most excitable and thus most likely to respond to inputs or transmit information to downstream targets [11], [12], [59].

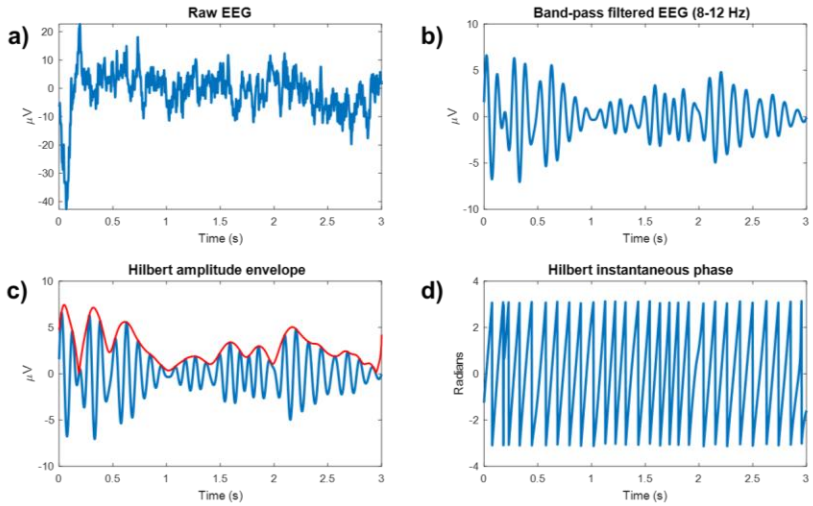

Figure 5. Overview of the process used to extract oscillatory features from EEG data. (a) Raw EEG from a single channel and epoch. (b) Band-pass filtered signal isolating the target oscillatory band. (c) Hilbert-derived amplitude envelope showing moment-to-moment power fluctuations. (d) Instantaneous phase obtained from the analytic signal, reflecting the temporal evolution of the oscillation's phase angle.

2.2.2 Functional roles of frequency bands

The continuous spectrum of neural oscillations is conventionally divided into discrete frequency bands, each associated with distinct cognitive functions and neural mechanisms (summarised in Table 2). This parcellation, while somewhat arbitrary, reflects real differences in how oscillatory frequencies contribute to information processing [9].

Delta oscillations (approximately 1-4 Hz) are the slowest conventional brain rhythms and are prominently associated with sleep, particularly slow-wave sleep, though they also appear during certain cognitive states and in pathological conditions [91].

Theta oscillations (approximately 4-8 Hz) play a central role in memory encoding, retrieval and spatial navigation, particularly through their prominence in hippocampal-cortical interactions [92]. Theta rhythms facilitate memory processes by integrating distributed neural structures into coherent networks, providing a temporal framework for organising sequential information and coordinating the encoding of episodic memories [93]. In working memory tasks, theta oscillations show increased synchronisation in frontal and central regions during memory maintenance [94].

Alpha oscillations (approximately 8-13 Hz) serve multifaceted roles in visual attention, sensory inhibition and the regulation of cortical excitability [95], [96]. Alpha activity exhibits an inhibitory function that suppresses task-irrelevant sensory processing and protects internal representations from external interference [13]. During working memory retention, alpha power increases (event-related synchronisation, ERS), signifying active inhibition of visual input to protect memory representations, whereas alpha power decreases (event-related desynchronisation, ERD) during encoding, indicating active visual processing [95].

Beta oscillations (approximately 13-30 Hz) are primarily associated with motor control, sensorimotor integration and the maintenance of the current cognitive or motor set [97]. Beta-band synchronisation supports the maintenance of steady-state motor output and posture. Beyond motor functions, beta oscillations play important roles in large-scale neuronal interactions and sensory integration [98].

Gamma oscillations (approximately 30-100 Hz) represent the fastest conventional frequency band and are intimately linked to local cortical processing, feature binding and conscious perception [19], [99]. Gamma rhythms facilitate synchronisation and information transfer across distributed neural assemblies, supporting the integration of visual information and the binding of distributed feature representations into coherent perceptual objects [11]. The phase of slower oscillations, particularly alpha and theta, can modulate gamma amplitude

through cross-frequency coupling, creating a hierarchical organisation of information flow [100].

Table 2. The frequency bands, associated cognitive functions and characteristic scalp distributions. Each band is defined by its approximate frequency range (may vary across studies) and linked to specific cognitive processes and scalp patterns.

Frequency band	Range (Hz)	Typical cognitive functions	Typical scalp distribution
Delta (δ)	1-4	Sleep stages, deep meditation, attention, motivation, reward processing	Frontal-central, widespread
Theta (θ)	4-8	Memory encoding/retrieval, attention, meditation, emotional processing	Frontal-midline, medial temporal
Alpha (α)	8-13	Visual attention, inhibition, sensory gating, cortical idling, relaxed wakefulness	Occipital-parietal (strongest over Oz)
Beta (β)	13-30	Motor control, active thinking, focused attention, cognitive processing, sensorimotor	Central (motor cortex), frontal
Gamma (γ)	>30	Feature binding, perceptual integration, consciousness, attention, memory encoding	Local, task-dependent, widespread

An important difference between oscillatory analysis and traditional ERP approaches lies in the dynamic, time-varying nature of oscillations versus the stationary, phase-locked peaks characteristic of ERPs. While ERPs reflect the average response to repeated stimuli, capturing only phase-locked activity, oscillatory analysis measures changes in oscillatory power and phase over time, allowing both phase-locked and non-phase-locked (induced) activity to be examined [19]. Oscillations therefore reflect ongoing cognitive activity, with their amplitude, phase and frequency modulations deliver information about cognitive states and processes in ways that ERPs cannot capture.

Although oscillations provide rich information about neural dynamics, EEG captures them indirectly. The recorded signal is shaped by the geometry of cortical sources, the conductivity of tissues and the spatial mixing of multiple sources. Understanding these limitations is essential for interpreting oscillatory measures and for distinguishing genuine neural interactions from artefacts of volume conduction.

2.2.3 Methodological challenges in interpreting oscillatory activity

While oscillatory analysis provides rich information about brain dynamics, it also introduces significant methodological challenges. The advantages of oscillatory measures stem from their ability to capture both amplitude and phase information, which together provide a comprehensive picture of neural dynamics and enable the assessment of dynamic connectivity between brain regions [86]. Phase information is particularly crucial because it reveals the temporal relationships between oscillations in different regions, allowing researchers to identify synchronised networks and understand how information flows through the brain [12].

However, the interpretation of oscillatory activity from scalp-level EEG recordings is complicated by several fundamental challenges inherent to the physics of volume conduction and the spatial properties of EEG signals. Spatial smearing occurs because electrical potentials generated by neural sources propagate through the brain tissue, cerebrospinal fluid, skull and scalp, each with different conductivity properties, before reaching the recording electrodes [29]. This volume conduction process causes the activity from a single neural source to be detected by multiple electrodes and conversely, each electrode records a mixture of activity from multiple underlying sources.

The mixed nature of sources represents a related challenge, wherein each recorded EEG channel contains contributions from numerous cortical and subcortical sources, as well as non-neural artefacts [45]. This mixing problem is particularly severe for connectivity analyses because it can create spurious correlations between channels that do not reflect genuine neural communication but rather the shared influence of a common underlying source [28]. When two electrodes both record activity from the same neural source, they will necessarily show correlated signals, even if the underlying neural populations are not functionally connected.

This phenomenon, known as the volume conduction problem, represents one of the most significant challenges in EEG connectivity analysis and will be addressed in greater detail in subsequent sections.

Limitations of scalp-level interpretation extend beyond spatial resolution to involve fundamental ambiguities in source localisation. The inverse problem in EEG is mathematically ill-posed, meaning that infinitely many source configurations could theoretically produce the same scalp distribution [31]. While various source localisation algorithms attempt to resolve this ambiguity by imposing additional constraints (such as MNE [48] or Beamformer [101] approaches), these methods introduce their own assumptions and limitations that affect the reliability of source-level inferences.

These methodological challenges are not unique to oscillatory analysis but influence any metric derived from EEG signals, including connectivity measures. The spatial smearing and source mixing problems directly impact the validity of functional connectivity estimates, potentially leading to overestimation of connectivity strength and the detection of spurious connections that do not reflect genuine neural communication [102]. Addressing these challenges requires careful methodological choices in preprocessing, analysis and interpretation, including the use of appropriate connectivity metrics that are designed to be robust to volume conduction effects.

2.3 Brain connectivity concepts

2.3.1 Introduction to brain connectivity

Brain connectivity research aims to characterise the patterns of anatomical links and functional interactions that enable coordinated activity across distributed neural networks. This field recognises that cognitive functions occur not from isolated brain regions but from the dynamic interplay of multiple areas working together. Three conceptually different types of connectivity: structural, functional and effective connectivity (as illustrated in Figure 6) are typically compared in the neuroscience literature [60], [102].

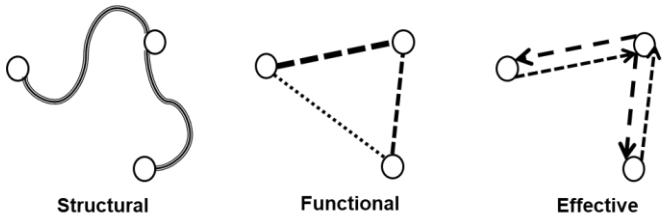

Figure 6. Three different types of connectivity: structural, functional and effective connectivity.

Structural connectivity refers to the physical, anatomical connections between brain regions, comprising the white matter fibre tracts that provide the substrate for neural communication. These connections can be characterised using diffusion tensor imaging (DTI) or other diffusion-weighted MRI techniques that trace the orientation and integrity of axonal bundles [60]. Structural connectivity is relatively stable over short timescales.

Functional connectivity is defined as the statistical dependence between the activity of different brain regions, typically measured as the temporal correlation, coherence or phase synchronisation between signals recorded from those regions [37], [102]. Functional connectivity is inherently symmetric. If region A is functionally connected to region B, then B is equally connected to A and it does not imply directionality or causality. Rather, it identifies regions that show coordinated activity patterns, suggesting they participate in common functional networks. Functional connectivity can be estimated from various neuroimaging modalities, including fMRI, EEG and MEG. In EEG research, functional connectivity is typically assessed through measures of phase synchronisation, amplitude correlation or spectral coherence, which quantify the consistency of temporal relationships between oscillatory signals [59].

Effective connectivity extends beyond mere statistical dependence to characterise the causal influence that one neural system exerts over another, incorporating directionality and often attempting to model the underlying mechanisms of interaction [37]. Effective connectivity methods, such as Granger causality, partial directed coherence and dynamic causal modelling, aim to determine not only which regions interact but also the direction and strength of causal influences.

This study focuses specifically on functional connectivity in EEG, leveraging the excellent temporal resolution of electrophysiological recordings to characterise the millisecond-scale dynamics of neural synchronisation that support cognitive processes. EEG-based functional connectivity analysis offers unique advantages for studying the temporal dynamics of brain networks, capturing rapid changes in connectivity patterns that occur during cognitive tasks.

2.3.2 Phase synchronisation

Phase synchronisation represents a fundamental mechanism of neural communication, wherein oscillations in different brain regions maintain consistent phase relationships over time despite potential variations in amplitude [12], [59]. This phenomenon reflects the temporal coordination of neural activity, synchronising periods of increased excitability across regions to support information transfer. Unlike amplitude-based measures of connectivity, which can be influenced by common input or volume conduction effects, phase synchronisation specifically captures the temporal alignment of oscillatory cycles, providing insight into the dynamic coordination of neural populations. Phase information can be extracted from EEG signals using two main approaches. The Hilbert transform method involves band-pass filtering the signal to isolate a specific frequency band, then applying the Hilbert transform to obtain the analytic signal [86] [103]. This approach is computationally efficient and provides good temporal resolution for analysing phase dynamics in narrow frequency bands [86]. Wavelet-based phase extraction offers an alternative that provides simultaneous time-frequency localisation without requiring separate filtering steps [86]. Complex Morlet wavelets directly generate both amplitude and phase information through their complex-valued coefficients.

Once phase information has been extracted from signals recorded at different locations, various metrics can quantify the consistency of phase relationships over time (see Figure 7). Phase locking refers to the phenomenon wherein the phase difference between two oscillating signals remains relatively constant, indicating synchronised activity [103]. Perfect phase locking occurs when the phase difference is constant over time, while partial phase locking is characterised by a phase difference that fluctuates around a preferred value with limited variance. The degree of phase locking can be quantified by examining the distribution of phase differences across time points or trials. These metrics, which will be detailed in Section 2.4, transform the continuous phase information into scalar values that quantify the strength of synchronisation.

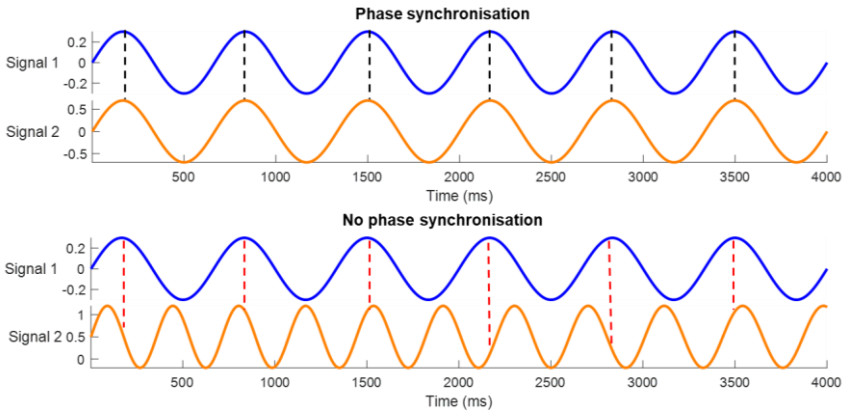

Figure 7. Illustration of phase synchronisation between two oscillatory signals with different frequencies are shown across time points. Stable phase differences indicate phase-locking, whereas varying phase differences indicate no synchronisation.

2.3.3 Sensor space vs. source space approaches

A fundamental question in EEG connectivity analysis concerns whether to estimate connectivity at the sensor level (scalp electrodes) or at the source level (estimated cortical generators). This choice of decision has great implications for the interpretability, spatial precision and validity of connectivity estimates, as sensor-level and source-level signals have fundamentally different properties due to the physics of volume conduction.

Sensor-level signals represent the electrical potentials recorded directly at scalp electrodes, reflecting the summed activity of all neural sources whose electrical fields reach the scalp surface. Due to volume conduction, each sensor records a mixture of activity from multiple underlying cortical and subcortical generators, with the contribution of each source depending on its strength, orientation and distance from the electrode [29]. This mixing has several important consequences for connectivity analysis (see Figure 8 for further illustration). First, it creates instantaneous correlations between sensors that do not reflect genuine neural communication but rather the shared influence of common sources [28]. Second, volume conduction causes spatial smearing, in which activity from a single source is distributed across multiple electrodes, making it difficult to determine the precise location of the generating source [32]. Third, the mixing of sources means that connectivity estimates between sensors may reflect not only direct connections between the underlying sources but also indirect connections caused by third regions or common input from a shared source.

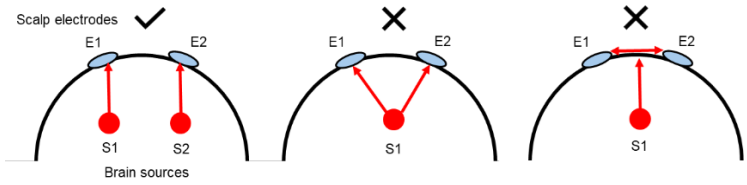

Figure 8. Illustration of how neural sources project to the scalp EEG electrodes. Left: ideal one-to-one mapping between a source and a single electrode. Middle and right: realistic spreading of a single source across multiple electrodes, producing overlapping scalp projections.

The interpretation of synchrony at the scalp level is therefore inherently ambiguous and potentially misleading. High correlation between two sensors could indicate genuine functional connectivity between the underlying neural populations, volume conduction from a common source, or some combination of both [28]. This ambiguity is particularly problematic for connectivity metrics that are sensitive to zero-lag correlations, as these metrics cannot distinguish between genuine zero-lag and spurious zero-lag correlations induced by volume conduction [33]. The spatial resolution of sensor-level connectivity is also limited, as it is constrained by the number and spacing of electrodes and cannot resolve activity from sources that are close together or have similar scalp projections.

Source-level signals, in contrast, represent estimates of the activity of neural sources within the brain, obtained by applying inverse solutions to the sensor-level data [31], [80]. Source reconstruction methods, such as MNE, beamformers or DIPFIT, attempt to solve the inverse problem by determining the configuration of cortical sources that best explains the observed scalp potentials. While the inverse problem is mathematically ill-posed and requires additional constraints to obtain a unique solution, source reconstruction can substantially improve the spatial resolution of connectivity estimates by reducing the mixing of sources and providing more direct access to the activity of distinct neural populations [28].

Source-space connectivity analysis offers several advantages over sensor-level approaches. First, by estimating the activity of spatially distinct sources, it reduces the influence of volume conduction on connectivity estimates [28]. Second, source reconstruction enables connectivity analysis in anatomically defined regions of interest, facilitating comparison with structural connectivity data and integration with findings from other neuroimaging modalities [104]. Third, source-level analysis can reveal connectivity patterns that are obscured at the sensor level due to spatial smearing or cancellation effects [28].

However, source reconstruction also introduces its own challenges and limitations. The accuracy of source estimates depends on the quality of the forward model, the appropriateness of the inverse method and its regularisation parameters and the signal-to-noise ratio of the data [31]. Errors in source localisation can propagate to connectivity estimates, potentially creating spurious connections or obscuring genuine ones. Additionally, source reconstruction typically requires individual anatomical MRI scans to construct accurate head models, which may not be available in all research or clinical settings. Even with source reconstruction, some degree of spatial leakage remains, where the estimated activity of one source contains contributions from nearby sources [105], [106].

Given the complementary strengths and limitations of sensor-level and source-level approaches, there is a clear need for methods that improve spatial resolution without requiring full source reconstruction. ICA represents one such intermediate approach, providing spatial filtering that separates mixed sensor signals into independent components, each representing a distinct source or artefact [44], [52]. ICA requires spatial independence on the components, allowing temporal relationships between components to be analysed without the confound of spatial mixing. This makes ICA particularly suitable for connectivity analysis, as it addresses the volume conduction problem while remaining computationally flexible and not requiring individual anatomical data. The theoretical foundations and practical applications of ICA will be explored in detail in Section 2.5.

2.4 Connectivity metrics and their theoretical foundations

2.4.1 The volume conduction problem revisited

The volume conduction problem represents the most fundamental challenge in EEG connectivity analysis, happening from the physical properties of electrical field propagation through biological tissues. When neurons generate electrical currents through synaptic activity, these currents create electrical fields that spread instantaneously through the surrounding brain tissue, cerebrospinal fluid, skull and scalp [29]. This instantaneous propagation means that activity from a single neural source is detected simultaneously at multiple recording electrodes (Figure 9a), creating correlations between sensors that do not reflect genuine neural communication but rather the passive spread of electrical fields. The mathematical consequence of volume conduction is the production of zero-lag correlations between recording sites. If two electrodes both detect activity from the same underlying source, their signals will be perfectly correlated at zero-time lag, regardless of whether the neural populations generating that activity are functionally connected [33]. This creates a fundamental ambiguity in interpreting connectivity measures: observed synchronisation could reflect genuine neural communication (which may itself occur at zero lag due to reciprocal connections or common input), or it could be an artefact of volume conduction from a single source being detected at multiple locations.

The implications of volume conduction for connectivity analysis are serious and complicated. First, it leads to spurious connectivity, in which connectivity metrics detect strong relationships between sensors that do not correspond to any genuine functional interaction between the underlying neural populations [28]. These spurious connections can dominate connectivity matrices, obscure genuine functional relationships and leading to incorrect conclusions about network organisation. Second, volume conduction causes overestimation of synchrony, inflating connectivity values beyond what would be observed if only genuine neural communication were measured [102]. This overestimation is particularly problematic when comparing connectivity across conditions, groups or frequency bands, as differences in the spatial distribution of sources or in signal-to-noise ratios can differentially affect the magnitude of volume conduction artefacts.

Importantly, not all zero-lag correlations are spurious. Genuine neural synchronisation can occur at zero lag due to common input from a third region, reciprocal connections with negligible conduction delays or electrical coupling via gap junctions [33]. Thus, removing all zero-lag interactions eliminates both spurious and potentially meaningful connectivity. This trade-off motivates the development of metrics that selectively discount zero-lag interactions while preserving non-zero lag synchrony. Figure 9b shows the comparison between spurious

connectivity and genuine connectivity patterns. This creates a dilemma for connectivity analysis: methods that eliminate zero-lag interactions to avoid volume conduction artefacts may also discard genuine zero-lag synchronisation, potentially missing important functional relationships. This finding highlights the need for careful consideration of the trade-offs between sensitivity to genuine connectivity and robustness to volume conduction artefacts when selecting connectivity metrics. The following sections will detail specific connectivity metrics that have been developed to address the volume conduction problem, ranging from classical phase-based measures that are highly sensitive to volume conduction to more sophisticated metrics that explicitly discount zero-lag interactions.

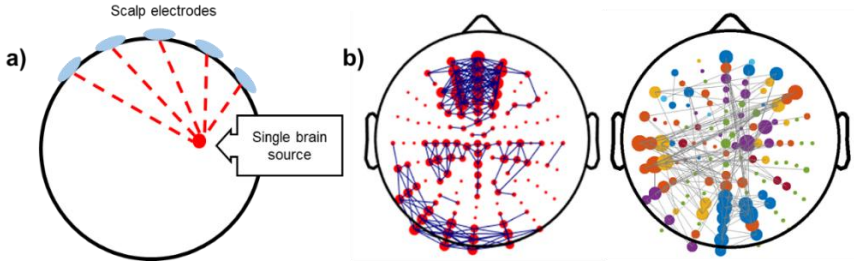

Figure 9. The volume conduction problem in EEG connectivity. (a) A single brain source generates electrical fields that spread instantaneously through the head. (b) Comparison between spurious connectivity (left) and genuine connectivity (right) patterns.

Before discussing modern connectivity metrics designed to address volume conduction, it is essential to understand the classical measures that dominated early EEG connectivity research. These metrics: (1) correlation and (2) coherence, are sensitive to both amplitude and phase relationships, making them highly susceptible to volume conduction artefacts. Understanding their limitations motivates the development of phase-based and zero-lag-insensitive measures discussed in subsequent sections.

The simplest measure of connectivity between two signals is the Pearson correlation coefficient, which quantifies the linear relationship between their amplitudes:

$$r_{xy} = \frac{\sum_{t=1}^{T}(x_t-\bar{x})(y_t-\bar{y})}{\sqrt{\sum_{t=1}^{T}(x_t-\bar{x})^2}\sqrt{\sum_{t=1}^{T}(y_t-\bar{y})^2}} \quad (4)$$

where x_t and y_t are the signal values at time t, $\bar{x}$ and $\bar{y}$ are the mean values and T is the number of time points. Correlation ranges from -1 (perfect negative correlation) to +1 (perfect positive correlation), with 0 indicating no linear relationship. The problem with correlation is that it is sensitive to both amplitude covariation and phase relationships. Two signals can show high correlation due to: (1) genuine functional coupling, (2) volume conduction from a shared source or (3) amplitude fluctuations driven by a common non-neural activity. Correlation cannot distinguish between these scenarios, making it unsuitable for inferring functional connectivity from EEG data.

Meanwhile, coherence extends correlation to the frequency domain, quantifying the consistency of amplitude and phase relationships between two signals within specific frequency bands. Coherence is computed as:

$$C_{xy}(f) = \frac{|S_{xy}(f)|^2}{S_{xx}(f)\cdot S_{yy}(f)} \quad (5)$$

where $S_{xy}(f)$ is the cross-spectral density between signals x and y at frequency f and $S_{xx}(f)$ and $S_{yy}(f)$ are the power spectral densities of x and y, respectively. Coherence ranges from 0 (no consistent relationship) to 1 (perfect consistent relationship) at each frequency. Coherence can be decomposed into amplitude and phase components. High coherence can come from: (1) consistent phase relationships (phase synchronisation), (2) correlated amplitude fluctuations

(amplitude coupling) or (3) both. This makes coherence difficult to interpret as different neural mechanisms can produce similar coherence values.

The fundamental problem with both correlation and coherence is their sensitivity to zero-lag relationships and volume conduction. When two electrodes record activity from the same underlying source due to volume conduction, they will show perfect correlation and coherence at zero phase lag, regardless of whether the underlying neural populations are functionally connected. This makes these classical measures highly vulnerable to spurious connectivity. In terms of phase, volume conduction produces 0˚ or 180˚ phase differences between electrodes. If two electrodes have the same polarity projection from a source, they will be in phase (zero phase difference). If they have opposite polarity projections, they will show a 180˚ phase difference. Neither case reflects genuine neural interaction. These limitations motivated the development of phase-based measures that ignore amplitude fluctuations and focus exclusively on phase relationships, such as the Phase Locking Value (PLV).

2.4.2 Phase-based measure

2.4.2.1 Phase Locking Value

The PLV represents one of the most widely used metrics for quantifying phase synchronisation between neural signals, offering a straightforward and intuitive measure of the consistency of phase relationships over time [103], [107]. PLV quantifies the extent to which the phase difference between two signals remains constant across trials or time windows, with values ranging from 0 (no phase locking) to 1 (perfect phase locking).

Mathematically, PLV is defined as the absolute value of the mean phase difference across N trials or time points:

$$PLV = \left|\frac{1}{N}\sum_{n=1}^{N} e^{i\Delta\phi_n}\right| \quad (6)$$

where $\Delta\phi_{\mathrm{n}} = \phi_1(n) - \phi_2(n)$ is the phase difference between signals 1 and 2 at trial or time point n, i is the imaginary unit and N is the total number of trials or samples [108]. The exponential term $e^{i\Delta\varphi_n}$ represents a unit vector in the complex plane with angle $\Delta\varphi_{\mathrm{n}}$. When phase differences are consistent across trials, these vectors point in similar directions and their mean has a large magnitude (PLV close to 1). When phase differences are random or highly variable, the vectors point in different directions and their mean has a small magnitude (PLV close to 0). PLV is thus insensitive to the absolute phase relationship between signals, caring only about the consistency of that relationship.

PLV has several properties that have contributed to its widespread adoption. First, it is amplitude-independent, meaning that it is not influenced by variations in signal amplitude and thus specifically captures phase synchronisation rather than amplitude covariation [103]. This makes PLV particularly suitable for analysing oscillatory connectivity, where phase relationships are thought to be more directly related to neural communication than amplitude relationships. Second, PLV is frequency-specific, as it is typically computed on band-pass filtered signals or wavelet coefficients corresponding to specific frequency bands, allowing examination of synchronisation in different frequency ranges. Third, PLV is computationally efficient and conceptually straightforward to implement and interpret.

However, PLV has a critical limitation: it is highly sensitive to volume conduction [33], [34], [107]. Because volume conduction creates instantaneous correlations between sensors, it produces zero-lag phase relationships that PLV will detect as strong synchronisation. When two electrodes record activity from the same underlying source, their phases will be identical (or differ by a constant offset), resulting in a PLV of 1 regardless of whether the underlying neural populations are functionally connected. This sensitivity to volume conduction means that PLV connectivity matrices often show strong connections between neighbouring electrodes or between electrodes with similar scalp projections, reflecting spatial proximity and volume conduction rather than genuine functional connectivity. Despite this limitation, PLV remains useful in specific analysis settings. Under controlled conditions, PLV provides a straightforward and robust estimate of phase synchronisation, making it a reliable reference point for evaluating

more advanced connectivity measures. In practice, PLV often serves as a baseline against more sophisticated metrics that attempt to address volume conduction. The development of volume conduction-insensitive measures, discussed in the next section, was motivated largely by the limitations of PLV and similar classical metrics.

2.4.3 Zero-lag-insensitive measures

2.4.3.1 Imaginary coherence (ImCoh)

ImCoh was one of the first metrics developed to address volume conduction by focusing exclusively on the imaginary part of the complex coherence. The key insight is that volume conduction produces real-valued coherence (zero or 180˚ phase differences), whereas genuine neural interactions with non-zero phase lags produce complex-valued coherence with a non-zero imaginary component. The complex coherence is defined as:

$$Coh_{xy}(f) = \frac{S_{xy}(f)}{\sqrt{S_{xx}(f) \cdot S_{yy}(f)}} \tag{7}$$

where $S_{xy}(f)$ is the complex cross-spectral density. The imaginary part of coherence is:

$$ImCoh_{xy}(f) = Im\left(\frac{S_{xy}(f)}{\sqrt{S_{xx}(f) \cdot S_{yy}(f)}}\right) \tag{8}$$

ImCoh ranges from -1 to +1 with non-zero values indicating a consistent non-zero phase lag between signals. Because volume conduction produces zero-lag relationships (zero imaginary coherence), ImCoh is insensitive to volume conduction artefacts. The advantage of ImCoh is its robustness to volume conduction and reference effects. Studies have shown that ImCoh reveals connectivity patterns that are obscured by spurious correlations in classical coherence measures . The limitation is that ImCoh discards all zero-lag interactions, including potentially genuine zero-lag synchronisation. Additionally, ImCoh is sensitive to the magnitude of phase lags (small phase lags produce small ImCoh values even if phase synchronisation is strong). This motivated the development of metrics that focus on phase consistency rather than phase lag magnitude, such as phase-lag index (PLI) and weighted phase-lag index (wPLI).

2.4.3.2 Phase-Lag Index and weighted Phase-Lag Index

PLI was developed to quantify phase synchronisation while explicitly discounting zero-lag interactions [34], [109]. The fundamental insight underlying PLI is that volume conduction produces instantaneous correlations with zero or 180-degree phase differences, whereas genuine neural communication typically involves non-zero phase lags due to conduction delays, synaptic transmission times. By focusing exclusively on the asymmetry of the phase difference distribution, that is, whether phase differences are consistently positive or consistently negative, PLI can detect genuine phase synchronisation while being insensitive to zero-lag relationships. Mathematically, PLI is defined as:

$$PLI = |\langle sign(\Delta\phi_n)\rangle| \tag{9}$$

where $\Delta\phi_n$ is the phase difference at time point or trial n and $sign(\cdot)$ is the signum function that returns +1 for positive values, -1 for negative values and 0 for zero [34]. PLI thus measures the absolute value of the mean sign of phase differences, ranging from 0 (no consistent phase lead or lag) to 1 (perfectly consistent phase lead or lag). If one signal consistently leads the other in phase (all phase differences positive or all negative), PLI will be 1. If phase differences are symmetrically distributed around zero, PLI will be 0, even if there is strong phase locking at zero lag.

The key advantage of PLI is its insensitivity to volume conduction and reference effects [34]. Because volume conduction produces zero-lag correlations, PLI effectively removes their contribution. This makes PLI particularly valuable for sensor-level connectivity analysis. Studies have demonstrated that PLI can reveal connectivity patterns that are obscured by volume conduction artefacts in PLV and other zero-lag-sensitive measures [34], [102], [110]. However, PLI has an important limitation: by using only the sign of phase differences, it

discards information about the magnitude of phase lags, treating a small phase lag the same as a large phase lag as long as they have the same sign [66]. This can reduce PLI's sensitivity to genuine phase synchronisation, particularly when phase differences are small.

The wPLI was developed to address these limitations while retaining PLI's insensitivity to zero-lag interactions [66]. wPLI weights the contribution of each phase difference by its magnitude, giving more weight to large phase lags and less weight to small phase lags that are more likely to be influenced by noise. Mathematically, wPLI is defined as:

$$wPLI = \frac{|\langle |Im(S_{xy})| \cdot sign(Im(S_{xy}))\rangle|}{\langle |Im(S_{xy})|\rangle} \quad (10)$$

where $\mathrm{Im}(S_{xy})$ is the imaginary part of the cross-spectral density and the angle brackets denote averaging over trials or time windows. This weighting makes wPLI more robust to noise and more sensitive to genuine phase synchronisation than PLI, while maintaining insensitivity to zero-lag interactions.

A further improvement, the debiased weighted Phase Lag Index (dwPLI), addresses the positive bias that can affect wPLI estimates, particularly for short data segments or low numbers of trials [66]. dwPLI applies a debiasing correction that provides more accurate estimates of connectivity strength, especially in scenarios with limited data:

$$dwPLI = \frac{\sum_k (Im(S_{xy,k}))^2}{\sum_k |Im(S_{xy,k})|^2} \quad (11)$$

where $S_{xy,k}$ is the cross-spectrum for trial/segment k and $Im(S_{xy,k})$ is the imaginary part. The sums run over all trials or time segments. This metric was used successfully in Chapter 3 of this thesis to characterise functional connectivity in aesthetic perception.

It is important to note that the complete elimination of zero-lag interactions is not without cost. Genuine neural synchronisation can occur at zero lag and removing all zero-lag connectivity may discard functionally meaningful information [33]. The choice between zero-lag-sensitive measures (like PLV) and zero-lag-insensitive measures (like PLI and wPLI) should be guided by the specific research question, the spatial resolution of the data and whether source reconstruction or spatial filtering methods have been applied.

2.4.4 Graph theory metrics for network analysis

While connectivity metrics quantify the strength of pairwise relationships between brain regions, graph theory provides a mathematical framework for characterising the organisation of entire brain networks [36], [111], showing properties that are not apparent from examining individual connections in isolation. In graph theory terms, a brain network is represented as a graph $G = (V, E)$, where V is a set of nodes (representing brain regions, electrodes or independent components) and E is a set of edges (representing functional connections between nodes).

Nodes in EEG connectivity networks typically represent either individual electrodes (in sensor-space analysis), estimated cortical sources (in source-space analysis) or independent components (in ICA-based analysis). Meanwhile, **edges** represent functional connections between nodes, with edge weights typically derived from connectivity metrics such as PLV, wPLI, or coherence [111]. Networks can be either binary (edges are either present or absent) or weighted (edges have continuous values representing connection strength).

Node strength (also called degree in binary networks) is a fundamental local measure that quantifies the total connectivity of a node, computed as the sum of edge weights connecting that node to all other nodes in the network [111]:

$$s_i = \sum_{j \in V} w_{ij} \quad (12)$$

where s_i is the strength of node i, and w_{ij} is the weight of the edge connecting nodes i and j. High node strength indicates that a region is strongly connected to many other regions, suggesting it plays an important role in network communication.

Clustering coefficient measures the extent to which a node's neighbours are also connected to each other, quantifying local network segregation or cliquishness [112]. For a node i, the clustering coefficient is defined as:

$$C_i = \frac{2t_i}{k_i(k_i-1)} \tag{13}$$

where t_i is the number of triangles (sets of three mutually connected nodes) involving node i and k_i is the degree (number of connections) of node i. High clustering indicates that a node is part of a densely interconnected local community, suggesting modular organisation.

Path length quantifies the average number of edges that must be traversed to travel between any two nodes in the network, providing a measure of network integration [113]:

$$L = \frac{1}{n(n-1)} \sum_{i \neq j} d_{ij} \tag{14}$$

where n is the number of nodes and d_{ij} is the shortest path length between nodes i and j. Short path lengths indicate efficient communication and high global integration.

Betweenness centrality identifies nodes that lie on many shortest paths between other nodes, serving as important hubs or bottlenecks for information flow [111], [113]:

$$b_i = \sum_{j \neq k} \frac{\sigma_{jk}(i)}{\sigma_{jk}} \tag{15}$$

where σ_{jk} is the number of shortest paths between nodes j and k, and $\sigma_{jk}(i)$ is the number of those paths that pass through node i. High betweenness centrality indicates that a node plays a critical role in connecting different parts of the network and its removal would significantly disrupt network communication.

Modularity quantifies the extent to which a network can be subdivided into distinct communities or modules which is groups of nodes that are densely connected internally but sparsely connected to nodes in other modules [114]:

$$Q = \frac{1}{2m} \sum_{ij} \left[w_{ij} - \frac{k_i k_j}{2m} \right] \delta(c_i, c_j) \tag{16}$$

where m is the total number of edges, $k_i$is the degree of node i, c_i is the module assignment of node i, and $\delta(c_i, c_j) = 1$ if nodes i and j belong to the same module and 0 otherwise. High modularity indicates strong community structure, which is thought to support specialised processing within modules while allowing flexible integration across modules.

Small-worldness characterises networks that combine high local clustering (like regular lattices) with short path lengths (like random networks) [112]. Small-world networks are thought to optimise the trade-off between local specialisation and global integration. Small-worldness is quantified as:

$$\sigma = \frac{C/C_{\text{rand}}}{L/L_{\text{rand}}} \tag{17}$$

where C and L are the clustering coefficient and path length of the observed network, and C_{rand} and L_{rand} are the corresponding values for a random network with the same number of nodes and edges. Values of $\sigma > 1$ indicate small-world organisation.

Participation coefficient measures the extent to which a node connects to nodes in other modules [111], identifying connector hubs that integrate information across communities:

$$P_i = 1 - \sum_{m=1}^{M} \left(\frac{k_{im}}{k_i}\right)^2 \quad (18)$$

where k_{im} is the number of connections from node i to nodes in module m, $k_i$is the total degree of node i, and M is the number of modules. High participation coefficient indicates that a node distributes its connections across many modules, serving as an integrative hub.

An important consideration in graph theory analysis is the choice of thresholding strategy for converting weighted connectivity matrices into graphs suitable for analysis [111]. Common approaches include applying an absolute threshold (retaining only edges above a certain strength), a proportional threshold (retaining a fixed percentage of the strongest edges), or using data-driven methods to identify significant connections. Each approach has advantages and limitations, and the choice can significantly affect network metrics. Graph theory metrics provide powerful tools for characterising brain network organisation and have revealed important details into how network topology relates to cognitive function. Some of these metrics will be particularly relevant in Chapter 3, where they will be applied to characterise connectivity patterns in the analysis.

2.5 ICA: Theory and applications in EEG

2.5.1 Core principles of ICA

ICA is a computational method for separating a multivariate signal into additive, statistically independent subcomponents, providing a powerful approach for blind source separation [51]. In the context of EEG, ICA addresses the fundamental problem that each scalp electrode records a mixture of activity from multiple neural sources as well as various artefacts [44], [52].

The theoretical foundation of ICA is on linear mixing model (Figure 10) that describes how observed signals arise from the combination of underlying sources [44]. For EEG data, this model can be expressed as:

$$X = A \cdot S \quad (19)$$

where X is an $n \times t$ matrix of observed signals (n electrodes $\times$ t time points), S is an $m \times t$ matrix of source signals (m independent components $\times$ t time points) and A is an $n \times m$ mixing matrix that describes how each source projects to the scalp electrodes. In standard ICA applications to EEG, we assume that the number of sources m does not exceed the number of electrodes n [44], [51]. In practice, when ICA is applied to EEG data with n electrodes, it produces exactly n independent components. This is because ICA decomposes the n-dimensional signal space into n maximally independent components. Each row of X represents the time course recorded at one electrode, each row of S represents the time course of one independent component and each column of A represents the spatial distribution (scalp topography) of one component.

The two unknowns problem

The goal of ICA is to estimate both the source signals S and the mixing matrix A from the observed data X alone [51], without prior knowledge of the sources or their mixing. This is accomplished by finding a demixing matrix W such that:

$$S = W \cdot X = A^{-1} \cdot X \quad (20)$$

where W is the inverse of A.

This presents a fundamental challenge where we have only one known quantity (X, the observed EEG data) and two unknowns (A and S) [44], [51], [52]. So the question is, how can we solve for two unknowns with only one equation? The answer lies in making use of the specific assumptions about the statistical properties of the source signals. ICA uses mathematical constrains and optimisation strategies to make this seemingly impossible problem solvable. The key is that if we make certain assumptions about the sources, we can narrow down the space of possible solutions until we find the unique decomposition that best satisfies

those assumptions. These assumptions, detailed below, provide the constraints needed to solve the two unknowns problem.

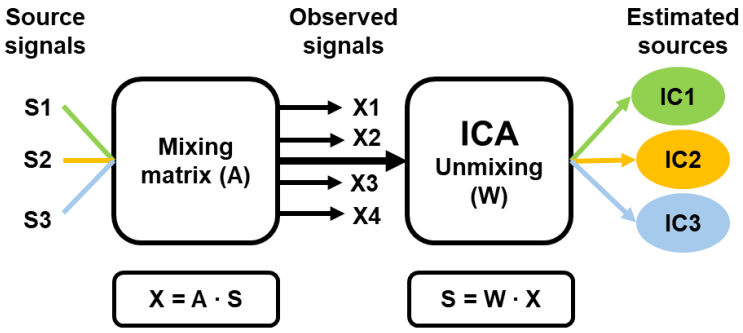

Figure 10. Schematic of the ICA model: observed EEG signals X from a linear mixing of underlying sources S via mixing matrix A. ICA estimates an unmixing matrix W to recover maximally independent components.

Core assumptions of ICA

ICA achieves this separation by making use of several fundamental assumptions about the source signals:

The first assumption is statistical independence: the source signals are assumed to be statistically independent of each other, meaning that knowing the value of one source provides no information about the values of other sources [51]. This independence assumption is stronger than mere uncorrelatedness (zero covariance) and requires that higher-order statistical relationships are also absent. This assumption is reasonable for EEG because different neural sources (e.g. visual cortex, motor cortex) and artefacts are generated by distinct physiological processes that operate independently.

The second assumption is non-Gaussianity: the source signals are assumed to have non-Gaussian probability distributions [51]. This assumption is critical because of the Central Limit Theorem, which states that the sum of independent random variables tends toward a Gaussian distribution [51]. Since the observed EEG signals are mixtures (sums) of independent sources, they will be more Gaussian than the individual sources. ICA exploits this property by searching for a demixing matrix that produces components with maximally non-Gaussian distributions, as these are most likely to correspond to the original independent sources. Non-Gaussianity can be measured using statistics such as kurtosis (fourth-order moment) or negentropy (deviation from Gaussian entropy). Neural signals and artefacts typically have non-Gaussian distributions (e.g. eye blinks have sharp peaks, alpha oscillations have rhythmic structure), making this assumption well-suited for EEG.

The third assumption is stationarity: ICA assumes that the mixing process is stationary, meaning that the mixing matrix A does not change over time [44], [51], [52]. In other words, the way sources project to electrodes remains constant throughout the recording. This assumption implies that sources do not move or change their spatial distributions during the recording period. For EEG, this is generally reasonable over short time scales (minutes to hours), as neural sources are anchored to cortical anatomy and electrode positions remain fixed.

The fourth assumption is sufficient number of observations: ICA typically assumes that the number of underlying neural and artefactual sources does not exceed the number of EEG sensors ($m \leq n$), ensuring that the recorded signals contain sufficient information to estimate the contributing sources [51], [52], [115]. In practice, when applied to n-channel EEG, ICA produces exactly n independent components, each representing a distinct source or a combination of sources.

The last assumption is linear and instantaneous mixing: The mixing process is assumed to be linear, such that each EEG electrode records a weighted sum of simultaneously active sources due to volume conduction [44], [52]. Moreover, the mixing is assumed to be

instantaneous, meaning that signal propagation delays from sources to sensors are negligible relative to the sampling rate. Under this assumption, each EEG observation reflects the concurrent contribution of all sources at a given time point, without temporal smearing or lag effects [115]. This is a reasonable approximation for EEG, as electromagnetic propagation through the head occurs at the speed of light, far faster than typical EEG sampling rates (e.g. 512 Hz corresponds to ~2 ms sampling intervals).

From covariance to identity matrix

ICA addresses a problem: both the mixing matrix A and the underlying sources S are unknown. The idea is to transform the signal step by step until covariance matrix becomes an identity matrix. Once this is achieved, the remaining task is to identify the rotation that produce statistically independent components. The following section outlines this process.

The first step in most ICA algorithms is whitening (also known as sphering) [51], which transforms the observed data X so that its covariance matrix becomes the identity matrix:

$$Z = V \cdot X \tag{21}$$

where V is a whitening matrix chosen such that the covariance of Z is the identity matrix I:

$$Cov(Z) = I \tag{22}$$

The identity matrix has ones on the main diagonal and zeros elsewhere. This means that after whitening: (1) each component has unit variance (diagonal elements = 1) and (2) all components are uncorrelated (off-diagonal elements = 0). In other words, whitening removes all second-order dependencies from the data. This greatly simplifies the ICA problem: after whitening, any remaining structure must come from higher-order statistics, which are precisely what ICA utilises to identify independent components. Whitening is typically achieved using Singular Value Decomposition (SVD), a matrix factorisation technique that decomposes the covariance matrix into its eigenvalues and eigenvectors [51], [52]. Under the assumption of zero mean (which can be achieved by subtracting the mean from each channel), the covariance matrix and its inverse can be determined by SVD. This gives us a concrete mathematical solution to the first part of the problem.

After whitening, the data are uncorrelated but not yet independent. The next step is to find a rotation matrix R [116] that transforms the whitened data into statistically independent components:

$$S = R \cdot Z = R \cdot V \cdot X \tag{23}$$

Different ICA algorithms determine R by optimising a measure of statistical independence. Common criteria include: (1) maximising non-Gaussianity (e.g. using kurtosis or negentropy), (2) minimising mutual information or (3) maximising entropy of the outputs. Once optimal rotation is found, the demixing matrix is obtained as:

$$W = R \cdot V \tag{24}$$

And the estimated sources follow as:

$$S = W \cdot X \tag{25}$$

This two-step procedure: whitening followed by rotation provides a clear conceptual pathway in solving the ICA problem.

Different ICA algorithms and how they differ

Various ICA algorithms implement these principles through different optimisation strategies. The Infomax algorithm maximizes the mutual information between the input and output of a

neural network, which is equivalent to maximising the entropy of the output [51]. The FastICA algorithm uses a fixed-point iteration scheme to maximise non-Gaussianity, measured by kurtosis or negentropy [51]. The JADE (Joint Approximate Diagonalization of Eigenmatrices) algorithm jointly diagonalises a set of fourth-order cumulant matrices [117]. While these algorithms differ in their computational approaches, they all aim to find components that are maximally independent and non-Gaussian.

An important property of ICA is that it imposes spatial independence on the components while allowing them to have arbitrary temporal relationships [44], [116]. This is in contrast to Principal Component Analysis (PCA), which finds spatially and temporally uncorrelated components but does not enforce statistical independence [51]. The preservation of temporal relationships is crucial for connectivity analysis, as it means that temporal correlations or phase synchronisation between independent components can reflect genuine functional connectivity rather than spatial mixing [44].

2.5.2 ICA for EEG source separation and artefact removal

EEG recordings are unavoidably contaminated by a range of physiological and non-physiological artefacts. These include eye blinks, eye movements, muscle activity, cardiac signals and line noise where each of which can obscure or distort the underlying neural activity. Because these artefacts often overlap in time with brain signals and propagate broadly across the scalp, simple filtering or epoch rejection may be insufficient. This motivates the use of ICA, which provides a practical solution to the source separation problem, enabling the isolation of neuronal activity from artefacts and the decomposition of mixed scalp signals into spatially distinct components (Figure 11) [45], [52].

ICA is particularly effective at isolating common EEG artefacts, including [45]:

- Eye blinks: Large-amplitude, stereotyped waveforms with strong frontal scalp distributions
- Eye movements: Lateral frontal distributions with opposite polarity over left and right hemispheres
- Muscle artefacts: High-frequency, irregular activity with focal distributions over temporal or frontal regions
- Cardiac artefacts: Rhythmic activity at the heart rate frequency
- Line noise: Narrow-band activity at 50 Hz

Once artefactual components are identified, they can be removed so that the EEG can be reconstructed without them. This approach to artefact removal has several advantages over traditional methods such as rejection of contaminated epochs. First, it preserves more data, as entire epochs need not be discarded due to transient artefacts. Second, it can remove artefacts that are temporally overlapping with neural signals of interest, which would be impossible with epoch rejection. Third, it allows artefact removal without manually identifying contaminated segments [45].

Beyond artefact removal, ICA enables analysis of EEG data at the level of functionally distinct sources rather than at the level of mixed scalp signals. The key is that ICA executes spatial independence while allowing temporal relationships to be analysed subsequently [44]. Because the components are spatially independent by construction, any temporal correlation or phase synchronisation observed between components cannot be attributed to spatial mixing or volume conduction. Instead, such relationships must reflect genuine functional connectivity between the underlying neural sources. This makes ICA-based connectivity analysis a powerful approach that combines some of the benefits of source reconstruction (reduced volume conduction) with the computational flexibility of sensor-level analysis.

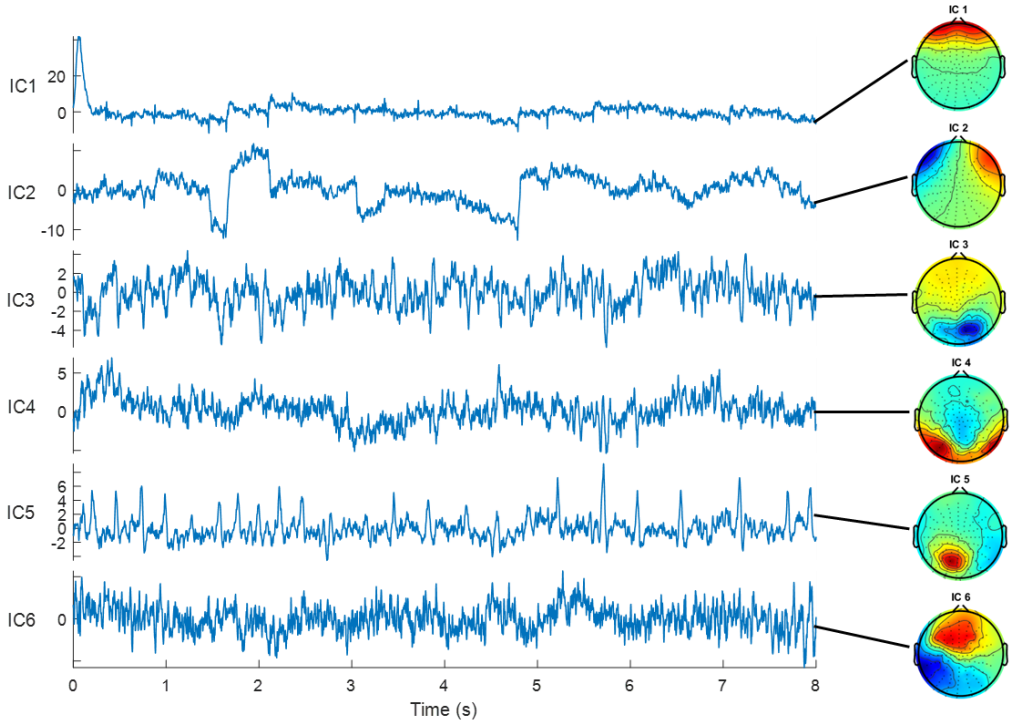

Figure 11. ICA decomposition of EEG data, showing the temporal activation patterns of six independent components (IC1-IC6) together with their corresponding scalp topographies. IC1-IC2 are eye movements; IC3-IC5 are occipital-related components and IC6 is a motor-related component.

The process of applying ICA to EEG typically involves several steps:

1. Preprocessing: Continuous EEG data are filtered to remove slow drifts and high-frequency noise, and potentially downsampled to reduce computational demands.
2. ICA decomposition: An ICA algorithm (such as Infomax [118] or FastICA [119]) is applied to estimate the demixing matrix W and the independent components S.
3. Component classification: The resulting components are inspected and classified as either neural or artefactual based on their spatial, temporal and spectral characteristics.

2.5.3 Automated component classification: ICLabel

While ICA effectively separates EEG signals into independent components, the challenge remains to classify these components as either neural or artefactual. Manual classification based on visual inspection of component properties is time-consuming, subjective and requires considerable expertise, limiting the scalability and reproducibility of ICA-based analyses. Automated classification methods address these limitations by using machine learning algorithms trained on large datasets of manually labelled components to predict component classes based on their spatial, temporal and spectral features. ICLabel is an automated component classification tool that uses a deep neural network trained on over 200,000 manually labelled independent components to classify components into seven categories: brain, muscle, eye, heart, line noise, channel noise and other [54]. ICLabel analyses multiple features of each component, including its spatial topography (scalp map), power spectrum, autocorrelation function and relationship to other components, to predict the probability that the component belongs to each category. The output is a set of probabilities summing to 1, indicating the likelihood that the component represents each artefact type or neural activity. Figure 12 illustrates four example components (IC1, IC2, IC4, IC11), showing their scalp maps, time-series activity, spectral profiles and classification probabilities.

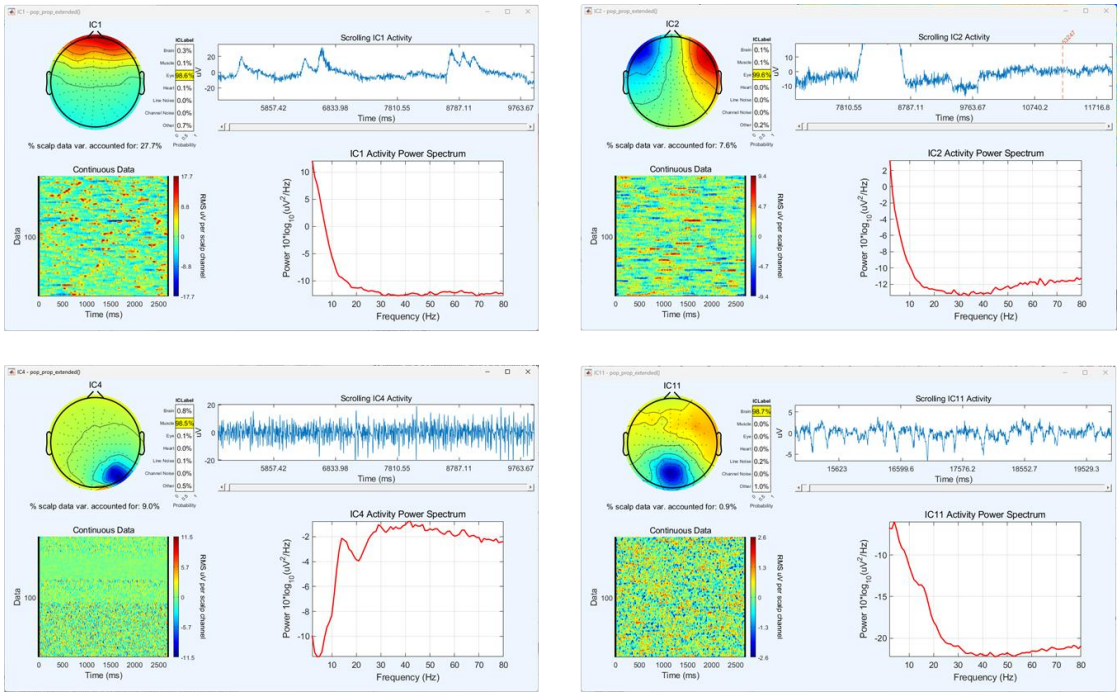

Figure 12. Example independent components (ICs) extracted from EEG data using ICA. Each panel includes the scalp topography, activation time-series, trial-wise heatmap and spectrum, with ICLabel classifications. IC1–2 correspond to eye movements, IC4 to muscle activity and IC11 to an occipital brain component.

ICLabel has been integrated into the EEGLAB toolbox and is widely used in automated EEG processing pipelines [54]. The typical workflow involves running ICA decomposition, applying ICLabel to classify components and then removing components that are classified as artefacts with high confidence. Thresholds for component rejection are typically set based on the predicted probability of the "brain" category, with common values being 80-90%. For example, components with less than 80% probability of being brain-related might be rejected, while those with higher probabilities are kept. The choice of threshold involves a trade-off between removing artefacts (which requires a lenient threshold that may also remove some neural components) and preserving neural signals (which requires a stringent threshold that may retain some artefacts).

The DISCOVER-EEG pipeline demonstrates the integration of ICA and ICLabel into a fully automated EEG processing workflow [120]. This pipeline applies ICA for source separation, uses ICLabel for automated artefact identification and removes artefactual components before computing connectivity and network metrics. Such automated approaches enhance reproducibility, reduce analysis time and enable the processing of large datasets that would be impractical to analyse manually. While automated classification tools like ICLabel have greatly improved efficiency and objectivity, they are not foolproof. Classification accuracy depends on the quality of the training data and the representativeness of the training set. Therefore, it remains good practice to visually inspect at least a subset of classified components.

2.6 Software tools

The implementation of EEG connectivity analysis requires sophisticated software tools that provide functions for data import, preprocessing, artefact removal, connectivity estimation and visualisation. Two open-source MATLAB-based toolboxes are the widely used platforms for EEG and MEG analysis: EEGLAB and FieldTrip [52], [121]. Both toolboxes offer extensive functionality, active development communities and comprehensive documentation, though they differ in their design philosophies and specific capabilities.

2.6.1 EEGLAB

EEGLAB is an interactive MATLAB toolbox for processing continuous and event-related EEG, MEG and other electrophysiological data, providing a comprehensive group of tools for data import, preprocessing, ICA decomposition, time-frequency analysis and visualisation [52]. Developed by the Swartz Center for Computational Neuroscience at UC San Diego, EEGLAB has become one of the most widely used platforms for EEG analysis, with thousands of users worldwide and an extensive system of plugins that extend its core functionality [122].

EEGLAB's design philosophy emphasises user-friendliness and flexibility, providing both a graphical user interface (GUI) for interactive analysis and a scripting interface for automated batch processing [52]. The GUI allows users to explore their data, test different analysis parameters and visualise results without writing code, making EEGLAB accessible to users with limited programming experience. At the same time, all GUI operations can be performed via command-line functions, making it possible to build reproducible analysis scripts and automated pipelines for processing large datasets. Figure 13 illustrates the EEGLAB's GUI overview window and its plotting options, while Figure 14 provides an example of a corresponding analysis script for automated preprocessing.

Key features include comprehensive preprocessing functions (filtering, re-referencing, epoch extraction, baseline correction), ICA decomposition using multiple algorithms (Infomax, FastICA, JADE), automated artefact detection and removal including ICLabel for component classification [54], time-frequency analysis (using FFT, wavelets and Hilbert transform) and extensive visualisation tools [52]. EEGLAB also supports the import of data from numerous EEG systems and file formats. For connectivity analysis, EEGLAB supports coherence and phase-synchronisation analyses primarily through its plugin system (e.g. SIFT [122], FieldTrip), while basic spectral measures are available in the core toolbox.

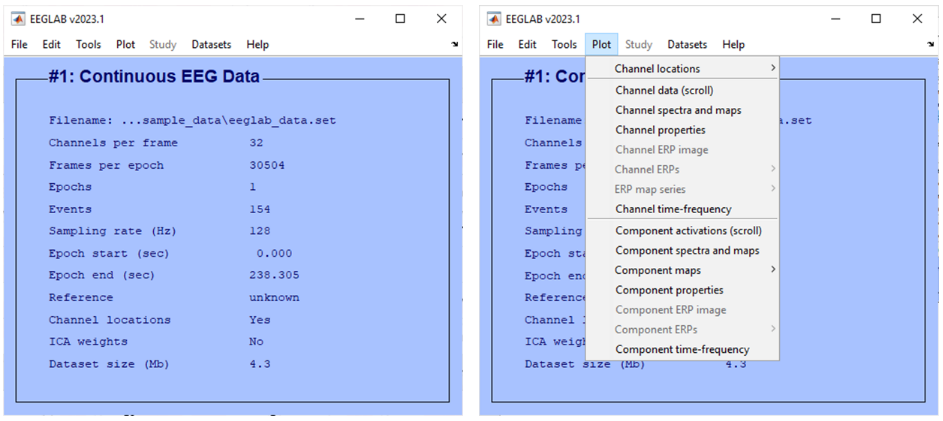

Figure 13. EEGLAB graphical user interface (GUI) showing the dataset overview window and the available plotting options for channel- and component-level visualisation. The interface provides access to data inspection, spectral analysis, time-frequency plots and ICA-related visualisations.

```
% open EEGLAB
[ALLEEG EEG CURRENTSET ALLCOM] = eeglab('nogui');

input_path = './input/';
output_path = './output/';

% load EEG set file
EEG = pop_loadset('filename',input_file,'filepath',input_path);

% High-pass filter at 1 Hz
EEG = pop_eegfiltnew(EEG, 'locutoff',1);

% Low-pass filter at 45 Hz
EEG = pop_eegfiltnew(EEG, 'hicutoff',45);

% run ICA
EEG = pop_runica(EEG, 'icatype', 'runica', 'extended',1,'interrupt','off');

% do ICLabel
EEG = pop_iclabel(EEG, 'default');

% remove eye, muscle and channel noise artifacts based on thresholds
BrainTh = NaN;
MuscleTh = 0.8;
EyeTh = 0.9;
HeartTh = 0.9;
LineNoiseTh = 0.9;
ChannelNoiseTh = 0.8;
OtherTh = NaN;
EEG_1 = pop_icflag(EEG, [BrainTh BrainTh;MuscleTh 1;EyeTh 1;HeartTh 1;LineNoiseTh 1;ChannelNoiseTh 1;OtherTh OtherTh]);

% epoching uncleaned set
set_file = [input_filename '_epochs'];
EEG_2 = pop_epoch( EEG_1, {  '53247'  }, [-2  11], 'newname', set_file, 'epochinfo', 'yes');

% save uncleaned file
output_file = fullfile(output_path, [set_file '.set']);
[ALLEEG EEG CURRENTSET] = pop_newset(ALLEEG, EEG_2, 2,'setname', set_file,'savenew', output_file,'gui','off');
```

Figure 14. Example MATLAB analysis script demonstrating a typical EEGLAB preprocessing workflow, including filtering, ICA decomposition, automated component classification using ICLabel and epoch extraction.

2.6.2 FieldTrip

FieldTrip is a MATLAB toolbox for advanced analysis of MEG, EEG and invasive electrophysiological data, developed at the Donders Institute for Brain, Cognition and Behaviour in the Netherlands [121]. While EEGLAB emphasises user-friendliness and interactive analysis, FieldTrip is designed for flexibility and methodological accuracy, providing a set of functions for analyses while requiring more programming expertise from users.

FieldTrip's design philosophy centres on integrated functions that can be combined in flexible analysis pipelines, with each function performing a specific operation (e.g. filtering, artefact rejection, time-frequency analysis, source reconstruction, connectivity estimation) and passing standardised data structures between functions [121]. This integrated approach provides maximum flexibility for implementing custom analysis workflows but requires users to have a good understanding of the analysis steps and their parameters. Figure 15 provides an example FieldTrip analysis script, showing the pipeline used for preprocessing and ERP computation. Key strengths include extensive source reconstruction capabilities (MNE, beamformers, DIPFIT), advanced connectivity methods (coherence, Granger causality, phase synchronisation, directed connectivity), sophisticated statistical testing using cluster-based permutation tests [123] and comprehensive time-frequency analysis (wavelets, multitapers, Hilbert transform).

For connectivity analysis, FieldTrip provides a unified framework through its *ft_connectivityanalysis* function, which computes a wide range of connectivity metrics (coherence, PLV, PLI, wPLI, Granger causality, partial directed coherence and many others) [121]. This function can operate on sensor-level data, source-reconstructed data or any other time series, making it highly versatile. FieldTrip also provides functions for computing graph theory metrics and for visualising connectivity networks. In practice, many researchers use both EEGLAB and FieldTrip, leveraging the strengths of each toolbox for different aspects of their analyses [86]. For example, EEGLAB might be used for initial preprocessing and ICA decomposition (taking advantage of its GUI and ICLabel integration), while FieldTrip might be used for advanced connectivity analysis and source reconstruction. The two toolboxes can work together through data conversion functions (e.g. *eeglab2fieldtrip* and *fieldtrip2eeglab*).

```
% Add FieldTrip to MATLAB path and initialize defaults
ft_defaults;

input_path = './input/';
latency_window = [-1 10];     % Time window for trial selection
erp = cell(1,10);              % Preallocate ERP cell array

%  SUBJECT-LEVEL PREPROCESSING AND ERP COMPUTATION
for i = 1:10

    % Load EEGLAB dataset
    EEG = pop_loadset('filename', input_file{i}, 'filepath', input_path);

    % Convert EEGLAB structure to FieldTrip format
    data = eeglab2fieldtrip(EEG, 'raw');

    % Baseline correction
    cfg = [];
    cfg.demean = 'yes';
    cfg.baselinewindow = [-0.5 0];
    data = ft_preprocessing(cfg, data);

    % Select latency window
    cfg = [];
    cfg.latency = latency_window;
    data_latency = ft_selectdata(cfg, data);

    % Compute ERP for this subject
    cfg = [];
    cfg.channel = 'all';
    erp{i} = ft_timelockanalysis(cfg, data_latency);
end

%  GRAND AVERAGE ERP ACROSS SUBJECTS
cfg = [];
cfg.latency = [-1 1];
cfg.layout  = 'l28biosemi.lay';
ga_erp = ft_timelockgrandaverage(cfg, erp{:});
```

Figure 15. Example FieldTrip preprocessing and ERP analysis script. The script demonstrates the pipeline structure characteristic of FieldTrip, including data import, conversion from EEGLAB format, baseline correction, latency selection and computation of subject-level and grand-average ERPs.

2.7 Conclusion

This chapter established the theoretical foundations for analysing EEG signals, emphasising that scalp-recorded activity reflects the coordinated dynamics of distributed neural populations. It also highlighted that understanding cognition requires methods capable of capturing how these interactions evolve over time, while accounting for the spatial mixing introduced by volume conduction.

What remains unknown is how these principles manifest during real cognitive experiences. Aesthetic perception is a rich and temporally extended process that engages multiple stages of visual and evaluative processing. The theoretical considerations outlined here imply that such experiences should be reflected in time-resolved patterns of large-scale neural interaction, yet these dynamics have rarely been examined directly. Building on this theoretical foundation, Chapter 3 applies these concepts to empirical data, investigating how functional connectivity unfolds during the perception of abstract and figurative paintings. This provides the first step toward linking the theoretical mechanisms described in this chapter with the neural processes that support naturalistic aesthetic experience.

3. SENSOR-SPACE CONNECTIVITY DURING AESTHETIC PERCEPTION

3.1 Introduction and rationale

3.1.1 Context, theoretical background and rationale

The ability to create and appreciate art is one of humanity's most unique cognitive abilities. Archaeological evidence traces artistic expression back tens of thousands of years, revealing that the drive to create visual representations has been with us since the earliest days [124]. Among all the types of art, visual art occupies a particularly prominent place in human culture. Remarkably, the human brain can rapidly recognise and differentiate between different artistic styles, often within a fraction of a second of viewing an artwork [5]. Understanding how the brain achieves this and more broadly, how neural processes support aesthetic perception and appreciation, represents a central goal of neuroaesthetics, an interdisciplinary field that bridges neuroscience, psychology and art history [2], [3].

A foundational theme in visual art is the interplay between figurative (representational) and abstract (non-representational) styles. Figurative artworks depict recognisable objects, scenes or figures from the real world, relying on representational content that can be readily identified by viewers. In contrast, abstract artworks dismiss representational content, instead using colours, forms, lines and textures to create compositions that do not depict identifiable objects [125], [126]. This stylistic difference is not merely a matter of artistic details but reflects fundamentally different approaches to visual communication and may engage distinct perceptual and cognitive processes for the viewer. When we look at a figurative painting, our brain can draw on its extensive experience with recognising objects and scenes. When viewing abstract art, our brain must process the visual information without the assistance of familiar content, thus, potentially requiring different cognitive strategies.

Theoretical models of aesthetic appreciation propose that the processing of visual art unfolds through multiple stages as introduced in Chapter 1, from early perceptual analysis to higher-level cognitive and affective evaluation [5], [6]. One influential framework is the model of aesthetic appreciation and aesthetic judgements proposed by Leder et. al (Figure 16). This model suggests that when we view an artwork, our brain first performs perceptual analysis, extracting visual features such as complexity, contrast, symmetry and colour relationships. Processing then proceeds through implicit memory integration (where the artwork is compared with stored visual experiences) and explicit classification (including recognition of artistic style and interpretation of content). Finally, the viewer engages in cognitive mastering (making sense of the artwork) and evaluative judgement (forming aesthetic preferences) [5], [6].

Neuroimaging research using fMRI has provided supporting evidence for this multi-stage architecture. Studies have associated occipital and parietal brain regions (the areas involved in visual processing) in the early perceptual analysis of artworks. Frontal and limbic regions, which support higher-order thinking and emotion, become engaged during evaluative and affective responses to art [2], [7], [8]. Critically, Leder's model proposes that different types of artworks may engage these processing stages to different degrees. Abstract artworks, lacking recognisable content, may place greater demands on perceptual analysis and cognitive mastering, whereas figurative artworks may facilitate explicit classification and semantic interpretation [5].

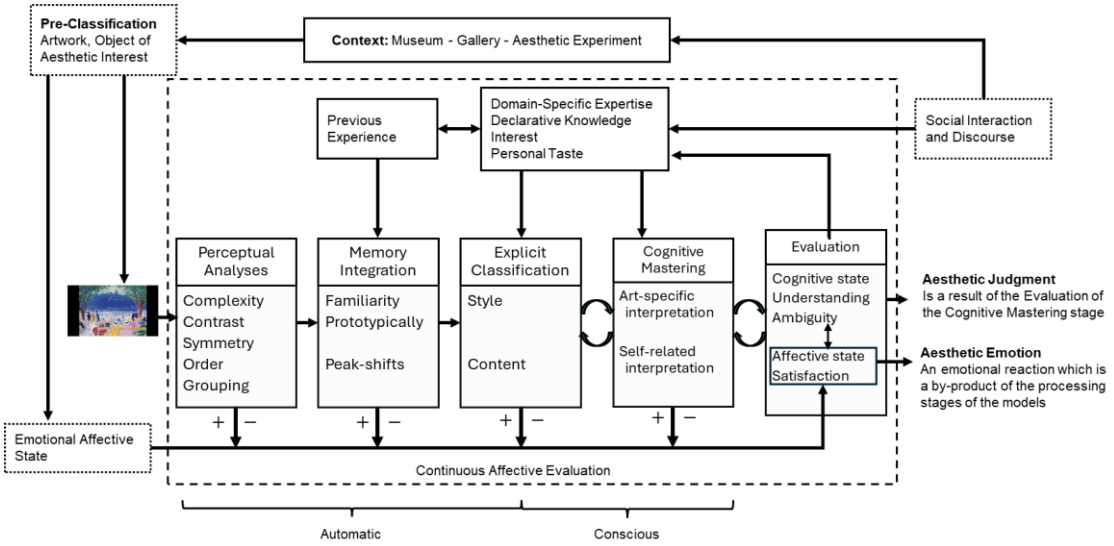

Figure 16. Model of aesthetic appreciation and aesthetic judgement, adapted from [6]. The model proposes that aesthetic processing unfolds through multiple stages, from early perceptual analysis through cognitive mastering and evaluative judgement, with different artwork types potentially engaging these stages to different degrees.

Research-based evidence supports the idea that abstract and figurative artworks engage partially separate neural processes [127], [128]. Behavioural studies have demonstrated that viewers process these two styles differently, with abstract art often causing stronger perceptual engagement and figurative art facilitating semantic interpretation [125], [129]. Neuroimaging studies using fMRI have revealed that viewing abstract versus representational art activates partially overlapping but distinct brain networks. Abstract art tends to engage visual processing regions more strongly, consistent with the idea that viewers must work harder to extract meaning from non-representational visual information and figurative art recruits regions involved in object recognition and semantic processing, reflecting the activation of stored knowledge about depicted objects and scenes [43], [130].

While fMRI has been invaluable for mapping the spatial organisation of aesthetic processing, its poor temporal resolution cannot capture the rapid, dynamic neural processes that unfold during the first few hundred milliseconds of visual perception. EEG, by contrast, offers corresponding advantages, providing millisecond-scale temporal resolution that can track the time course of aesthetic processing from early perceptual stages through later cognitive evaluation and inter-regional communication during extended and naturalistic art viewing [131]. Previous EEG studies have identified several components associated with aesthetic processing, including early visual components (P1, N1), components sensitive to perceptual features such as symmetry (N300-400) and later components associated with evaluative judgement (late positive potential, LPP) [42], [131].

Most early EEG research on aesthetic perception focused on ERPs, which is the averaged brain responses that are phase-locked to stimulus onset. ERPs provide valuable information about the timing of neural processes, but they capture only part of the picture. ERPs reflect synchronised, phase-locked activity but miss induced oscillatory activity that occurs at variable phases across trials. More fundamentally, ERPs tell us about activity at individual brain locations but do not reveal how different brain regions communicate and coordinate their activity. Recent advances in EEG analysis have enabled investigation of neural oscillations and functional connectivity (the dynamic patterns of coordinated activity across distributed brain regions). As discussed in Chapter 2, neural oscillations in different frequency bands (delta, theta, alpha, beta, gamma) play distinct functional roles in perception, attention and memory [9], [12]. Functional connectivity analysis, which quantifies the statistical dependencies between signals recorded from different brain regions, can reveal how these regions communicate and coordinate their activity during cognitive tasks [12], [59]. Rather than asking

"which brain regions are active?", connectivity analysis asks, "how do active brain regions interact?". This network-level perspective is particularly important for understanding complex cognitive processes like aesthetic perception, which likely involve coordinated activity across multiple brain systems.

The application of functional connectivity analysis to aesthetic perception is especially promising for several reasons. First, it can reveal not only which brain regions are active during art viewing, but also how these regions interact dynamically to support the perceptual and cognitive processes involved in aesthetic experience [38]. Second, more recent perspectives in neuroaesthetics emphasise that aesthetic experience is not only spatially distributed but also dynamically unfolds over time through interactions among large-scale neural networks. Understanding aesthetic perception therefore requires moving beyond identifying isolated active regions toward investigating how neural systems communicate and coordinate. Previous studies have demonstrated that aesthetic appreciation involves coordinated activity across distributed networks spanning visual, parietal and frontal regions [38], [132]. However, most connectivity studies have focused on aesthetic judgement (beautiful vs. not beautiful) rather than on the processing of different artistic styles.

A critical methodological consideration for sensor-level EEG connectivity analysis is the problem of volume conduction. As established in Chapter 2, volume conduction produces instantaneous, zero-lag correlations across electrodes due to passive field spread rather than genuine neural interactions [28], [33]. This issue is addressed in the connectivity analysis described in Section 3.4.

3.1.2 Research gap

Despite growing interest in the neural basis of aesthetic perception, several important gaps remain in our understanding of how the brain processes different artistic styles.

First, while previous studies have identified brain regions involved in viewing abstract versus figurative art using fMRI [43], [130], the temporal dynamics of style-related processing remain poorly understood. The rapid recognition of artistic style that can occur within a few hundred milliseconds of viewing an artwork suggests that style-related processing begins at early perceptual stages, but the time course of this processing has not been systematically characterised.

Second, most EEG studies of aesthetic perception have focused on averaged ERPs [39], [41], [133], [134], [135], which capture only phase-locked responses and may miss important induced oscillatory activity that is time-locked but not phase-locked to stimulus onset [19]. As discussed in Chapter 2 (Section 2.1.3), ERPs provide limited information about the dynamic, oscillatory coordination of neural populations that may be critical for aesthetic processing. Oscillatory activity in different frequency bands reflects different aspects of neural processing [9]. Moreover, ERPs tell us about activity at individual locations but not about how brain regions communicate [102]. Investigating oscillatory power and functional connectivity in different frequency bands can provide more insights into the neural mechanisms supporting style perception [98]. Do abstract and figurative artworks engage different oscillatory rhythms? Do they evoke different patterns of inter-regional communication? These questions require going beyond traditional ERP analysis.

Third, while some studies have investigated functional connectivity during aesthetic judgement (beautiful vs. not beautiful) [38], [65], few have investigated whether different artistic styles evoke distinct patterns of functional connectivity. If abstract and figurative artworks engage different perceptual and cognitive processes, as suggested by theoretical models [5] and behavioural evidence [125], these differences should be reflected in distinct patterns of inter-regional communication. Characterising these connectivity differences could provide important insights into the neural mechanisms underlying style-specific processing.

Fourth, most connectivity studies have examined relatively short time windows or have averaged connectivity across entire viewing periods [62], potentially obscuring rapid changes in network organisation that occur as processing unfolds. Aesthetic processing is thought to progress through multiple stages from early perceptual analysis through later cognitive evaluation and emotional response [5]. If different processing stages engage different neural

networks, connectivity patterns should change dynamically over time [62], [63]. Examining connectivity at multiple discrete time points can reveal how functional networks reconfigure as aesthetic processing unfolds.

Finally, as emphasised in Chapter 2, the choice of connectivity metric is critical for obtaining valid estimates of functional connectivity from sensor-level EEG data. Many previous studies have used metrics such as coherence or PLV that are highly sensitive to volume conduction [33], [34], [106], potentially leading to spurious connectivity estimates. The application of volume conduction-insensitive metrics such as dwPLI [66] to aesthetic perception has been limited, representing a methodological gap that needs to be addressed.

3.1.3 Objectives of present chapter

Aesthetic perception unfolds though multiple neural stages, beginning with early sensory responses, progressing through oscillatory dynamics and ending with coordinated network activity. To reflect this progression, this chapter is organised to first examine the stimulus-evoked responses (ERPs), then characterise the time-dependent oscillatory power changes and finally investigate the temporal dynamics of functional connectivity. This structure creates a clear narrative from basic neural activation to network-level organisation.

The primary objective of this chapter is to investigate how the brain processes abstract and figurative paintings during the naturalistic free-viewing condition using high-density EEG. The specific objectives are as follows:

1. To identify the key early neural activations associated with the perception of abstract and figurative paintings and determine whether they evoke distinct stimulus evoked responses.
2. To characterise how oscillatory power evolves over time during aesthetic perception and to determine whether different artistic styles modulate frequency-specific patterns of synchronisation and desynchronisation.
3. To determine whether abstract and figurative painting evoke significantly different patterns of functional connectivity and if so, to characterise the spatial distribution, frequency-specific and temporal dynamics of these differences.
4. To explore the network topology underlying aesthetic perception by identifying regions that serve as important hubs and assessing how network organisation differs between artistic styles.

This study utilises sensor-level connectivity analysis using dwPLI, a method that addresses volume conduction concerns while remaining computationally flexible and not requiring individual anatomical MRI scans (Chapter 2, Section 2.4.3). While sensor-level analysis has inherent spatial limitations due to source mixing (Chapter 2, 2.3.3), the combination of a volume conduction-insensitive metric and high-density recording (128 channels) provides adequate spatial sampling for characterising large-scale network dynamics.

The findings from this study establish what can be achieved with methodologically rigorous sensor-space approaches. While it is not possible to pinpoint connectivity to specific anatomical locations, which is a limitation inherent to sensor-level analysis, the temporal and frequency-specific dynamics of functional networks supporting aesthetic perception can be characterised. These findings provide a foundation for future investigations that may employ complementary spatial filtering methods, such as the ICA approach validated in Chapter 4, to further improve spatial resolution. By addressing the identified research gaps with appropriate methodological accuracy, this study aims to advance our understanding of the neural mechanisms supporting aesthetic style perception and to demonstrate the value of time-resolved, frequency-specific connectivity analysis for characterising the dynamic brain networks underlying aesthetic experience.

3.2 Experiment details

This section describes the experimental design, participants, stimuli, procedures and data acquisition methods used to investigate functional connectivity during aesthetic perception.

3.2.1 Participants

A total of 29 university students (15 female; mean age = 23.14 ± SD = 3.81 years) volunteered to participate in this study. All participants were right-handed, had normal or corrected-to-normal vision and reported no history of neurological or psychiatric disorders. The participant's lateral dominance was determined using the Edinburgh Handedness Inventory [136] and to exclude potential confounding handedness effects on connectivity, only right-handed participants were selected for the study.

A customised version of the Art Expertise Assessment [137] was used to evaluate the participant's level of experience and knowledge in the field of visual arts. On the art expertise scale, participants scored an average of 4.66 (SD = 4.30) out of a maximum possible score of 45, indicating minimal exposure to art and art-related expertise. This low level of art expertise was intentional. Non-expert viewers were deliberately recruited because the study aimed to investigate spontaneous perceptual processing of artistic styles rather than expert aesthetic judgement. Art experts might engage different cognitive strategies when viewing artworks, drawing on extensive training and knowledge that could alter connectivity patterns. By studying non-expert viewers, the more universal perceptual processes that most people engage when encountering visual art can be captured. This approach is consistent with previous neuroaesthetics research examining style perception in non-expert viewers [125], [138].

Prior to the EEG experiment, each participant was asked to complete a Positive and Negative Affect Schedule (PANAS) [139] questionnaire to measure the participant's actual emotional state and verify that they were able to perform the given experiment. Participants were also briefed about the nature of the study, the risks and benefits and their right to withdraw at any time. Written informed consent was obtained from every participant confirming their participation and permission for the data to be used for research and publication purposes. The study was approved by the local ethics committee of the university in accordance with the Declaration of Helsinki. All documents related to the data collection are provided in Appendix A-Appendix E.

3.2.2 Stimuli

The stimuli consisted of 80 digital colour images of paintings selected from the less familiar works of famous Hungarian artists arranged into two experimental conditions: 40 abstract and 40 figurative paintings. The paintings collected for the figurative condition belong to the representational art category. The paintings show easily recognisable real-world figurative objects, such as people (faces, portrait and groups), animals, still life and various scenes (landscapes, townscapes, etc.). The abstract condition group consists of non-representational (showing non-recognisable shapes, colours or forms) and highly abstract figurative paintings. For each condition, paintings were selected carefully in terms of content, complexity and visual features to create a balanced, non-biased set of stimuli. Each painting was viewed once by each participant. The full collection of the paintings used in the experiment is provided in Figure A-1 and A-2 in Appendix F.

All images were presented in full colour on a monitor (resolution 1920 × 1080 pixels, 60 Hz refresh rate). Images were sized to fit within the display while maintaining their original aspect ratios. The 80 paintings were presented in fixed pseudo-randomised order across participants to counterbalance sequence effects.

3.2.3 Experimental procedure

The study was performed in the Bioelectric Brain Imaging Laboratory of the Faculty of Information Technology at the University of Pannonia. Each trial began with a 1 s numeric cue (1-80) followed by an 8 s viewing period during which participants freely observed a single painting. The cue was introduced to maintain subjects' attention and help them focus on the centre of the screen. After each painting, a 4 s blank black screen was shown prompting the

subject to response (“Like” or “Dislike”) via button press. Figure 17 illustrated the experimental protocol. Participants were instructed to minimise head movements and blinking during stimulus presentation while maintaining natural free viewing behaviour. The measurements took place in a single session for each subject without breaks. Total experiment duration was approximately 18 minutes. Importantly, participants were not explicitly informed about the difference between abstract and figurative conditions, nor were they asked to categorise or judge the paintings according to style. This approach was intended to investigate spontaneous, implicit processing of artistic style rather than explicit categorisation processes.

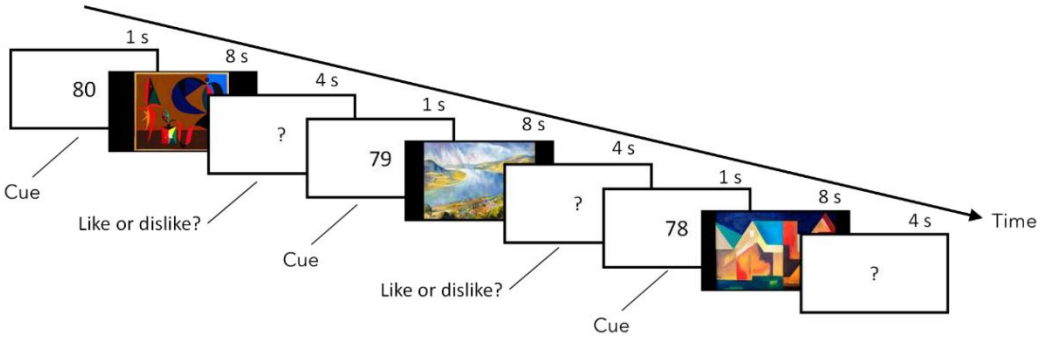

Figure 17. Experimental protocol showing the sequence of events in each trial: numeric cue (1 second), painting presentation (8 seconds) and response period (4 seconds).

Stimulus presentation and behavioural recording were implemented using Psychtoolbox-3 [18] (Psychophysics Toolbox Version 3) and synchronised with a special-purpose trigger unit [19] was used to generate event triggers for the EEG device. Stimulus onset events were created by displaying a 1 × 1 cm white square on the right edge of the display simultaneously with the painting, which was then registered by a display-mounted light sensor. The light sensor and the mouse micro-switches were connected to the trigger unit to generate hardware trigger signals for the stimulus and response, respectively, that were then sent to the EEG device for digitisation.

3.2.4 Recording setup

EEG activity was recorded using a 128-channel BioSemi ActiveTwo system (BioSemi B.V., Amsterdam, Netherlands) with Ag/AgCl active electrodes arranged according to the BioSemi equiradial ‘ABC’ layout (Figure 18) [140]. Conductive saline gel (Signa) ensured stable electrical contact between the electrodes and the scalp. DC electrode offset values were maintained below 40 μV throughout the session. The analog EEG signal was low-pass filtered at 410 Hz (-3 dB) and digitised at a sampling rate of 2048 Hz. Data were stored in BDF format for offline processing.

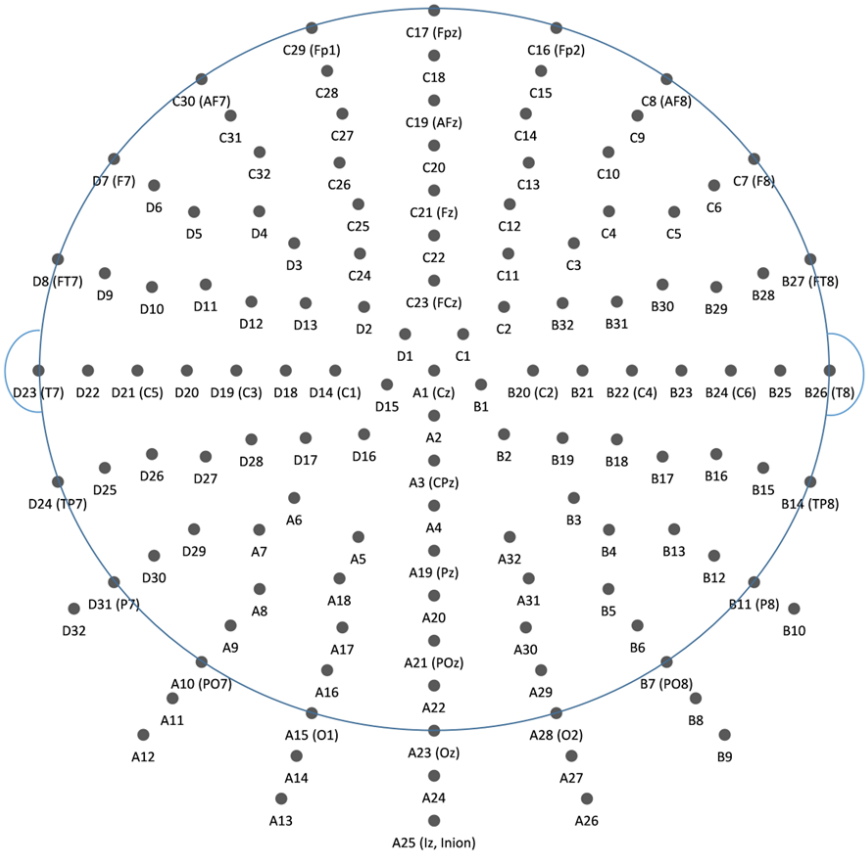

Figure 18. Biosemi equiradial 'ABC' electrode layout showing the positions of all 128 electrodes. This high-density configuration provides comprehensive scalp coverage, allowing detailed spatial characterisation.

3.2.5 Preprocessing steps

The EEG data processing was performed using the EEGLAB Toolbox [52] in three key steps: (i) pre-processing, (ii) removing unwanted noise and artefacts and (iii) segmenting the data into epochs. The raw EEG signals were filtered with 1 Hz and 40 Hz cut-off frequency high- and low-pass zero-phase finite-impulse-response (FIR) filters (EEGLAB *eegfiltnew* filter) to remove slow drifts and high-frequency noise, respectively. These cut-off values are widely recommended for cognitive EEG research because they preserve the frequency range of interest while minimising artefacts [77]. Next, the data were downsampled from 2048 Hz to a 512 Hz sampling rate to reduce computational load while maintaining sufficient temporal resolution for ICA and time-frequency decomposition [44].

The filtered EEG datasets were inspected for bad channels (having extremely high or low amplitudes or excessive noise), which were then interpolated in EEGLAB using spherical spline interpolation (16 subjects, average number of bad channels: 3), a method shown to preserve spatial topography and avoid biasing ICA decomposition [47], [52]. After interpolation, the dataset was re-referenced to the average reference, a standard approach that improves spatial neutrality and improves ICA performance in high-density EEG recordings [29]. ICA [44] was then performed to separate eye, muscle and channel noise artefacts from the neural signals (further details can be found in Chapter 2, Section 2.5). The resulting independent components (ICs) were labelled as potential artefacts using the ICLabel EEGLAB plugin [54]. Eye blinks, muscle and channel noise artefact components with a confidence level above 80% as recommended [54] were removed from the component set to reconstruct the artefact-free signals. Datasets that still showing artefacts after cleaning were further inspected and the remaining artefactual ICs with <80% confidence level were removed manually before epoching. Figure 19 illustrates the complete preprocessing pipeline.

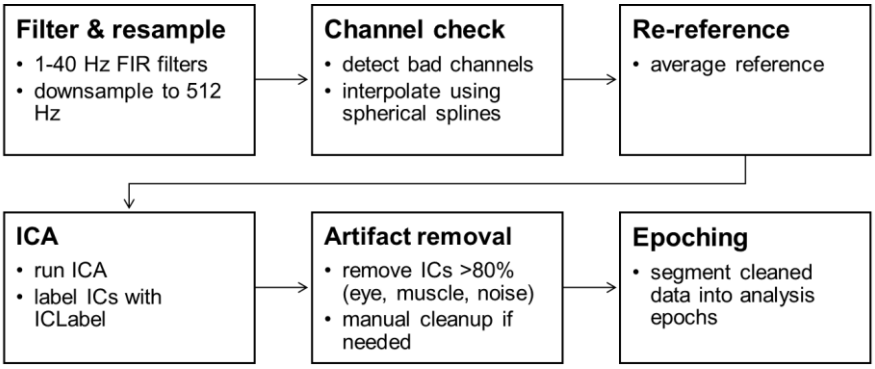

Figure 19. EEG preprocessing pipeline.

3.3 Preliminary analyses

Preliminary EEG analyses were conducted to characterise neural responses associated with the perception of abstract and figurative paintings. These analyses serve two purposes. First, they establish that our experimental manipulation (abstract versus figurative paintings) produces measurable differences in brain activity. Second, they inform the selection of time windows and frequency bands for subsequent connectivity analysis.

I performed two complementary analyses: ERP and ERSP analysis. ERPs capture phase-locked responses, the neural activity that occurs at consistent timing relative to stimulus onset across trials. ERSPs were computed using time-frequency analysis, which quantifies changes in spectral power over time relative to a baseline. All EEG analyses were performed using custom MATLAB scripts [141] in combination with the EEGLAB [52] and FieldTrip [121] toolboxes.

3.3.1 Event-Related Potentials

ERPs reveal the time course of neural responses by averaging brain signals across many trials, time-locked to stimulus onset. This averaging cancels out activity that varies randomly across trials while preserving activity that consistently occurs at specific times after the stimulus.

After pre-processing, the EEG data were segmented to stimulus-locked 2 s epochs (with -1 s pre-stimulus and 1 s post-stimulus intervals). Following the baseline (-500 to 0 ms) correction, the trials were labelled as ‘figurative’ or ‘abstract’ depending on the style of the stimulus, creating datasets for the two conditions. After epoch averaging, the ERP waveforms (Figure 3.4) showed peaks at approximately 120 ms, 250 ms and 450 ms. A well-known effect in event-related potential research is that temporal precision decreases as the signal extends further from the stimulus. The paintings were presented for 8 s but, as shown in Figure 20, the ERP waveform after 1 s post-stimulus is hardly distinguishable from the baseline period. After approximately one second, the probability of phase locking and synchronisation across trials sharply decreases, resulting in strong signal cancelation and a low signal-to-noise ratio after epoch averaging. This temporal decay motivated our decision to focus connectivity analysis on the 0-1 second post-stimulus window, where phase-locked activity is strongest and signal-to-noise ratio is highest.

Figure 21 illustrates the spatial distribution of the ERPs from 0 to 1100 ms. These maps show that the potential distribution is dominated by occipital area activations, with hardly any detectable activations in other areas. This spatial pattern has important implications. The strong occipital activity confirms that participants were visually engaged with the paintings. However, the limited activity in other regions does not necessarily mean those areas were not involved in aesthetic processing. Rather, it likely reflects a limitation of ERP analysis: ERPs capture only phase-locked activity, missing induced oscillatory activity that may be critical for higher-level processing but occurs at variable phases across trials.

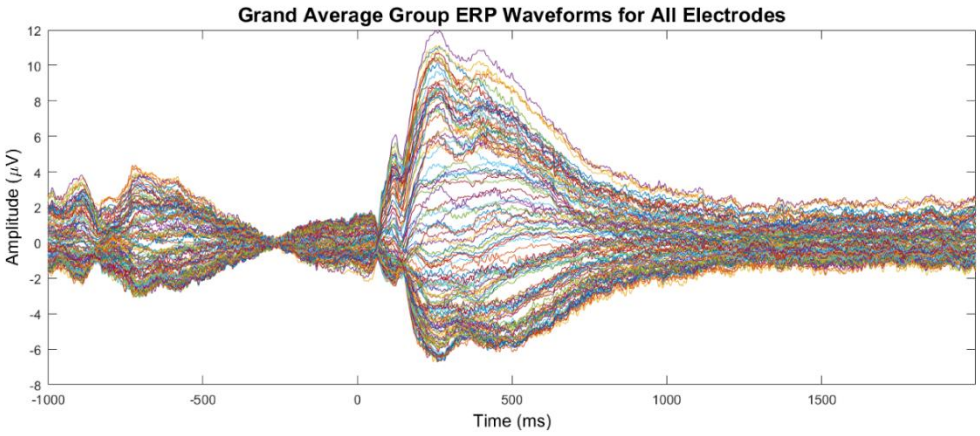

Figure 20. Grand average group ERP waveforms of all electrodes in the figurative condition. Time 0 represents the presentation of the stimulus that lasts 8 s. Note the amplitude peaks around 120, 250 and 450 ms and the drop at 900 ms onwards. Different waveform colours represent different EEG channels.

The ERP analyses revealed condition-related activity but also highlighted limitations. The strong posterior focus and relative lack of detectable activity in other regions suggest that ERPs alone provide an incomplete picture of aesthetic processing. Theoretical models propose that aesthetic appreciation involves distributed processing across visual, parietal and frontal regions. Yet ERPs show primarily occipital activity. This discrepancy likely reflects the fact that ERPs capture only phase-locked responses. Higher-level cognitive processes involved in aesthetic appreciation such as attention allocation, memory retrieval, semantic interpretation and evaluative judgement may involve neural activity that is time-locked to stimulus onset but not phase-locked. This induced activity would be invisible to ERP analysis but could be revealed through time-frequency (ERSP) and connectivity analyses. Moreover, ERPs tell us about activity at individual locations but not about how different brain regions communicate. Aesthetic processing almost certainly involves coordinated activity across distributed regions. To investigate this inter-regional coordination, connectivity analysis is needed, as it investigates relationships between signals from different locations. These considerations motivated the primary analysis approach: functional connectivity analysis, described in Section 3.4.

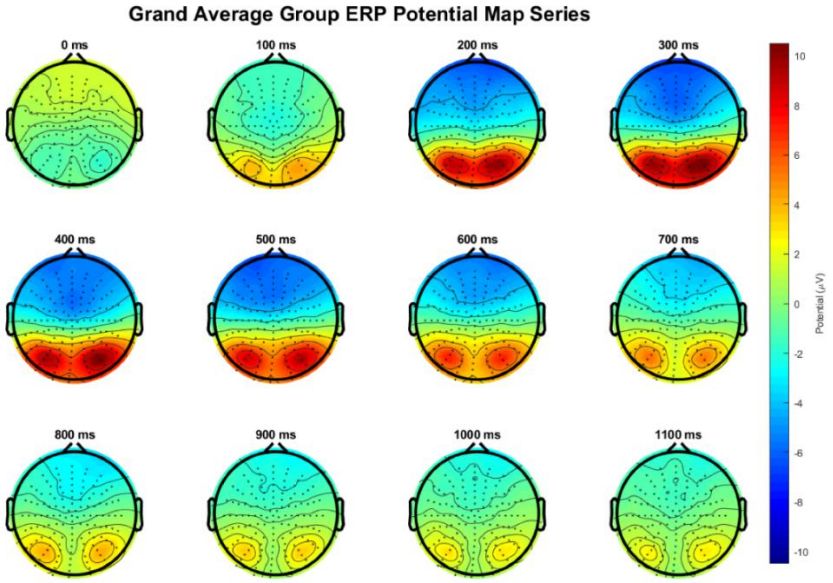

Figure 21. Grand average group ERP map series from 0 to 1100 ms post-stimulus in the figurative condition. Values are in μVolts. Note the dominance of occipital areas throughout the time interval with hardly any detectable activity in other areas.

3.3.2 Event-Related Spectral Perturbation

While ERPs capture phase-locked responses, they do not reflect the induced oscillatory activity that varies in phase across trials [19]. To characterise these time-dependent changes in oscillatory power, ERSP analysis was performed [142]. ERSP provides a time-frequency representation of how spectral power changes in relative to a pre-stimulus baseline [143], allowing both early and sustained neural processes to be examined. This is computed at the single-subject level for each electrode and condition, producing ERSP matrices based on:

$$ERSP(t,f)_{dB} = 10\log_{10}\left(\frac{P(t,f)}{P_{baseline}(f)}\right) \quad (26)$$

where $P(t,f)$ represents the spectral power at time t and frequency f for the trial-averaged time-frequency decomposition. $P_{baseline}(f)$ is the mean spectral power at frequency f during the baseline period (-1000 to 0 ms). ERSP values are expressed in decibel (dB) units normalises inter-subject variability and provides a symmetric scale for increases (synchronisation) and decreases (desynchronisation) in power. Positive ERSP values indicate event-related synchronisation (ERS), reflecting increased oscillatory engagement, whereas negative values indicated event-related desynchronisation (ERD), typically associated with active information processing or release of inhibition [85]. The ERSP time-frequency plot derived from the fully pre-processed data (Figure 22) shows an early broadband power modulation within the first 500 ms, followed by sustained band-specific modulations extending throughout the viewing period. Early changes likely reflect initial sensory processing, whereas later sustained modulations reflect prolonged attentional and integrative processes during aesthetic perception.

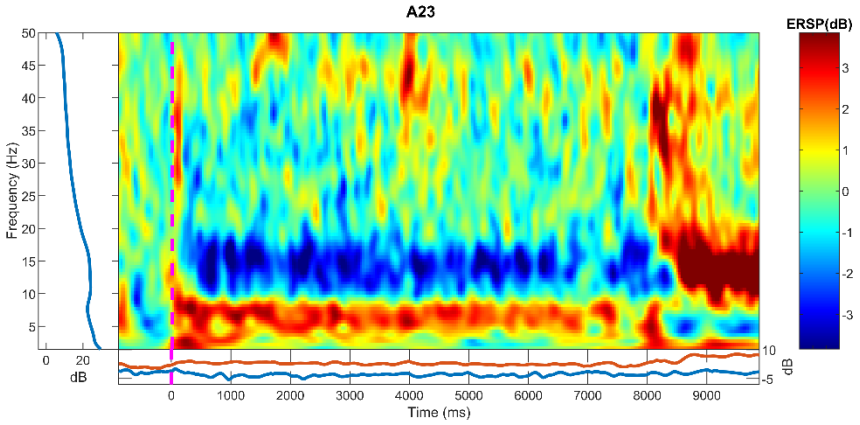

Figure 22. Time-frequency representation (ERSP) for channel A23 from a single participant, covering the full analysis epoch including pre-stimulus baseline, 0-8 s painting viewing period and post-stimulus interval. Spectral power changes are shown relative to stimulus onset at 0 ms. Stimulus-related activity ends at 8s when painting disappears, after which the plot reflects post-stimulus dynamics.

For group-level analysis, these ERSPs were first converted back to absolute power because averaging in dB space is not mathematically appropriate. For each subject, electrode and condition, the ERSP matrix was transformed using

$$P = 10^{\left(\frac{ERSP_{dB}}{10}\right)} \quad (27)$$

and power values were then accumulated across frequency bins corresponding to the oscillatory bands (delta, theta, alpha, beta and gamma). This produced band-limited power time courses for every electrode and condition.

After processing all participants, absolute power values were averaged across subjects for each band, time point and electrode. The resulting group-level averages were converted back to decibel units, producing condition-specific maps of band-limited power. Figure 23 illustrates

this procedure using the alpha band as an example, showing the topographic power distribution for the abstract and figurative conditions. As the two maps show only subtle differences when looked roughly at the scalp level, a condition-difference map (figurative minus abstract) for each frequency band was computed to examine task-related differences. Difference maps were used because absolute power varies across subjects and electrodes. Thus, subtracting conditions isolates task-related effects by removing global power differences and improve sensitivity to subtle condition-specific modulations.

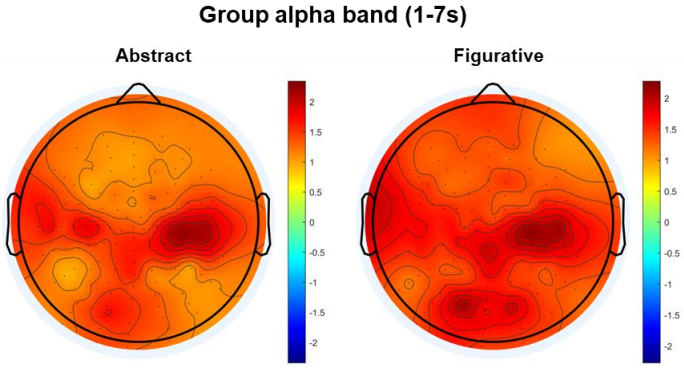

Figure 23. ERSP topographic maps of alpha band activity for the abstract and figurative conditions from 1 to 7 seconds of the painting viewing.

For visualisation, band-limited power was averaged across a post-stimulus window from 1 to 7 seconds and scalp topographies were generated using the 128-channel montage. The oscillatory power was averaged across 1-7 s post-stimulus to capture sustained neural dynamics during prolonged free viewing while excluding the initial transient ERP-dominated response (<1 s). This window reflects ongoing perceptual and cognitive engagement rather than early stimulus-locked responses. Activity after 7 s reflects trial offset and onset of response-related and preparatory processes, rather than ongoing aesthetic processing. Thus, including 7-8 s interval would mix task-related oscillatory activity with end-of-trial and motor-preparatory processes, reducing interpretability. The 1-7 s window therefore isolates stable, task-related oscillatory dynamics. These maps summarise the spatial distribution of oscillatory power differences between conditions for delta, theta, alpha, beta and gamma bands as shown in Figure 24. Because each frequency band showed distinct and sustained task-related modulations, these ERSP results indicate the specific oscillatory ranges in which connectivity differences are most likely to occur.

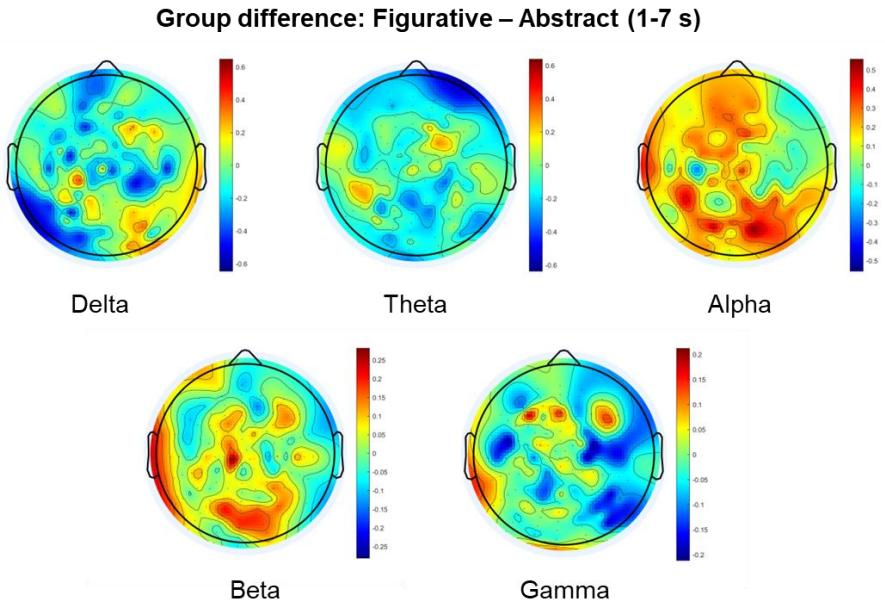

Figure 24. The group difference ERSP topographies illustrating power distribution across five frequency bands: delta, theta, alpha, beta and gamma. Different frequency bands show distinct spatial distributions, reflecting their different functional roles in aesthetic processing.

The time-frequency analysis revealed spatially distributed and sustained oscillatory activity across multiple frequency bands. This finding has important implications: (1) The widespread patterns of oscillatory power changes across different scalp regions suggest that aesthetic processing engages distributed neural systems, not just focal visual area; (2) Different frequency bands show different spatial distributions, suggesting that different oscillatory rhythms support different aspects of aesthetic processing; (3) The sustained nature of oscillatory changes (across the 1-7 second window) indicates that aesthetic processing involves ongoing neural dynamics, not just brief, transient responses.

However, like ERPs, time-frequency analysis has limitations. It tells about oscillatory activity at individual locations but not about how different locations interact. The spatially distributed patterns suggest that different brain regions are engaged, but cannot determine whether and how these regions communicate with each other. To investigate inter-regional communication, how distributed brain regions coordinate their activity during aesthetic perception, functional connectivity analysis is needed. The ERPs and time-frequency results informed the connectivity analysis by: (1) Confirming that all five frequency bands show task-related activity, justifying analysis of connectivity in each band; (2) Revealing the temporal window (0-1 second) where activity is strongest, guiding the selection of time points for connectivity analysis; (3) Showing spatial patterns that suggest distributed processing, motivating a network-level analysis approach. The next section describes functional connectivity analysis, which directly investigates how brain regions interact during aesthetic perception.

3.4 Connectivity analysis

The preliminary analyses revealed spatially distributed and temporally extended neural responses to abstract and figurative paintings. While these analyses demonstrate that aesthetic perception engages widespread brain activity, they cannot reveal how different brain regions communicate and coordinate their activity. This section describes our functional connectivity analysis, which investigates inter-regional communication during aesthetic perception.

Aesthetic experience during prolonged and naturalistic viewing is thought to occur from the integration of perceptual, attentional, memory-related and evaluative processes, which are supported by coordinated activity across distributed neural systems [6], [38]. The spatially distributed patterns observed in our preliminary analyses suggest that multiple brain regions are

engaged during aesthetic perception. However, engagement alone does not tell us how these regions interact. Do they operate independently, each contributing separately to aesthetic processing? Or do they communicate and coordinate, forming functional networks that support integrated aesthetic experience? Functional connectivity analysis addresses these questions by quantifying the statistical dependencies between neural signals recorded from different brain regions. Strong connectivity between two regions suggests they are communicating and coordinating their activity, potentially working together to support specific aspects of aesthetic processing.

The present analysis focuses on sensor-space connectivity which is the connectivity estimated between scalp electrodes rather than between identified neural sources. As discussed in Chapter 2 (Section 2.3.3), sensor-space analysis has inherent limitations due to volume conduction and source mixing.

These limitations can be reduced with the proper choice of connectivity metric (dwPLI, described below) and remaining constraints are acknowledged in interpretation. The methodological implications and interpretational constraints of sensor-space connectivity are discussed in detail in Section 2.3.3. These limitations provide critical motivation for Chapter 4 which focuses on validating ICA as a spatial filtering method that could, in future research, be integrated with connectivity analysis to improve spatial information. The spatially distributed and temporally extended patterns observed in the preliminary analyses therefore suggest that a network-level approach is necessary to fully characterise the neural mechanisms underlying aesthetic perception.

3.4.1 Connectivity metric calculation

A fundamental challenge for EEG connectivity analysis is volume conduction, which causes electrical activity from a single source to spread instantaneously through the head and produce zero-lag correlations across electrodes that do not reflect genuine neural communication. Traditional phase-based connectivity measures, such as the PLV and coherence, are highly sensitive to zero-lag correlations and therefore vulnerable to spurious connectivity estimates [23], [24].

To mitigate this issue, functional connectivity in the present study was estimated using the dwPLI, originally proposed by Vinck et al. [66]. More details on phase-based and amplitude-based connectivity measures, including PLV, PLI and their respective sensitivities to volume conduction, is provided in Chapter 2 (Section 2.4). Here, the focus is limited to the rationale for selecting dwPLI as the most appropriate measure for the present sensor-space analysis. The dwPLI improves upon earlier phase-based measures through three key features:

1. dwPLI focuses on phase differences that deviate from zero (and 180 degrees), effectively ignoring instantaneous correlations that likely arise from volume conduction. Only non-zero phase lags, which suggest genuine neural communication with conduction delays contribute to the connectivity estimate.
2. Not all non-zero phase differences are equally reliable. dwPLI weights each phase difference by its magnitude (how far it is from zero or 180 degrees), giving more weight to consistent, non-zero phase relationships and less weight to small, potentially noisy phase differences. This weighting reduces sensitivity to noise.
3. Earlier versions of the phase lag index could show upward bias (overestimation) due to finite sample sizes. The dwPLI applies a mathematical correction that removes this bias, providing more accurate connectivity estimates.

These properties make dwPLI well-suited for sensor-space EEG connectivity analysis. By explicitly discounting zero-lag interactions, dwPLI substantially reduces spurious connectivity from volume conduction. The weighting and debiasing features further enhance the reliability of connectivity estimates.

While dwPLI substantially reduces volume conduction artefacts, it cannot completely eliminate all effects of source mixing inherent to sensor-space recordings. Some residual volume conduction effects may remain, particularly when (1) sources have asymmetric

configurations that produce small non-zero phase lags; (2) multiple sources project to the same electrodes with different phase relationships or (3) genuine neural synchronisation occurs at or near zero lag. Additionally, by discounting zero-lag interactions, dwPLI may miss genuine neural synchronisation that occurs with negligible conduction delays (e.g. between nearby brain regions or through fast, direct connections). These trade-offs are inherent to sensor-space connectivity analysis. The dwPLI represents a methodologically rigorous choice that prioritises precision (avoiding false positives from volume conduction) while accepting some cost to sensitivity (potentially missing genuine zero-lag synchronisation). Connectivity patterns were interpreted with appropriate caution, acknowledging these limitations (see Section 3.5.3).

Connectivity was computed at four discrete time points relative to stimulus onset. These time points were -300 ms (pre-stimulus baseline), 100 ms post-stimulus, 300 ms post-stimulus and 500 ms post-stimulus. This approach of analysing connectivity at discrete time points rather than averaging across the entire viewing period was motivated by the goal of capturing the dynamic progress of functional networks as processing unfolds from early perception through later cognitive stages. The specific time points were selected based on the ERP results (Section 3.3.1), which showed distinct peaks at approximately 100, 300 and 500 ms as well as previous aesthetic perception research identifying these time windows as relevant for perceptual analysis and cognitive processing.

Connectivity was also computed separately for five frequency bands: delta (1-4 Hz), theta (4.5-8 Hz), alpha (8.5-13 Hz), beta (13.5-30 Hz) and gamma (30.5-100 Hz). These frequency bands correspond to well-established standard EEG spectrum, each associated with distinct cognitive functions as detailed in Chapter 2 (Section 2.2.2 and Table 2). Examining connectivity separately in each frequency band allows for the identification of frequency-specific communication electrodes that may support different aspects of aesthetic processing [12].

By employing dwPLI, the present study aims to capture non-instantaneous, physiologically meaningful phase-synchronisation patterns while minimising false positives arising from volume conduction. Taking into consideration that different cognitive processes are associated with different types of figurative and abstract art, connectivity differences are expected to be frequency-related. At the same time, it was expected that any remaining near-zero-phase synchronisation should remain observable, highlighting the fundamental limitations of sensor-space connectivity analysis. These methodological constraints emphasise the need to move beyond sensor-level analyses. Chapter 4 therefore examines the reliability of ICA in identifying meaningful neural components, establishing whether ICA provides a sufficiently stable basis for subsequent source-space connectivity approaches.

3.4.2 Statistical analysis

To identify significant differences in connectivity between abstract and figurative conditions, non-parametric cluster-based permutation tests were performed [123]. This approach effectively addresses the multiple comparisons problem in connectivity analyses by controlling the family-wise error rate while remaining sensitive to spatially extended patterns of connectivity differences, making it well-suited for EEG connectivity analysis [123]. Since the interest is in the differences between two conditions (abstract and figurative) executed for each subject, a within-subject design with two conditions was employed. A non-parametric Monte Carlo permutation test was performed using the *ft_freqstatistics*() function. A dependent samples one-tailed t-test was performed for each connection edge-time point pair with a randomisation level of 1000. The alpha level was set to 0.05 and FDR multiple comparison correction was applied.

The statistical analysis was proceeded in two complementary contrasts, first for **figurative > abstract**, then for **abstract > figurative** to denotes higher connectivity strength. Each contrast tests whether one condition shows significantly stronger connectivity weights (network edges) than the other. This two-sided approach was necessary because increases in one condition do not necessarily imply symmetrical decreases in the other. Testing both contrasts therefore allows the direction of the effects (which condition shows higher connectivity for each edge) to be determined without assuming that one style should dominate and provides a more complete understanding of style-related network differences. The null

hypothesis for both contrasts was that both painting styles produce equivalent connectivity patterns.

The Fieldtrip connectivity analysis function expects a binary input network, in which an edge is either present or missing, i.e., without a weight. This requires a preceding thresholding operation that can be problematic since one can use, e.g., the absolute threshold, which may result in widely varying network densities across conditions, or the proportional threshold, where the top x % strongest edges are retained [111]. This latter method can make very weak weights as important as strong weights in another network. To avoid this problem, the statistical calculation was adapted to operate directly on the weighted, non-thresholded network. The resulting significant edges ($p < 0.05$) identified by the permutation test were then retained as a binary mask. Next, the original connectivity matrices were proportionally thresholded to retain the strongest 5% of the edge, after which the statistical mask was applied. This ensured that only edges that were both (a) among the strongest connections and (b) statistically reliable were included in the final network visualisations. As connectivity matrices contain a large number of pairwise connections, uncorrected maps would inevitably include spurious effects. The masking procedure therefore serves to reduce false positives and preserve only meaningful, statistically supported network structure.

3.4.3 Results

This section presents the results of our functional connectivity analysis, examining how brain regions interact during the perception of abstract and figurative paintings. I first present node strength topographies, which reveal the overall organisation of functional networks. I then present the primary findings: significant connectivity differences between abstract and figurative conditions across time points and frequency bands.

3.4.3.1 Node strength topographies

To visualise the overall organisation of functional networks, I computed node strength for each electrode. Node strength is defined as the sum of all connection weights (dwPLI values) associated with a given electrode. Electrodes with high node strength are strongly connected to many other electrodes, suggesting they serve as important hubs in the functional network. Node strength values were then averaged across participants to produce group-level topographies. I computed node strength for the full frequency band (2-40 Hz, integrating across all five frequency bands) to provide an overview of network organisation. Figure 25 and Figure 26 show the temporal evolution of node strength, displayed as scalp topography time series for figurative and abstract conditions, respectively.

The temporal evolution of node strength reveals several distinct patterns across conditions. A clear increase in node strength first appears around 100 ms post-stimulus in the occipital region, reflecting the initial visual response common to both conditions. This is followed by a transient frontal enhancement at approximately 150 ms, again present in both conditions but with slightly different magnitudes. A third and more sustained increase occurs between 300-400 ms for the figurative condition, with activity spanning posterior and select frontal regions and between 350-550 ms for the abstract condition, exhibiting a slightly different spatial distribution. Together, these temporal patterns suggest that while early visual processing is shared across conditions, later stages diverge, likely reflecting differences in cognitive demands associated with interpreting representational versus non-representational content.

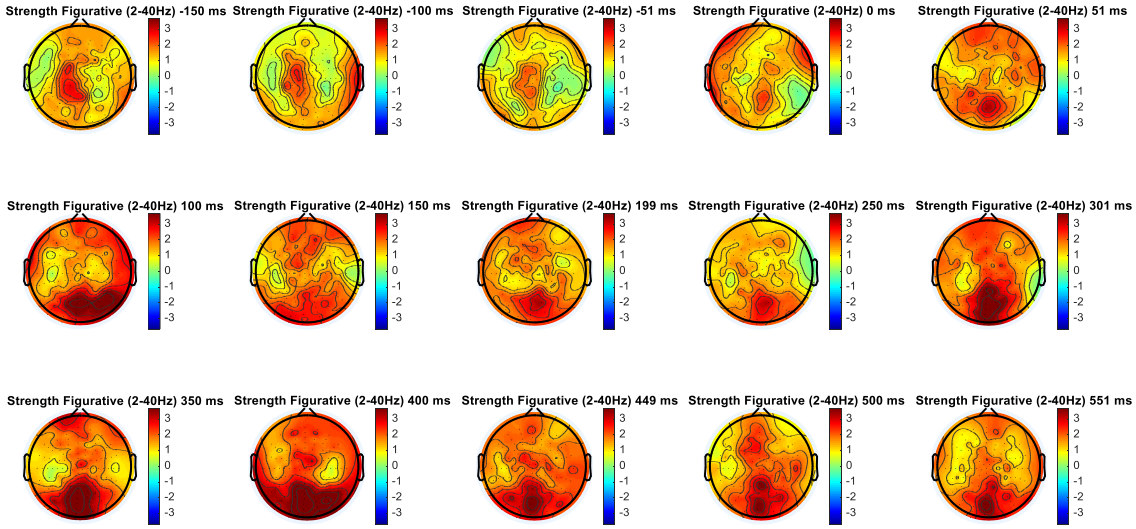

Figure 25. Group-averaged interpolated full-band node strength topography map time series of the figurative condition. Time starts at 150 ms pre-stimulus and stops at 551 ms post-stimulus. Stimulus is presented at 0 ms, time step is 50 ms. Warmer colours indicate higher node strength.

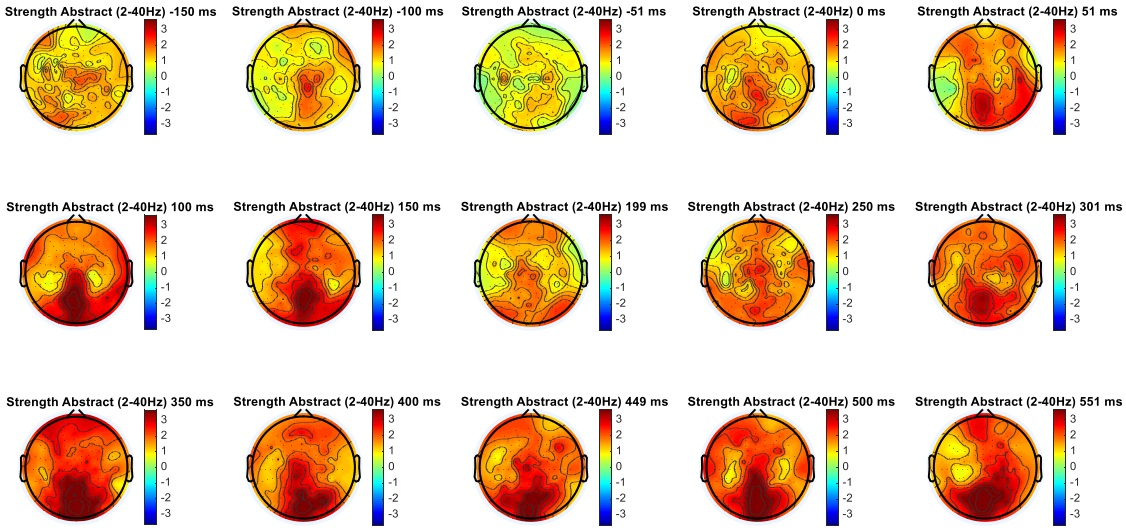

Figure 26. Group-averaged interpolated full-band node strength topography map time series of the abstract condition. Time starts at 150 ms pre-stimulus and stops at 551 ms post-stimulus. Stimulus is presented at 0 ms, time step is 50 ms. Warmer colours indicate higher node strength.

Thus, node analysis revealed that occipital region exhibited high connectivity, consistent with strong early visual activation observed in ERP maps. This overlap suggests that regions showing strong stimulus-evoked responses also act as hubs within the functional network. However, additional frontal and parietal nodes also showed increased in strength despite relatively weak (or non-existent) ERP amplitudes, indicating that connectivity analysis captures integrative processes not visible in ERP measures.

3.4.3.2 Network topology differences between abstract and figurative paintings

I present the functional connectivity network results for the five frequency bands and the two stimulus conditions here. These results are expressed as increases in connectivity of one condition relative to the other (i.e. figurative minus abstract for the figurative condition and abstract minus figurative for the abstract condition). For each band, network changes are shown at four selected time points (-300 ms baseline, 100, 300 and 500 ms post-stimulus). Node size

reflects relative node strength, while node colour indicates network modularity, with nodes sharing the same colour belonging to the same functional module.

The delta band results for abstract and figurative conditions across time points are shown in Figure 27. The figurative condition shows a significant increase in node strength (size) and interconnections at 100 ms (p = 0.0259), particularly in the left occipital and parietal regions. The node strengths further increase in the 300 ms (p = 0.0273) to 500 ms (p = 0.0247) interval, showing robust connectivity across various regions (frontal, temporal and parietal areas). Conversely, the abstract condition displays increased, dense and widespread connections in the frontal and posterior areas (temporal and occipital) from 100 ms (p = 0.0239) to 300 ms (p = 0.0233), which intensifies over time.

In the theta band (Figure 28), the highest figurative connection increase at 500 ms (p = 0.0234) was observed, initially with frontoparietal involvement at 300 ms (p = 0.0288) that becomes more right-hemisphere-dominant with stronger frontal connections by 500 ms. In comparison, the abstract condition reveals dense, increased connectivity, earlier than that seen in the figurative condition, at 100 ms (p = 0.0223) in the frontal, right parietal and occipital regions. This connectivity density then decreases from 300 ms (p = 0.0270) to 500 ms (p = 0.0306), with a noticeable shift towards the left temporoparietal region at 300 ms and central and left occipital areas at 500 ms.

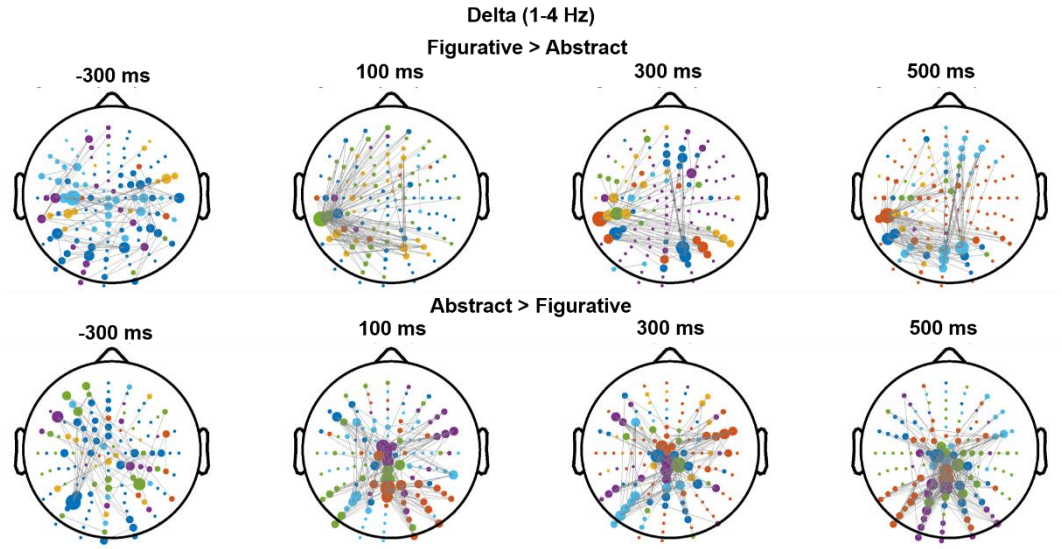

Figure 27. Location of increased connections for figurative > abstract (top) and abstract > figurative (bottom) conditions in the delta band at different time points relative to stimulus onset. Only the significant edges ($p < 0.05$) from the strongest 5% of the connections are retained and displayed.

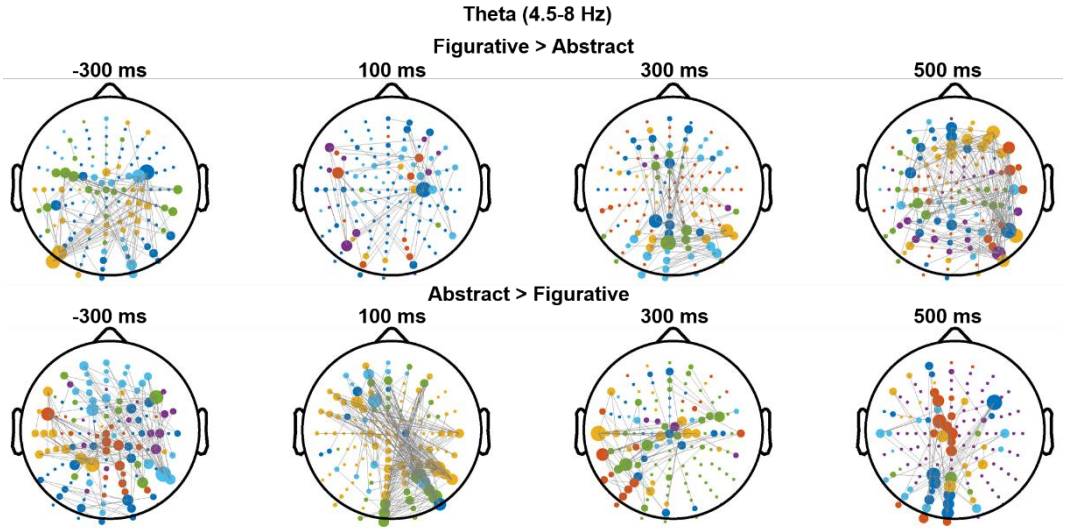

Figure 28. Location of increased connections for figurative > abstract (top) and abstract > figurative (bottom) conditions in the theta band at different time points relative to stimulus onset. Only the significant edges ($p < 0.05$) from the strongest 5% of the connections are retained and displayed.

The alpha band connectivity patterns (Figure 29) also progressed differently for both the abstract and figurative conditions. The figurative condition exhibits focused connectivity in the bilateral central regions, particularly in the left temporal area at 100 ms ($p = 0.0264$), progressing to denser connections in the fronto-occipital network by 300 ms ($p = 0.0267$) and shifting to the right frontal and posterior areas at 500 ms ($p = 0.0268$). The abstract condition, however, shows increased connectivity at 100 ms ($p = 0.0259$), with connections spanning from the occipital to frontal regions in both hemispheres. The connectivity pattern then shifts to the right hemisphere at 300 ms ($p = 0.0243$), involving the frontal, right temporal and left parietal areas, before becoming more distributed across the frontal, left temporal and occipital areas at 500 ms ($p = 0.0269$).

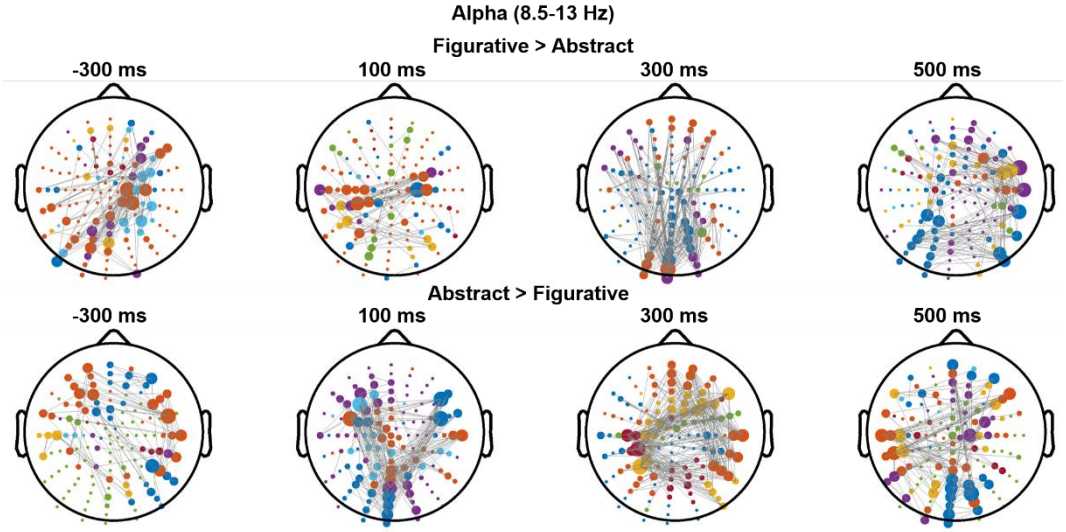

Figure 29. Location of increased connections for figurative > abstract (top) and abstract > figurative (bottom) conditions in the alpha band at different time points relative to stimulus onset. Only the significant edges ($p < 0.05$) from the strongest 5% of the connections are retained and displayed.

The beta band connectivity (Figure 30) reveals significant connectivity differences across time points for both conditions. For the figurative condition, increased connectivity can be observed

in the frontal and posterior regions, particularly at 100 ms (p = 0.0232) and 300 ms (p = 0.0232), with a higher beta connectivity in the frontoparietal network at 500 ms (p = 0.0260). In contrast, the abstract condition shows stronger connectivity, focusing in the occipital and parietal regions at 100 ms (p = 0.0252) and 300 ms (p = 0.0275), with frontal involvement at 300 ms. By 500 ms (p = 0.0256), the abstract condition displays more widespread beta connectivity across the scalp (occipital, parietal and central areas). Patterns varied across time points, indicating dynamic reconfiguration.

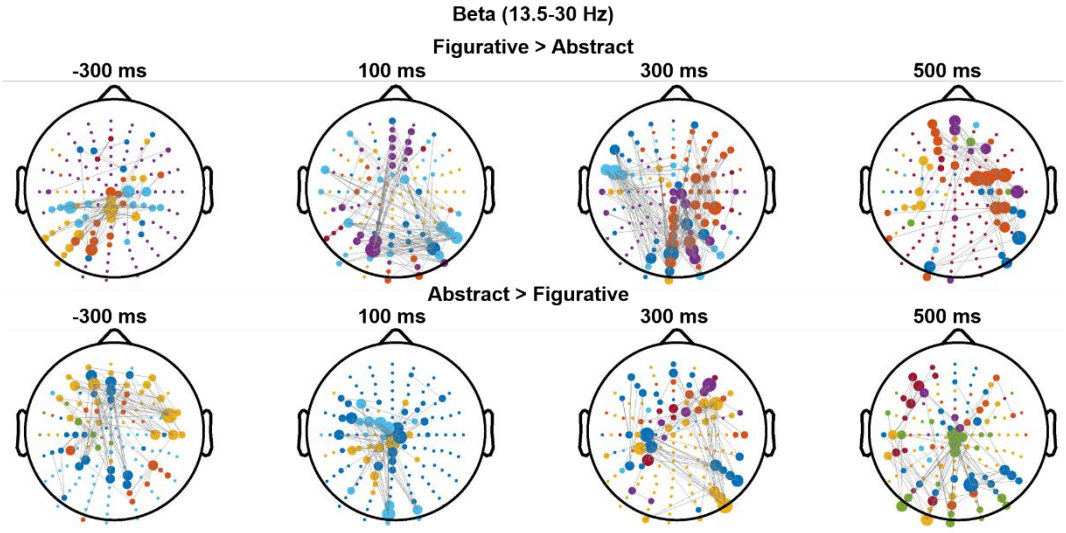

Figure 30. Location of increased connections for figurative > abstract (top) and abstract > figurative (bottom) conditions in the beta band at different time points relative to stimulus onset. Only the significant edges ($p < 0.05$) from the strongest 5% of the connections are retained and displayed.

The gamma band shows distinct temporal dynamics for both the abstract and figurative connections (Figure 31). Initially, at 100 ms, the figurative condition (p = 0.0245) exhibits increased connectivity with prominent nodes in the frontal and temporal regions, while for the abstract condition (p = 0.0252), the connectivity is mainly in the right frontal and left parieto-occipital regions, with relatively larger node strengths appearing in those areas. As processing continues to 300 ms, the figurative condition (p = 0.0254) displays extensive connections across the cortex, with larger nodes appearing in both the right frontal and occipital areas. The connections in the abstract condition (p = 0.0253) are more distributed in the frontal and occipital regions, similar to those seen at earlier time points but shifting to the right hemisphere. By 500 ms, the figurative condition (p = 0.0248) presents a more centralized connectivity whereas the abstract condition (p = 0.0245) shows widespread connectivity, particularly in the frontal and left temporal regions.

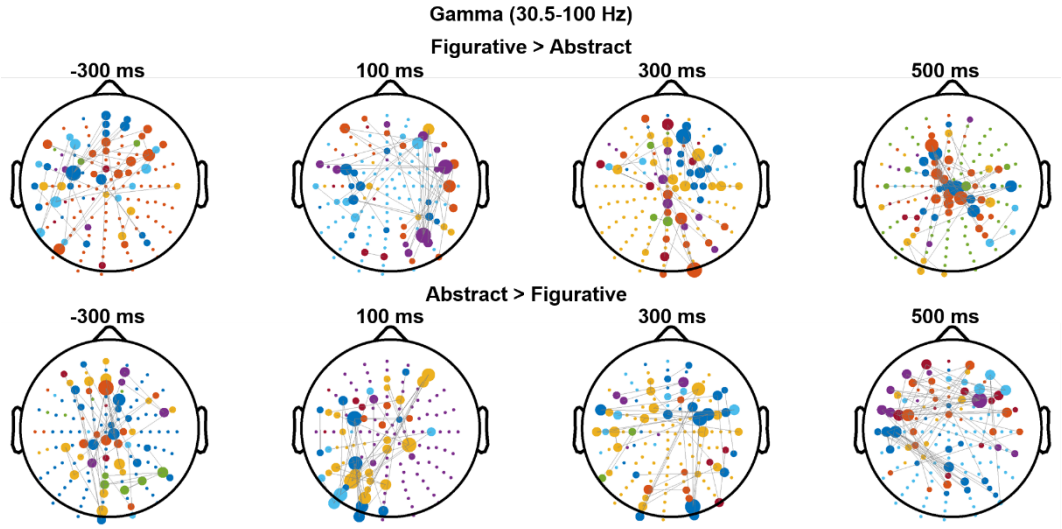

Figure 31. Location of increased connections for figurative > abstract (top) and abstract > figurative (bottom) conditions in the gamma band at different time points relative to stimulus onset. Only the significant edges ($p < 0.05$) from the strongest 5% of the connections are retained and displayed.

To summarise, across all bands, the strongest connectivity patterns consistently appeared over occipital and parietal regions, reflecting the visual nature of the task and the central role of posterior visual networks in aesthetic perception. Each frequency band, however, showed its own characteristic distribution. Delta and theta activity exhibited relatively diffuse patterns involving both frontal and posterior regions, consistent with their roles in large scale network integration and attentional processes. Alpha band activity was dominated by strong occipital-parietal hubs, aligning with alpha's well established involvement in visual attention and sensory processing. Beta band patterns were more distributed, with notable parietal and central involvement, reflecting beta's association with cognitive control and perceptual evaluation. Gamma band activity was more focal, with strong occipital hubs characteristic of local visual processing and feature binding.

The pattern of connectivity differences, whether abstract > figurative or figurative > abstract, varied across frequency bands, time points and brain regions, indicating complex, multi-dimensional differences in network organisation. The dynamic changes in connectivity patterns indicate continuous reconfiguration of functional networks, with the networks reorganising as processing progresses from early perceptual stages to later evaluative phases. These observations motivated the quantitative statistical comparison of connectivity between conditions, which I present next.

3.4.3.3 Statistical comparison of connectivity between abstract and figurative conditions

Statistical comparison of connectivity between abstract and figurative conditions using cluster-based permutation tests revealed significant differences at all time points and in all frequency bands (Table 3). This finding indicates that the processing of abstract and figurative paintings engages distinct patterns of functional connectivity from the earliest stages of perception (100 ms) through later cognitive processing (500 ms) and that these differences are expressed across multiple frequency bands.

Table 3. Mean p-values of the significantly different edges for the figurative and abstract conditions across five frequency bands (delta, theta, alpha, beta, gamma) at different time points (−300 ms, 100 ms, 300 ms, 500 ms).

	Mean *p*-values of the significant edge weight differences			
	−300 ms (Baseline)	**100 ms**	**300 ms**	**500 ms**
Figurative > Abstract				
Delta	0.0248	0.0259	0.0273	0.0247
Theta	0.0275	0.0292	0.0288	0.0234
Alpha	0.0299	0.0264	0.0267	0.0268
Beta	0.0263	0.0232	0.0232	0.0260
Gamma	0.0266	0.0245	0.0254	0.0248
Abstract > Figurative				
Delta	0.0258	0.0239	0.0233	0.0204
Theta	0.0250	0.0223	0.0270	0.0306
Alpha	0.0273	0.0259	0.0243	0.0269
Beta	0.0256	0.0252	0.0275	0.0256
Gamma	0.0246	0.0251	0.0253	0.0245

3.5 Discussion

This chapter focused on identifying the temporal dynamics of functional connectivity during the perception of abstract and figurative paintings using high-density EEG and a robust connectivity metric (dwPLI). The primary objective was to establish whether style-related categories produce differences in the neural communication, thereby providing a foundation for more advanced analysis in subsequent work. The findings reveal that different artistic styles engage distinct patterns of inter-regional communication from the earliest moments of perception through later cognitive processing, with differences expressed across the entire spectrum of neural oscillations. This section discusses the findings in relation to theoretical models of aesthetic perception, interprets the frequency-specific and time-varying connectivity patterns and critically evaluates the methodological approach and its limitations.

3.5.1 Summary of findings

First, significant connectivity differences between abstract and figurative paintings were identified at all time points (100, 300 and 500 ms post-stimulus) and in all frequency bands (delta, theta, alpha, beta, gamma), indicating that the processing of different artistic styles engages distinct patterns of inter-regional communication across multiple timescales and processing stages.

Second, connectivity differences appeared as early as 100 ms post-stimulus, within the first tenth of a second of viewing a painting. This rapid difference indicates that style-related processing begins at very early perceptual stages, well before explicit recognition or evaluative judgement could occur. The brain appears to rapidly distinguish between representational and non-representational visual information and engages different communication patterns almost immediately.

Third, connectivity differences did not just appear briefly and then disappear. Instead, they persisted through 300 ms and 500 ms post-stimulus, indicating sustained differential processing throughout the early-to-intermediate time window. This persistence suggests that abstract and figurative paintings don not just evoke different initial responses but they engage different processing modes that continue as aesthetic perception unfolds.

Fourth, each frequency band showed distinct spatial and temporal patterns of connectivity differences. Delta and theta bands showed relatively widespread connectivity involving frontal and posterior regions. Alpha band showed strong posterior connectivity differences, consistent with alpha's role in visual attention. Beta and gamma bands showed more focal patterns. These

frequency-specific patterns suggest that different oscillatory rhythms support different aspects of style-related processing.

3.5.2 Interpretation in theoretical context

The present findings can be interpreted within existing theories of aesthetic appreciation and prior research on the neural processing of art perception. The model of aesthetic appreciation proposed by Leder and et al. [5], [6] suggests that aesthetic processing unfolds through multiple stages, from early perceptual analysis through cognitive mastering and evaluative judgement. The model proposes that different types of artworks may engage these stages to different degrees, with abstract art potentially rely more heavily on perceptual processing due to the absence of recognisable content, while figurative art facilitates content-based interpretation and semantic processing.

The present findings of early-emerging (100 ms) connectivity differences are consistent with this model's prediction that style-related processing begins at early perceptual stages [6]. The involvement of multiple frequency bands and brain regions suggests that even within the first few hundred milliseconds, the brain engages distributed networks to process artistic style, rather than relying on a single region or processing stream. The observation of connectivity differences across all frequency bands suggests that abstract and figurative art engage multiple, parallel communication channels operating at different temporal scales.

Delta and theta bands may reflect differential engagement of large-scale networks supporting attention allocation, memory encoding and semantic processing. The fronto-posterior connectivity differences in these bands are consistent with the engagement of top-down control networks that may modulate perceptual processing based on stimulus characteristics. Alpha band connectivity differences, particularly the strong posterior alpha connectivity differences, are consistent with alpha's well-established role in visual attention and top-down control of sensory processing [13], [95]. Stronger alpha connectivity for abstract paintings may reflect greater demands on attentional mechanisms to process non-representational visual information. Beta-band differences may reflect differential engagement of networks supporting perceptual expectations and top-down predictions [97]. The processing of figurative art may benefit from stored object representations and perceptual templates, while abstract art may require more flexible, exploratory processing. Gamma band local gamma-band connectivity differences in posterior regions are consistent with gamma's role in feature binding and perceptual integration [99]. Different patterns of local synchronisation may reflect the distinct perceptual features and compositional structures of abstract versus figurative art.

The present findings extend previous research in several important ways. While previous fMRI studies identified brain regions involved in processing abstract versus figurative art [130], the present study reveals the rapid, dynamic evolution of functional networks on the timescale of tens to hundreds of milliseconds. Previous EEG studies primarily examined ERPs or power in specific frequency bands [132], [144], but few have systematically examined functional connectivity across multiple frequency bands. The present findings demonstrate that style-related differences are expressed across the entire frequency spectrum, suggesting multi-scale neural dynamics. By using dwPLI, a metric explicitly designed to be insensitive to volume conduction, the present study provides more confident estimates of genuine functional connectivity than previous studies using volume conduction-sensitive metrics.

The connectivity differences between abstract and figurative paintings likely reflect several cognitive processes. Perceptual analysis is one such process [5]. Abstract art lacks recognisable objects, requiring more extensive exploration of visual features (colours, shapes, textures) to construct a coherent perception. This may be reflected in stronger local connectivity in visual regions and different patterns of long-range connectivity supporting top-down attentional control. Object recognition and semantic processing represent another process. Figurative art activates stored object representations and semantic knowledge, potentially reflected in different patterns of connectivity involving regions supporting object recognition and semantic memory. Perceptual fluency is also relevant. Figurative art may benefit from greater perceptual fluency (ease of processing) due to the presence of familiar content, while abstract art may require more effortful processing [5]. Different connectivity patterns may

reflect these differences in processing demands. Finally, aesthetic evaluation plays a role. While the present study did not require explicit aesthetic judgements, implicit evaluative processes may begin early in perception. Different connectivity patterns may reflect different engagement of networks supporting aesthetic valuation.

3.5.3 Volume conduction and sensor-space limitations

While the present study employed dwPLI to address volume conduction concerns, it is important to acknowledge the inherent limitations of sensor-level connectivity analysis and to interpret findings with appropriate caution. As established in Chapter 2 (Section 2.4.1), the use of dwPLI substantially mitigates the volume conduction problem by explicitly discounting zero-lag interactions [66]. However, there are several important limitations that must be addressed.

First, there may be residual volume conduction effects. While dwPLI is insensitive to zero-lag interactions, volume conduction can also produce small non-zero phase lags due to asymmetries in source configuration or head geometry. Thus, dwPLI does not completely eliminate all volume conduction effects, though it substantially reduces them compared to zero-lag-sensitive metrics. Second, there is the issue of genuine zero-lag synchronisation. By discounting zero-lag interactions, dwPLI may also discard genuine neural synchronisation that occurs at zero lag due to common input or mutual connections with negligible conduction delays [33]. This represents a trade-off between sensitivity to genuine connectivity and robustness to volume conduction artefacts. Third, EEG suffers from source mixing: each electrode reflects a combination of multiple neural sources. Apparent connectivity may therefore arise from a single extended source or multiple overlapping sources rather than communication between distinct regions. As a result, the findings should be interpreted at the level of large scale functional networks rather than precise anatomical locations. Fourth, sensor space analysis lacks the anatomical precision of source reconstructed EEG or fMRI. Broad spatial patterns can be identified, such as posterior versus frontal activity, but specific cortical areas cannot be localised. Direct comparison with fMRI studies therefore requires caution.

3.6 Conclusion

The connectivity analysis demonstrates that abstract and figurative paintings evoke different connectivity patterns of large-scale neural communication. These differences emerge early by 100 ms and persist through later processing up to 500 ms, with each frequency band contributing differently. Together, the results show that aesthetic style perception involves dynamic, multi-frequency reconfiguration of functional networks.

However, these findings are constrained by the limits of sensor-level analysis. Connectivity can only be examined reliably within the first 500 ms after stimulus onset, yet participants viewed each painting for 8 seconds and made multiple, naturally occurring fixations throughout this period. Because these fixations occur at unpredictable times, they cannot be averaged in the same way as stimulus-locked ERPs and sensor-space connectivity cannot reveal the neural dynamics associated with individual fixations. Moreover, sensor-level data cannot resolve anatomical sources, distinguish direct from indirect pathways or identify the cortical sources underlying the observed network differences.

These limitations create a clear methodological need to analyse neural activity at the level of single fixations, using an approach that reduces source mixing without requiring anatomical head models. ICA offers such possibility but its reliability under naturalistic viewing conditions and across realistic preprocessing variations must be established before it can used to study fixation-locked neural dynamics.

Chapter 4 therefore evaluates whether ICA can consistently identify meaningful neural components, particularly fixation-related activity on a single-trial basis. Demonstrating ICA's robustness provides the methodological foundation needed for future component-space connectivity analyses that extend beyond the first 500 ms and capture the fixation-driven dynamics that unfold during naturalistic perception.

4. RELIABILITY OF ICA IN IDENTIFYING MEANINGFUL NEURAL RESPONSES DURING NATURALISTIC VIEWING

4.1 Introduction and Rationale

4.1.1 Natural viewing, eye movements and the challenge for EEG

When people view artworks in natural conditions, perception is driven not by single continuous visual episode but by a rapid sequence of eye movements. Natural or free viewing consists of two fundamental types of oculomotor events: saccades, which are rapid eye-movements that shift gaze from one location to another, and fixations, during which the eyes remain relatively stable and visual information is acquired. During art viewing, observes typically make three to four saccades per second, meaning that an 8-second trial will contain 20-30 discrete fixations. Each fixation represents a new sampling of the artwork and each saccade resets the visual input reaching the retina. Figure 32 illustrates this pattern of eye movements during naturalistic art viewing.

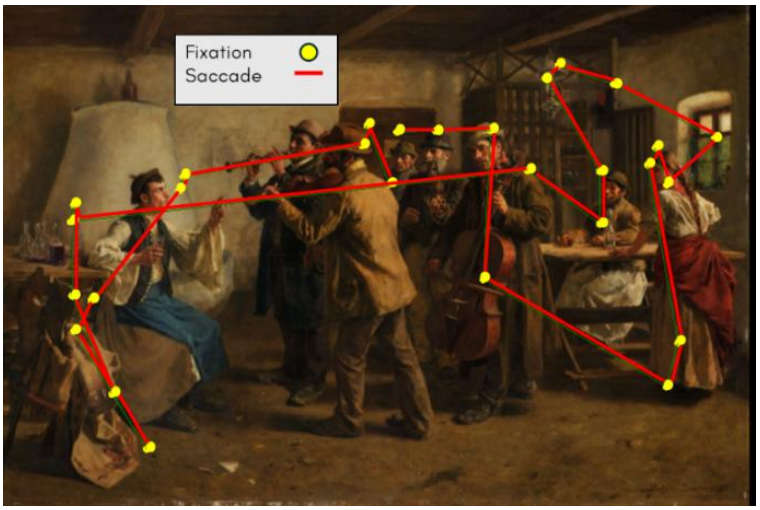

Figure 32. Illustration of an eye-tracking scanpath shown on a sample painting, showing fixations and saccades. Fixations occur when the eyes remain briefly stable on a single point, whereas saccades are the rapid movements that shift gaze from one point to another.

This viewing behaviour poses a fundamental challenge for EEG. Traditional ERP approaches assume that neural responses are time-locked to a single stimulus onset. In free viewing, however, the visual system is continuously re-stimulated by each saccade, producing overlapping neural responses and eye-movement artefacts that violate the assumptions of simple stimulus-locked averaging. As a result, the EEG signal during naturalistic art viewing is therefore a mixture of neural activity from multiple fixations, eye-movement artefacts and ongoing cognitive processes. Understanding aesthetic perception under these conditions requires methods that can isolate neural activity associated with each fixation. To address this, fixation-related potentials (FRPs) have become the standard approach for analysing EEG during natural viewing, as they time-lock the neural activity to fixation onset rather than stimulus onset [145], [146], [147]. Thus, allowing the study of neural processing that occurs each time the eyes land on a new region of an image.

A central component of FRPs is the lambda response (or wave), which is a sawtooth-shaped positive potential that occurs approximately 70-100 ms after saccade offset (i.e. fixation onset) [148], [149], [150]. It reflects the arrival of new visual information at primary visual cortex (V1) after each fixation or saccade activity [148], [149], [151]. Figure 33 illustrates a typical example of this response, showing the relationship between saccade onset, saccade offset and the subsequent lambda wave in occipital EEG recordings [151].

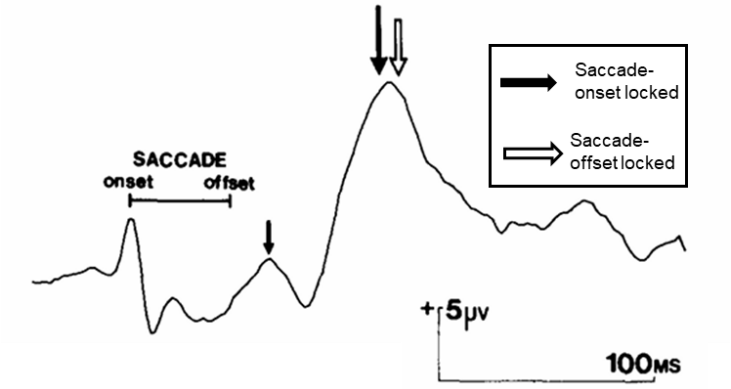

Figure 33. Example of a saccade locked lambda response adapted from Thickbroom et al. (1991). The waveform shows EEG activity time locked to saccade onset and offset. A prominent positive deflection appears approximately 70-100 ms after saccade offset (fixation onset), representing the lambda response associated with early visual cortical processing.

In the context of art viewing, this means that aesthetic perception is structured around a sequence of fixation-locked visual processing events, each initiated by a lambda response. Identifying lambda responses during art viewing is therefore scientifically meaningful as it reveals that aesthetic perception is composed of a sequence of fixation-locked processing cycles rather than a single continuous perceptual episode and provides a physiologically grounded marker for analysing how the brain processes each newly fixated region of an artwork. This insight reframes the interpretation of the connectivity results in Chapter 3, where static time windows captured the cumulative outcome of multiple fixation-specific processing cycles. By identifying lambda responses, it becomes possible to move beyond static windows and analyse aesthetic perception at the temporal resolution of individual fixations across the full 8-second viewing period.

4.1.2 Why ICA must be validated for free-viewing EEG

As established in Chapter 2 (Section 2.5), ICA offers a promising intermediate approach between sensor-level and full source reconstruction methods. ICA provides spatial filtering that separates mixed sensor signals into maximally independent components, each representing a distinct neural source or artefact [44], [152]. By imposing spatial independence on components while preserving temporal relationships, ICA addresses the volume conduction problem and enables connectivity analysis between spatially distinct sources rather than between mixed sensor signals. ICA also enables single-trial analysis in natural viewing paradigms by separating neural sources from eye related artefacts and other noise components. Thus, it becomes possible to study trial-by-trial brain activity even when the signal-to-noise ratio (SNR) is low and traditional averaging would cancel meaningful responses.

However, the reliability and validity of ICA decomposition depend critically on preprocessing choices and methodological parameters. Factors such as filtering, referencing, data length and channel interpolation can significantly affect ICA quality and the interpretability of resulting components [55], [67]. Previous research has used ICA extensively for artefact removal where it identifies and removes eye blinks, muscle activity and other non-brain signals [45], [101], [147], [153], [154]. This application has been very successful and is now standard practice. However, using ICA to extract neural components of interest such as specific brain signals that we want to analyse may require additional validation. This is particularly challenging in free-viewing paradigms because how do we know if ICA correctly identified a neural component? With artefacts like eye blinks, we can visually inspect the data and see obvious blinks. But with neural components representing cognitive processes, there is no obvious ground truth. Thus, the question is, how can we validate that ICA reliably extracts meaningful brain signals? This chapter addresses this validation challenge by investigating

ICA's ability to reliably detect and isolate a well-characterised visual component: the lambda response.

4.1.3 Rationale for using lambda response

Lambda responses possess several properties that make them exceptionally well suited for methodological validation.

First, they offer a verifiable ground truth: because saccades can be precisely detected using eye-tracking, each saccade provides a known time point at which a lambda response should occur. This gives us an objective benchmark for when the component ought to be active.

Second, lambda responses have a highly stereotyped signature. They consistently appear over occipital regions, exhibit positive polarity and occur at a predictable latency following each saccade. This regularity makes them straightforward to identify and evaluate.

Third, they occur frequently during natural viewing. People typically make three to four saccades per second, meaning that an eight-second viewing period contains roughly 20-30 saccades, each followed by a lambda response. This number of events provides a rich dataset for testing ICA performance. In other words, lambda responses sit exactly at the intersection of the main challenges of free-viewing EEG (e.g. dense eye-movement activity, low single-trial SNR and source mixing) and the main promise of ICA, which is its ability to unmix overlapping sources and recover meaningful neural components on trial-by-trial basis.

Lambda responses also originate primarily from a single, relatively focal source in V1, making them an ideal test case for assessing ICA's ability to isolate spatially distinct neural generators. Their biological validity further strengthens their suitability: lambda responses occur naturally during real-world visual exploration rather than being artificially induced in strict laboratory conditions.

Finally, they are directly relevant to aesthetic perception. Because lambda responses occur during art viewing as in the paradigm used in Chapter 3, validating ICA on these responses ensures that the methodology is directly applicable to the same dataset.

Reliability in this context refers to the consistent detection of the lambda component across participants and preprocessing pipelines, its stable spatial and temporal characteristics and its systematic alignment with saccade timing. Since ICA decomposition is highly sensitive to preprocessing choices, I systematically varied filtering settings, sampling rates and data lengths, allowing the identification of the parameter combinations that maximise the stability and reproducibility of ICA decompositions.

The validation strategy follows a systematic sequence. First, EEG is recorded while participants freely view paintings, with eye movements simultaneously tracked. Second, the EEG data are processed using a range of preprocessing parameters, including different filtering settings, sampling rates and data lengths. Third, ICA is applied to decompose the mixed EEG signals into independent components. Fourth, components are checked whether any corresponds to the lambda response using objective criteria derived from its known spatial, temporal and spectral characteristics. Fifth, the identified component is validated by confirming that its activity aligns with saccade timing detected by the eye-tracker. Finally, reliability is quantified by similarity index (SI) across preprocessing conditions to determine which parameter combinations produce the most robust ICA performance.

Demonstrating all of this for lambda responses would establish that ICA can reliably extract neural components with known, verifiable properties. This, in turn, provides confidence that ICA can be applied to extract other neural components even when comparable ground truth information is not available. Using lambda as a test case therefore serves two purposes: (i) it validates the stability of ICA decomposition under realistic processing variations and (ii) it provides evidence that ICA achieves meaningful signal separation, addressing the core limitation identified in Chapter 3.

4.1.4 Research gap and objectives

Despite extensive work using ICA in EEG research especially in artefact removal, several fundamental questions remain unanswered about its ability to isolate functionally meaningful neural component during natural viewing.

Firstly, although lambda responses are well-established at the sensor level, it is not yet known whether ICA can reliably extract them as distinct components across participant and preprocessing pipelines. This gap limits the confidence in using ICA for studying visual processing during free viewing settings and for further analysis such as connectivity.

A second major gap concerns preprocessing. Winkler et al. [67] emphasised that ICA performance is particularly sensitive to the choice of high-pass filtering and other parameters such as sampling rate and data length which can alter the ICA outcomes, yet no systematic evaluation exists using a consistent, physiologically meaningful reference component and the parameter combinations on the decomposition quality which remains under-study.

Finally, even if ICA can extract lambda components, it is unclear whether these components preserve enough temporal properties to allow single-trial detection of individual lambda responses. This is important as cognitive processes vary from trial to trial, thus single-trial analyses are essential for linking neural activity to behaviour. This chapter therefore makes two key contributions:

1. It establishes the lambda response as a meaningful neural component during naturalistic art viewing. This demonstrates that aesthetic perception unfolds as a sequence of fixation-locked processing cycles.
2. It provides a systematic validation of ICA preprocessing pipelines, using the lambda response as a ground truth physiological benchmark to determine which preprocessing choices produce reliable component extraction.

Additionally, to address the research gaps, this chapter aims to validate ICA as a method for extracting lambda response during natural viewing. Specific objectives are as follows:

1. **To determine whether ICA can reliably detect lambda components.**
   This include evaluating detection rates across participants and preprocessing conditions, and examining the consistency of component characteristics.

2. **To evaluate how preprocessing parameters influence ICA performance in successfully extracting lambda components.**
   High-pass filter cutoff, sampling rate, low-pass filter and data length were systematically varied to identify which parameters most strongly affect ICA performance. Based on prior literature, high-pass filter cutoff was expected to be the most critical factor.

3. **To assess whether ICA enables accurate single-trial detection of lambda responses.**
   Single-trial peak detection following individual saccades was evaluated and performance was compared sensor-level measures. ICA was expected to improve single-trial detection by separating lambda activity from overlapping neural signals and artefacts.

Together, these objectives provide a comprehensive methodological evaluation of ICA for studying saccade-related visual processing during natural viewing and establish a foundation for future work on component space connectivity analysis.

4.2 Experiment Details

This study used the same dataset described in Chapter 3, applying ICA to investigate whether lambda responses can be reliably detected and extracted from continuous EEG during naturalistic viewing. While Chapter 3 focused on functional connectivity between brain regions, this chapter examines ICA's ability to isolate individual neural sources, specifically, the lambda response component. This section describes the methods specific to ICA-based lambda detection; for details on participants, stimuli, experimental procedures and basic EEG acquisition, see Chapter 3, Section 3.2.

4.2.1 Participants and dataset

I analysed data from the same experiment described in Chapter 3, where participants viewed 80 art paintings during simultaneous EEG and eye-tracking recording. Of the original ten

participants where EEG and eye-tracker were recorded simultaneously, one was excluded due to excessive eye blinks that compromised both EEG and eye-tracking data quality. The final dataset included nine participants (two males, seven females; mean age = 23.4 years, SD = 4.7). All were right-handed university students with normal or corrected vision and no history of neurological disorders. Although the sample size is modest, nine participants is appropriate for a methodological validation study for two reasons. First, the aim here is to determine whether ICA reliably detects lambda components within individuals across different preprocessing conditions. The key question is not whether there are group-level effects that would require a larger sample for statistical power, but whether ICA performs reliably for each person. Second, each participant generated approximately 1800 (SD = 261.5) saccades during the experiment, providing a large number of events for stable ICA decomposition and validation.

Each participant completed 80 trials, with each trial consisting of viewing one painting for 8 seconds during which natural, free-viewing was encouraged. Every painting was viewed once and the full set of 80 paintings was presented in a fixed randomised order across participants. This free-viewing paradigm was ideal for lambda detection because it generated natural saccades with variable amplitudes, directions and intervals. During natural viewing of complex images, people make frequent saccades to explore different regions and details and this paradigm therefore reflects real-world painting viewing rather than an artificially controlled laboratory task. Augmenting the EEG data with synchronised eye-tracking measurement ensures precise identification of fixation-locked visual components especially the lambda response, which can serve as the benchmark for assessing ICA decomposition quality.

4.2.2 Eye movement data processing

Eye-tracking data were recorded simultaneously with EEG using a Tobii Pro Fusion screen-based eye-tracker (Tobii Technology, Sweden). The system samples eye position at 250 Hz with an accuracy of 0.3˚ of visual angle and precision of 0.2˚. Before the experiment, a standard 9-point calibration was performed to ensure accurate gaze measurement, typically achieving calibration errors less than 0.5˚. Recording eye movements was essential for the present study because the timing of each saccade provides the ground truth needed to identify when a lambda response should occur. Since lambda responses are tightly linked to saccade, precise saccade timestamps would allow the corresponding neural activity to be validated against ICA-derived components. Without eye-tracking, it would not be possible to determine whether an extracted component truly reflects lambda activity in the EEG.

Saccades and fixations were extracted from the continuous eye-tracking data using Tobii Pro Lab software (version 24.21.435 x64). The software implements the I-VT velocity-threshold algorithm [155], which classifies eye movements based on velocity. The default detection parameters recommended for free-viewing experiments was used: velocity threshold of 30˚/s, window length of 20 ms for velocity calculation, gap filling up to 75 ms for brief tracking losses and minimum fixation duration of 30 ms. These settings are standard for free-viewing experiments and have been validated in previous fixation-related EEG studies [146]. Only the 8-second painting viewing periods were analysed while the numeric cue and response intervals were excluded. A sample of the raw eye-tracking data exported from Tobii Pro Lab is shown in Table 4, illustrating the structure of the timestamped gaze and pupil measurements used for subsequent saccade detection.

Table 4. Sample raw eye-tracking data exported from Tobii Pro Lab.

Recording timestamp (µs)	Recording name	Recording Fixation filter name	Recording resolution height (px)	Gaze point X (DACS px)	Gaze point right X (DACS px)	Pupil diameter left (mm)	Eye position left X (DACS mm)
4830	S43_R01	Tobii I-VT (Fixation)	1050	406	403	3.293	182
8830	S43_R01	Tobii I-VT (Fixation)	1050	389	384	3.224	182

12830	S43_R01	Tobii I-VT (Fixation)	1050	404	391	3.226	181.9
16828	S43_R01	Tobii I-VT (Fixation)	1050	399	390	3.263	181.9

Several saccade parameters were extracted, including saccade magnitude (amplitude of the saccade in degrees of visual angle), saccade direction (angular direction of the saccade) and landing position (screen coordinates of the fixation following the saccade). To characterise the viewing behaviour underlying these parameters, the eye-movement data analysis confirmed that participants engaged in natural exploratory viewing. Mean fixation frequency was 3.10 fixations per second (SD = 0.61), while mean saccade frequency was 2.81 saccades per second (SD = 0.61). Further details on group statistics of the eye movements are provided in Figure A-3 in Appendix F. Saccade amplitudes averaged 4.61˚ (median = 3.73˚, SD = 3.50˚) and saccade directions showed uniform distribution across all angles, reflecting natural exploratory viewing rather than systematic scanning patterns. These parameters were used to examine relationships between saccade properties and lambda response characteristics. Table 5 presents example saccade parameters extracted using the I-VT algorithm, including direction, velocity and amplitude for both figurative and abstract viewing conditions.

Table 5. Example saccade parameters extracted from Tobii Pro Lab.

Condition	Event type	Start (ms)	Stop (ms)	Saccade direction (˚)	Average velocity (˚/s)	Peak velocity (˚/s)	Saccade amplitude (˚)
Figurative	Saccade	369	397	244.93	99.74	142.49	3.2
Figurative	Saccade	889	921	309.06	122.16	177.72	4.3
Abstract	Saccade	1264	1284	337.33	70.79	79.41	1.54
Abstract	Saccade	1584	1624	167.76	151.72	255.4	6.35

A critical technical step was synchronising eye-tracker saccade events with EEG data, as the two systems record independently with separate clocks. Initial alignment was established using hardware triggers from painting onsets (via photosensor) but a small residual temporal offset remained between the systems. To quantify this offset, the saccades detected by eye-tracker were compared with the corresponding saccade-related deflections in the horizontal and vertical EOG channels. As shown in Figure 34a, the eye-tracker saccade events were consistently lagged behind the EOG saccade peaks (electrodes EXG5 and EXG6) by approximately 16 ms. Therefore, a 16 ms temporal shift was applied to the eye-tracker timestamps. After this correction, the saccade events were precisely synchronised with EOG signals (Figure 34b), allowing accurate subsequent comparison between saccade timing and lambda component activity.

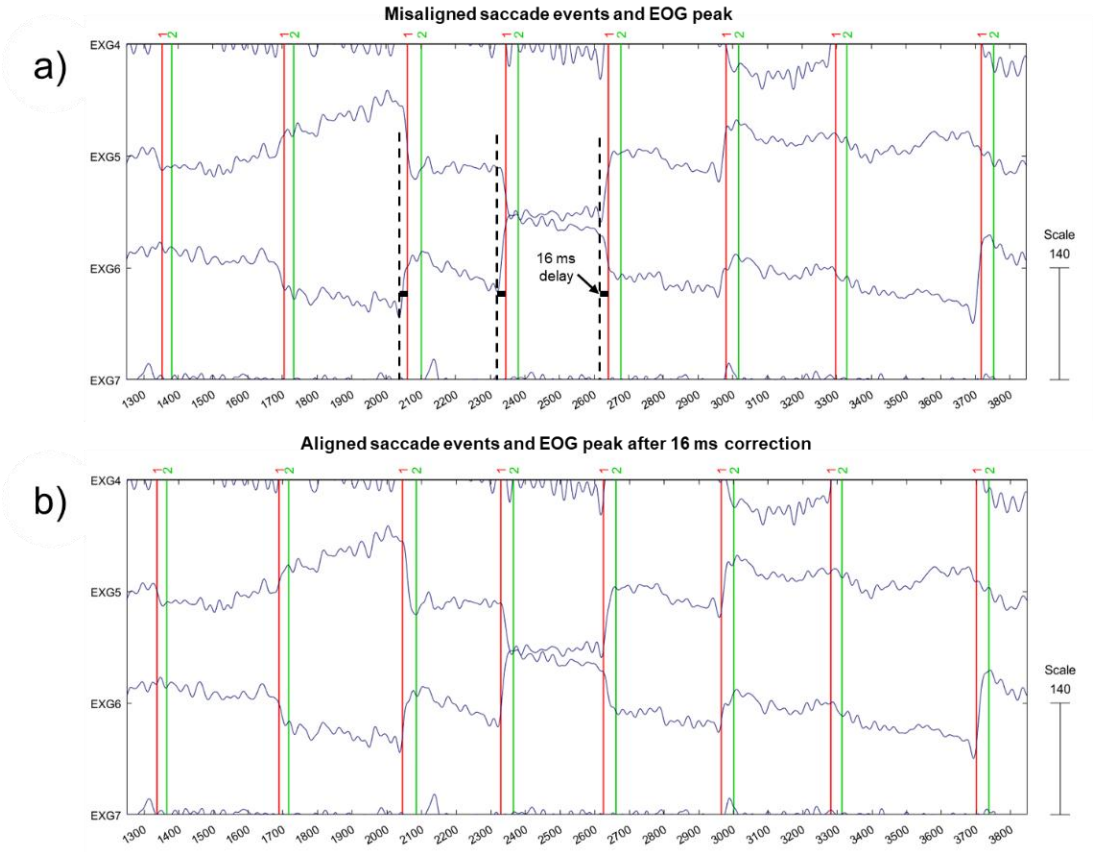

Figure 34. Synchronisation of eye-tracker saccade events with EOG signals. (a) Before synchronisation, the eye-tracker saccade onsets (red) and offsets (green) lag behind the corresponding EOG peaks by ~16 ms. (b) After applying a 16 ms temporal shift to the eye-tracker timestamps, the saccade events align precisely with the EOG peak.

4.3 Exploratory ICA decomposition and lambda identification

I begin by showing that ICA successfully identifies lambda components in exploratory analysis. I first tested whether ICA could detect lambda components at all using commonly-used preprocessing settings. I applied the preprocessing pipeline with 512 Hz sampling, 1 Hz high-pass filter and 40 Hz low-pass filter to all nine participants' datasets. This initial exploratory analysis would tell us whether lambda detection with ICA is feasible in principle. For all nine participants, visual inspection of the independent components revealed one component with characteristics strongly suggesting it represents lambda responses. Figure 35 shows the first eight independent components (ICs) for one participant (S8). IC1 and IC2 represent eye-related artefacts in which IC1 contains vertical eye movements and blinks, while IC2 contains horizontal eye movements. These artefact components are expected and show that ICA is successfully separating eye movement artefacts from neural activity. IC5 also stands out as a strong lambda candidate. The scalp topography shows a focal occipital-positive distribution centered around electrode Oz, exactly where lambda responses are known to be strongest. The spatial pattern shows a radial dipole originating from a central occipital location, matching the expected sources of lambda responses in primary visual cortex, V1. The ICLabel classified this component as “brain”, thus, confirming that this is likely neural rather than artefactual.

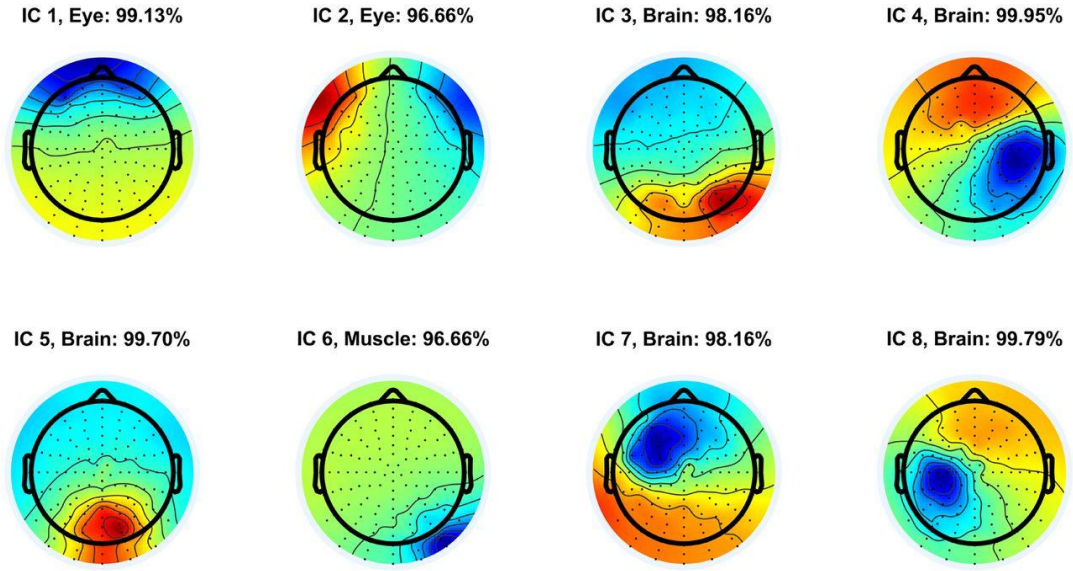

Figure 35. Classification probabilities assigned by the ICLabel algorithm. Components not belonging to the "Brain" class (cortical sources) represent artefacts. The components are sorted in decreasing order by increasing residual variance.

Moreover, Figure 36a shows the time-dependent activations of the first five independent components in one epoch for participant S8. Magenta vertical lines mark stimulus onsets (painting display), while black lines mark response events (button presses). Components IC1 and IC2 show the expected patterns of horizontal and vertical eye movements. In contrast, IC5 (the component with occipital topography, Figure 36b) shows something unique. The activation contains a distinct sequence of triangular pulses that appears only during the 8-second painting viewing intervals, not during the blank-screen response periods. The triangular waveform shape resembles the lambda waves described in past papers [148], [149], [151], [156], [157]. The zoomed-in segment with saccade onset (red) and offset (green) events from eye-tracker is shown in Figure 36c. The match between the two signals is very clear: almost every time a saccade ends, IC5 shows a positive peak afterwards. This consistent timing between the eye-tracking data and IC5 strongly suggests that IC5 reflects the lambda response.

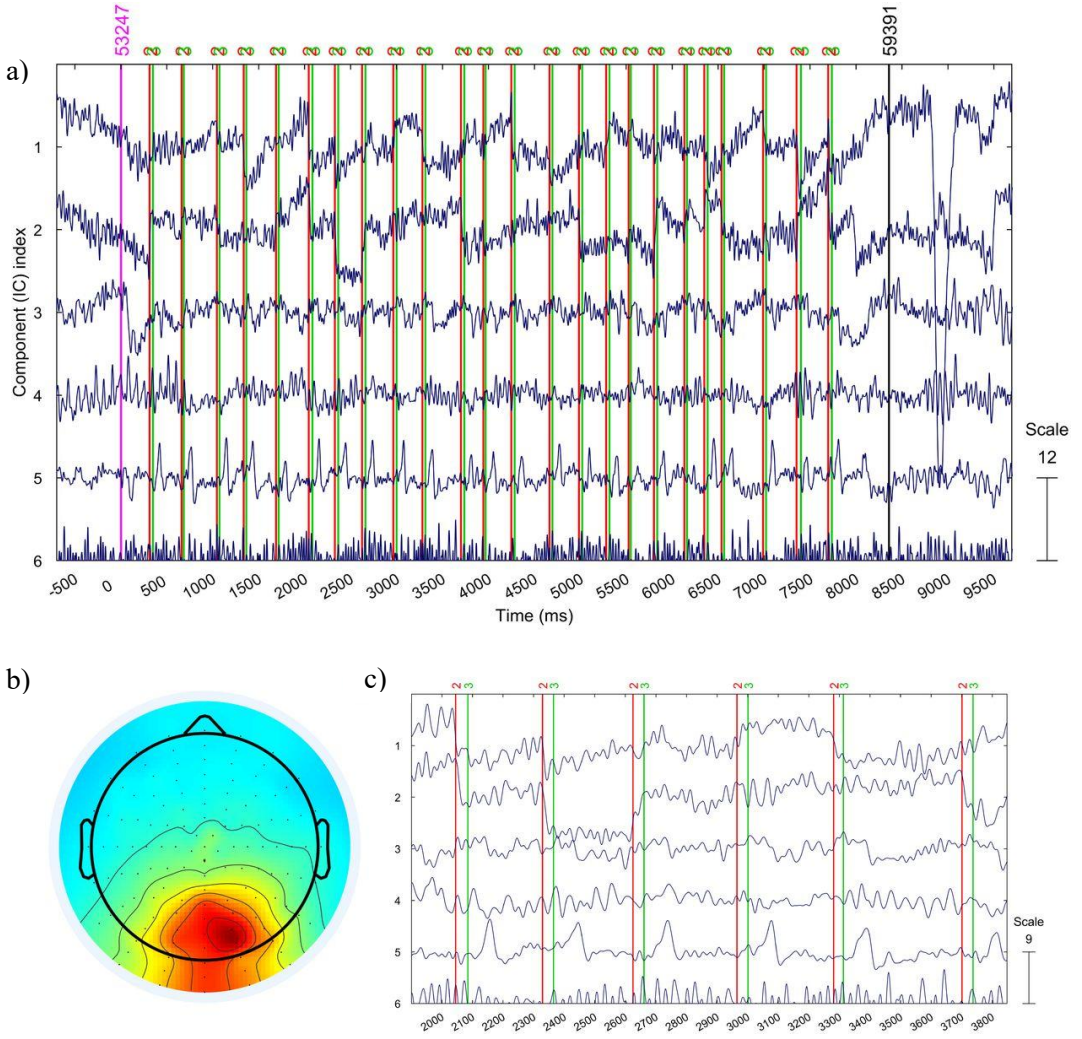

Figure 36. Independent component activations of participant S8 showing the five most important ICs after decomposition. (a) Time-course of the first five ICs in a 13 s epoch, with saccade onset (red) and offset (green) markers. (b) The scalp topography of IC 5 component. (c) A zoomed-in section of IC 5 showing how the triangular waves regularly follow saccades.

I observed similar results across all nine participants (Figure 37). Each participant had one component with occipital topography showing triangular waveform patterns time-locked to saccades during painting viewing. The consistency where nine out of nine participants showing identifiable lambda components, thus, suggests lambda detection with ICA is not chance but a reliable phenomenon. This exploratory finding established that ICA could identify lambda components in principle, motivating the systematic validation and parameter exploration that follows.

In addition to the lambda-related component, the exploratory ICA decomposition also revealed two additional occipito-parietal sources located over the left and right posterior regions, whose activity followed a consistent temporal sequence. As shown in Figure 38, IC5 shows the earliest and strongest peak, followed by IC4 and IC3, suggesting that occipital activity after each saccade/fixation unfolds across multiple sources rather than just a single source. This may suggest a progression of activity across occipital visual hierarchy, which ICA is able to separate into distinct components, although precise anatomical location cannot be inferred from sensor-level ICA.

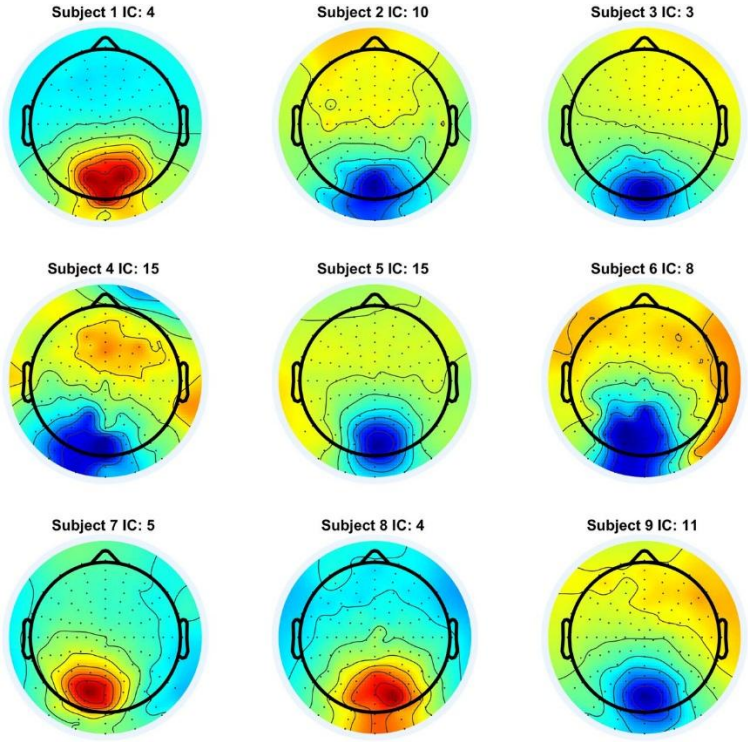

Figure 37. Projected scalp activation maps of the lambda components from each participant.

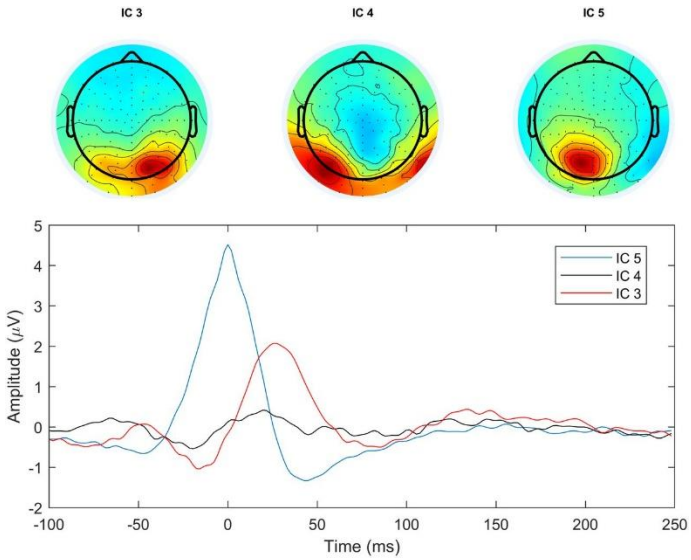

Figure 38. Occipital ICs with distinct topographies and sequential peak timing.

4.4 Lambda component validation

Having observed possible lambda components in all nine participants during the exploratory analysis, it is critical to validate that identified components genuinely represent lambda responses rather than other neural activity or artefacts. To establish this, three complementary validation approaches were implemented.

4.4.1 Validation through waveform morphology

To verify that ICA-extracted components genuinely represent lambda responses, I compared their waveforms with traditional saccade-locked averaged potentials from occipital electrodes. If the components represent the same neural activity producing lambda responses in sensor-level recordings, the waveforms should match. To test this, three types of averaged potentials

were generated. For saccade onset locked and saccade offset locked analyses, epochs from -50 to 200 ms were extracted around each saccade and averaged for the lambda component, for the combined O1-Oz-O2 electrodes and for individual occipital channels. Because lambda responses are more tightly linked to the arrival of new visual input after the eyes land, offset locked averages were expected to show clearer peaks. A third comparison used lambda peak locked averages, in which epochs from -150 to 150 ms were time locked directly to peaks detected in the lambda component. This eliminates temporal jitter from variable lambda latencies across saccades. In the following validation sections, a signal/waveform will always correspond to an epoch-averaged signal.

Correspondence between waveforms was quantified using a similarity index defined as the normalised dot product of two signals. Values range from -1 (opposite) to +1 (identical), with higher values indicating stronger match. If the ICA component truly reflects lambda activity, it should show high similarity to occipital sensor-level averages, sharper peaks in the component compared to individual electrodes (due to source separation) and highest similarity for peak-locked averages (eliminating jitter).

Saccade onset-locked comparison

Saccade-onset-locked epochs were averaged for the occipital electrodes O1 (A15), Oz (A23) and O2 (A28), and the resulting occipital mean waveform was compared with the averaged lambda IC (Figure 39a). The occipital average shows a saccadic spike potential occurring approximately 20 ms before saccade onset, followed by onset- and offset-related peaks. However, substantial differences between the occipital average and the lambda waveform were observed in the number and latency of the waveform peaks. Waveforms from the individual occipital electrodes are also shown (Figure 39b). The similarity index between the three-electrode occipital average and the lambda component (-50 to 200 ms) was SI = 0.7563.

An occipito-parietal electrode showing maximal activation in the lambda component scalp map (Figure 39c) was then identified (A17). The averaged A17 waveform and the lambda component are shown in Figure 39d. For visual comparison, the lambda component was scaled to the A17 peak amplitude (Figure 39e). Greater similarity in waveform shape and improved alignment of the dominant positive peak were observed compared with the occipital average. The similarity index between A17 and the lambda component was SI = 0.9759. The higher similarity for A17 suggests this particular electrode is optimally positioned for recording lambda responses in this participant, but even the best single electrode does not achieve the clarity of the ICA-separated component.

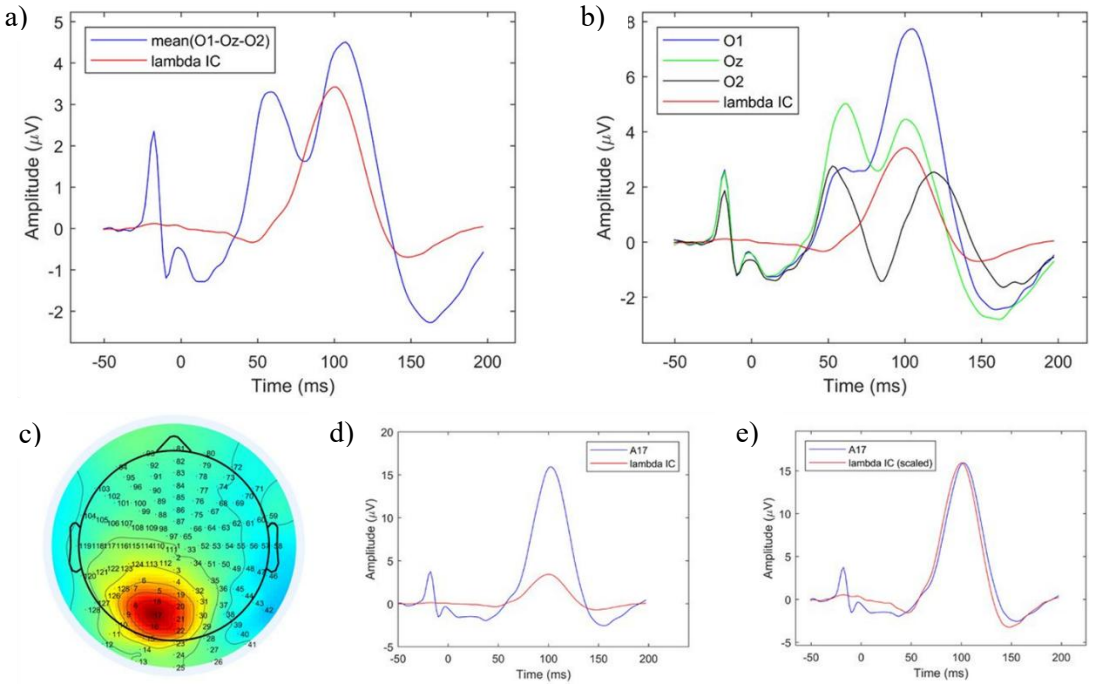

Figure 39. Saccade-onset-locked averages. (a) Averaged occipital activity (O1-Oz-O2) compared with the ICA-derived lambda component. (b) Individual occipital electrodes and the lambda component. (c) Scalp activity map showing A17 as peak activation electrode. (d) A17 onset-locked waveform versus lambda. (e) Same waveforms as in (b) with lambda scaled to match A17 waveform amplitude.

Saccade offset-locked comparison

A second comparison aligned the waveforms to saccade offset (Figure 40) which is slightly earlier than the onset-locked peaks. This timing makes physiological sense as the lambda response begins when new visual input reaches V1, which happens shortly after the eyes land, not when they begin moving. The lambda component waveform again shows a sharper; more distinct peak compared to sensor-level waveforms. Similarity indices for offset-locked averages were SI = 0.7934 for occipital average and SI = 0.9771 for electrode A17, which is very similar to onset-locked values. These high similarity values confirm that the lambda component represents the same neural activity visible in occipital electrode recordings, with improved separation.

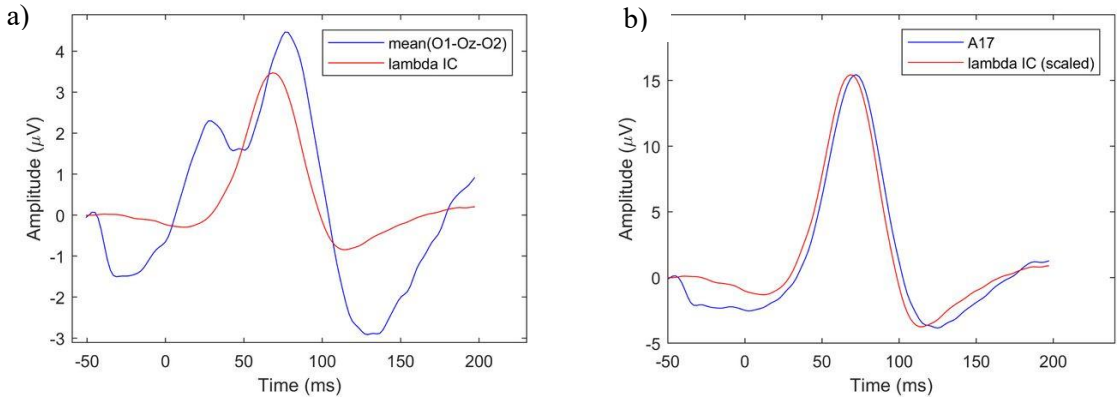

Figure 40. Saccade offset-locked averages. (a) Averaged O1-Oz-O2 waveform versus lambda component. (b) A17 offset-locked waveform versus scaled lambda signal. See Extended Data Figure 12-1 for saccade offset-locked ERP images of these electrodes.

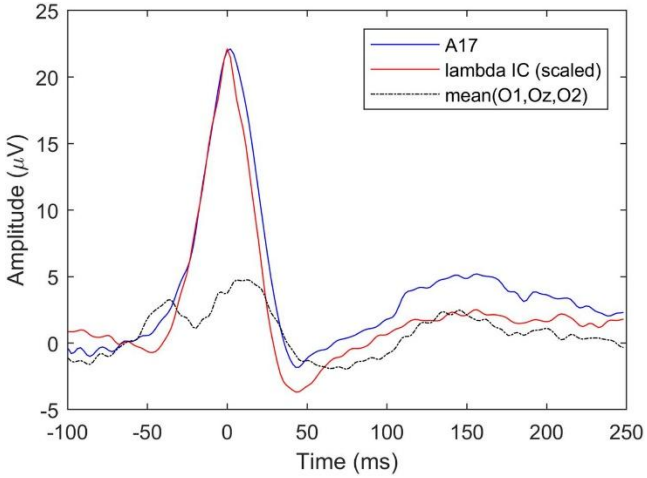

Figure 41. The average occipital O1-Oz-O2 and A17 lambda peak-locked ERPs versus the average ICA-detected lambda wave.

Lambda peak-locked comparison

The most stringent comparison used lambda peak locked averages (Figure 41). Instead of time locking to saccades, epochs were aligned to the peaks detected in the lambda component itself. This approach removes temporal jitter caused by variability in lambda latency across saccades; when lambda responses occur at different delays relative to saccade onset or offset, saccade locked averaging blurs the peak. Averaging lambda peak-locked epochs eliminates this blurring. Indeed, the lambda component waveform showed an extremely sharp peak at time zero (Figure 41). The occipital electrode waveforms also showed clear peaks aligned with the component, though with broader shapes due to source mixing at the scalp. Similarity indices for peak-locked averages were SI = 0.6954 for occipital average (somewhat lower because temporal alignment is optimized for the component rather than sensor signals) and SI = 0.9725 for electrode A17 which is the highest of all three comparison types. This very high similarity, almost near-perfect, provides strong evidence that the lambda component genuinely represents the same neural activity recorded at occipital electrodes, but with noticeably improved clarity.

Table 6 summarises similarity index values for all three comparison types, showing values for both the average occipital potential and the best single electrode, computed over the full epoch and also over a restricted window (-50 to 50 ms around lambda peak). All similarity indices are strong, ranging from 0.69 to 0.97, indicating good to excellent match. The best single electrode consistently shows higher similarity than the average of three electrodes, suggesting optimal electrode placement matters. The restricted time window shows slightly higher similarity, indicating correspondence is strongest during the lambda response itself. Peak-locked averages show the highest similarity (SI = 0.9725), confirming that temporal jitter affects sensor-level recordings more than component-level recordings. These waveform comparisons validate that ICA-extracted lambda components genuinely represent lambda responses, showing expected temporal characteristics and high similarity with sensor-level responses while providing improved clarity through source separation.

Table 6. Waveform similarity results for full saccade-related (-50 to 200 ms) and lambda peak-locked (-100 to 250 ms) epochs

	Saccade onset-locked epochs	**Saccade offset-locked epochs**	**Lambda peak-locked epochs**
Avg (O1, Oz, O2) versus lambda IC	0.7563 (0.7137)	0.7934 (0.7854)	0.6954 (0.6922)
A17 versus lambda IC	0.9759 (0.9791)	0.9771 (0.9781)	0.9725 (0.9862)

Similarity values obtained with comparing for the lambda template only (-50 to 50 ms) are in brackets.

4.4.2 Validation through lambda peak latencies

Lambda peak latencies provide a second, independent validation of the extracted component. Using detected lambda component peaks matched to saccades, onset-related and offset-related latencies were computed for each epoch and participant. These latency distributions allow us to assess whether the temporal behaviour of the extracted component aligns with established physiological characteristics of the lambda response. If the component reflected unrelated activity, the resulting latencies would be broad, inconsistent or systematically shifted. Instead, tight clustering around the timings would indicate that the extracted component corresponds to genuine lambda activity.

Figure 42 shows the distributions compiled from all detected lambda peaks across all nine participants. The onset related latency distribution (Figure 42a) had a mean of 101.33 ms (SD = 16.98 ms), forming an approximately normal distribution centered just above 100 ms. This aligns with previous lambda research [151], which typically reports onset related peaks around 100-120 ms. The offset related latency distribution (Figure 42b) had a mean of 64.86 ms (SD = 16.13 ms), again approximately normal and centered around 65 ms, matching the expected 60-80 ms range reported in the literature [151]. These results demonstrate that the ICA-detected peaks occur precisely within the expected physiological windows, providing strong validation that the extracted component reflects genuine lambda responses rather than spurious peaks or misidentified sources.

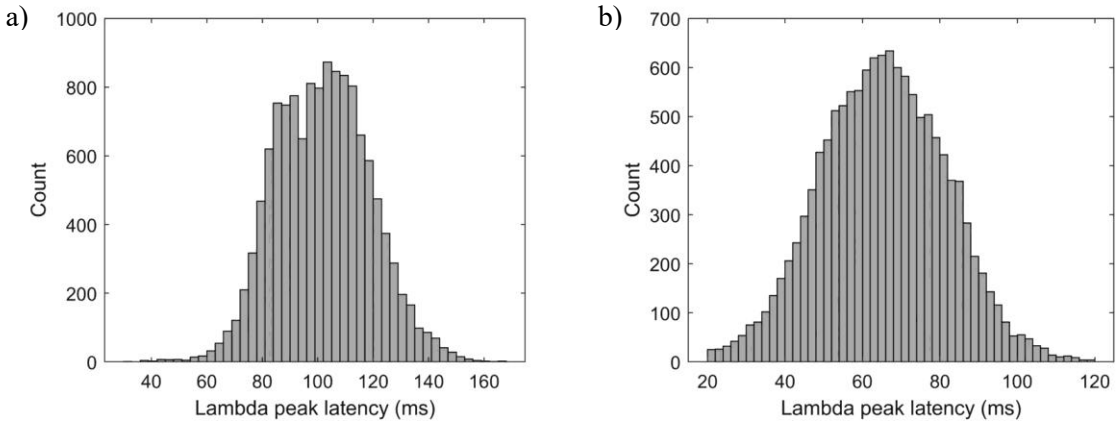

Figure 42. Distributions of all detected lambda peaks across the nine participants. (a) Onset-related latencies, approximately normally distributed around 100 ms. (b) Offset-related latencies, approximately normally distributed around 65 ms.

4.4.3 Validation through ground truth testing

The third validation approach uses synthetic data with known properties. Synthetic lambda signals was designed to mimic real lambda responses: triangular waveform shape with sharp rise and gradual decay, appropriate temporal characteristics (peak width ~100-150 ms), spectral content dominated by low frequencies (<30 Hz), occipital spatial distribution and time-locked to saccade offsets with realistic latency (~60-80 ms).

These synthetic signals were added to the real EEG data at various signal-to-noise ratios, applied them at different preprocessing pipelines and tested whether ICA could successfully extract them. Across a range of signal-to-noise ratios and preprocessing parameters, ICA successfully identified and extracted the synthetic lambda component. The extracted component showed high similarity with the original synthetic signal, confirming that ICA can separate lambda-like signals from background activity.

While synthetic signals are necessarily simplified compared to real neural activity, this ground truth validation provides important confirmation that ICA's mathematical principles are sound for lambda detection. Combined with the waveform-morphology and timing validations,

the combined evidence from all three independent approaches demonstrates that ICA genuinely detects lambda responses.

These three validation approaches (waveform morphology, timing verification and ground truth testing) all converged on the same conclusion: the identified components genuinely represent lambda responses. With this validation established using a standard preprocessing pipeline (512 Hz, 1 Hz high-pass, 40 Hz low-pass), the next step was to investigate how different preprocessing parameters influence ICA's ability to reliably detect lambda components. This systematic exploration was designed to determine which preprocessing choices are critical for successful detection and which parameters allow greater flexibility.

4.5 Effects of preprocessing parameters on ICA decomposition quality

In this section, since ICA had been shown to detect lambda components using a standard preprocessing pipeline (Section 4.3), next is to systematically test how different preprocessing parameters affect whether ICA can recover the lambda-related component. Manually searching for the lambda component among ~127 ICA outputs is tedious, time-consuming, subjective and not scalable, especially because component order and polarity vary across runs. To address this, we developed an automated single-trial lambda identification method that selects components based on the defining spatial and temporal characteristics of the lambda response.

The method first identifies components whose scalp-projected activity shows a clear maximum over the occipito-parietal region, defined a priori as electrodes A15-A31 in the Biosemi 128-channel layout (see Figure 18 in Section 3.2.4). This step assumes that the lambda response originates from an occipital radial equivalent dipole and therefore produces a focal activity pattern in this region. After selecting the component with the strongest occipito-parietal weighting, we performed polarity correction and applied peak detection to identify lambda responses. When eye-tracker data were available, peaks were accepted only if they occurred within 40-140 ms after saccade offset. When eye-tracker data were not available, peaks were detected using predefined prominence and interpeak distance thresholds, and only peaks whose inferred saccade-related latency fell within the expected 40-100 ms interval were retained. This procedure provides an objective and reproducible way to identify the lambda component and its corresponding peaks, and its performance was evaluated using Type I and Type II error rates relative to expert manual identification.

In total, 144 preprocessing combinations were tested: 3 sampling rates (512, 1024, 2048 Hz) × 4 high-pass filter cutoffs (0.1, 0.5, 1, 2 Hz) × 3 low-pass filter cutoffs (40, 80, 128 Hz) × 4 data length conditions (25%, 50%, 75%, 100%). These variations were necessary because the lambda response is small and temporally sharp, thus, filtering choices can either preserve its shape or distort it, which directly affects whether ICA can separate it as a distinct component.

4.5.1 Preprocessing considerations and pipeline implementation

The quality and interpretability of ICA decomposition are significantly influenced by preprocessing choices made before applying ICA to the EEG data [158], [159]. In general, filtering, referencing, channel handling and data length, all influence the statistical properties of the data and therefore the stability of the ICA. In the present study, these theoretical considerations guided the design of the preprocessing pipeline implemented in EEGLAB v2023.1 [152] running on MATLAB (R2023b) [141].

Filtering is a critical step because ICA assumes stationarity and independence. All filtering was performed using zero-phase FIR filters provided by EEGLAB's *pop_eegfiltnew* function. Filter steepness was determined automatically by the function based on the cutoff frequency and sampling rate, producing transition bands across the three sampling rates (512, 1024, 2048 Hz). High-pass filtering removes slow drifts and DC offsets, while low-pass filtering attenuates high-frequency noise and muscle artefacts. However, overly aggressive filtering can distort temporal structure and introduce artefacts [52]. To systematically evaluate these effects, high-pass cutoffs of 0.1-2 Hz and low-pass cutoffs of 40-128 Hz were tested.

Referencing also affects ICA because it changes the spatial distribution of the data. An average reference was used, as it removes the global mean field and often improves component independence [52]. Bad channels were identified through visual inspection and interpolated

using spherical splines [47]. While interpolation prevents noisy channels from dominating ICA, it also introduces spatial correlations [160], so interpolation was limited to cases where channels were clearly unusable.

Data length is another major determinant of ICA quality. Stable decomposition typically requires at least 20-30 times the square of the number of channels in time points [52], [161]. To assess this dependency directly, ICA performance was evaluated using 25%, 50%, 75% and 100% of the available continuous data (approximately 18 minutes of viewing time).

Based on these principles, each preprocessing configuration was defined as pipeline(fs, HP, LP), where *fs* is the sampling rate, *HP* the high-pass cutoff and *LP* the low-pass cutoff. The full preprocessing pipeline (Figure 43) consisted of:

1. **Resampling**: Raw data recorded at 2048 Hz were downsampled to 512, 1024 or 2048 Hz using EEGLAB's *pop_resample* function with anti-aliasing filtering. Lower sampling rates speed up processing while maintaining adequate temporal resolution for lambda responses.
2. **High-pass filtering**: Zero-phase FIR filters were applied at cutoffs of 0.1, 0.5, 1 or 2 Hz.
3. **Low-pass filtering**: Zero-phase FIR filters were also applied at cutoffs of 40, 80 or 128 Hz. For most analyses, 40 Hz was sufficient as it preserves all standard EEG frequency bands.
4. **Bad channel detection and interpolation**: Due to the small participant number, bad channels were identified through manual visual inspection. Three participants had bad electrodes: 8 channels for participant S2, 1 for S6 and 2 for S7.
5. **ICA decomposition**: The Extended Infomax algorithm [116] were then applied where it was implemented in EEGLAB's *runica* function, to the continuous (non-epoched) EEG data. Extended Infomax is an extension of the classic Infomax algorithm that handles both subgaussian and supergaussian source distributions. ICA produces as many independent components as input channels (126-128 components after bad channel interpolation). Further details on ICA are provided in Chapter 2 (Section 2.5).
6. **Component classification**: ICLabel, a machine learning classifier, was computed for automated component classification. ICLabel assigns each component to one of seven categories: brain activity, eye artefacts, muscle artefacts, heart artefacts, line noise, channel noise or other.
7. **Epoching**: As the final step, data were segmented into 13-second epochs spanning -2 to 11 seconds relative to stimulus (painting) onset. Each epoch included the full trial: 2 second pre-stimulus (that include the last 1 second response period and 1 second cue), 8-second painting and first 3 seconds of response period. Importantly, epoching was performed after ICA decomposition because ICA generally works better on longer continuous data segments.

These preprocessing decisions were essential not only for achieving high-quality ICA decomposition but also for ensuring that subsequent analyses (particularly the evaluation of lambda component reliability) were based on physiologically meaningful and interpretable components.

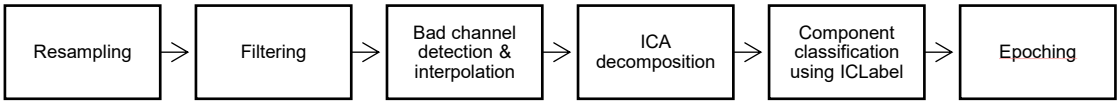

Figure 43. Overview of preprocessing pipeline and variable parameters.

4.5.2 Systematic exploration of the parameter space

To evaluate how preprocessing choices influence ICA's ability to recover the lambda component, the automated identification method described in Section 4.5 was applied to all 144 preprocessing pipelines. Each pipeline represented a unique combination of sampling rate, high-pass cutoff, low-pass cutoff and data length. ICA was also run separately for every configuration. For each decomposition, the method selected the component with the strongest

occipito-parietal projection and then applied polarity correction and peak detection to determine whether a valid lambda response was present. This approach allowed us to quantify for eavery preprocessing setting, whether ICA could successfully isolate and recovered the lambda-related component.

First, all 36 out of total 144 preprocessing combinations using 0.1 Hz high-pass filtering failed to produce identifiable lambda components. None one of these pipelines successfully extracted a lambda component for any participant. This represents zero percent detection rate for this sensitivity test. This finding is prominent because 0.1 Hz high-pass filtering is commonly used in EEG research, particularly for ERP analysis where researchers want to preserve very slow components. But for ICA-based lambda detection, 0.1 Hz filtering is completely insufficient. The likely explanation is that 0.1 Hz filtering leaves too many slow drifts and DC offsets in the data, which distort ICA decomposition by dominating the covariance structure, making it impossible to reliably separate neural sources [67].

In contrast, all 108 combinations using 0.5, 1 or 2 Hz high-pass filtering successfully produced identifiable lambda components in the representative participant used for the systematic parameter sweep. For this participant, the automated detection method correctly detected the lambda component in all 108 cases (True Positives = 108, False Negatives = 0). Thus, for the representative participant, the method achieved perfect classification performance across all 144 preprocessing configurations.

These results demonstrate that lambda component detection is a robust, reliable occurrence when appropriate preprocessing is used. As long as high-pass filter cutoff is 0.5 Hz or higher, lambda detection succeeds consistently. Figure 44 shows one epoch of the 108 successfully extracted lambda components. Despite differences in preprocessing parameters, all components show the characteristic triangular waveform pattern with peaks corresponding to saccades. This visual consistency provides initial evidence that different preprocessing parameters produce similar lambda components. In addition to waveform consistency, the extracted lambda components showed highly similar scalp topographies across all 108 successful preprocessing pipelines. Supplementary Figure A-5 in Appendix F presents the projected scalp maps of these components.

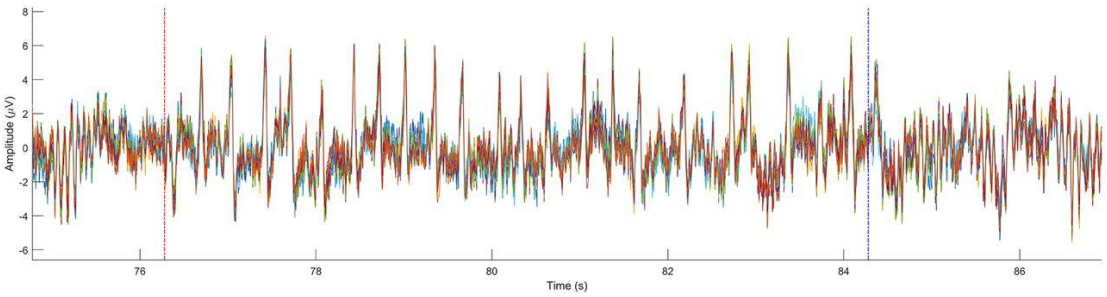

Figure 44. One epoch of the extracted lambda components obtained with different preprocessing settings. Epoch onset is marked by the red vertical line, while the offset is by the blue vertical line.

To quantify similarity between lambda components extracted under different preprocessing conditions, hierarchical cluster analysis (HCA) [162] was computed. This choice was appropriate because the primary goal was to determine whether ICA consistently identified lambda components and to compare how different preprocessing parameters affected detection quality. A pairwise correlation distances between all 108 lambda component topographies were computed, by taking one minus the Pearson correlation coefficient between component topographies, such that identical maps had a distance of zero. Then, Ward linkage clustering was then applied [163].

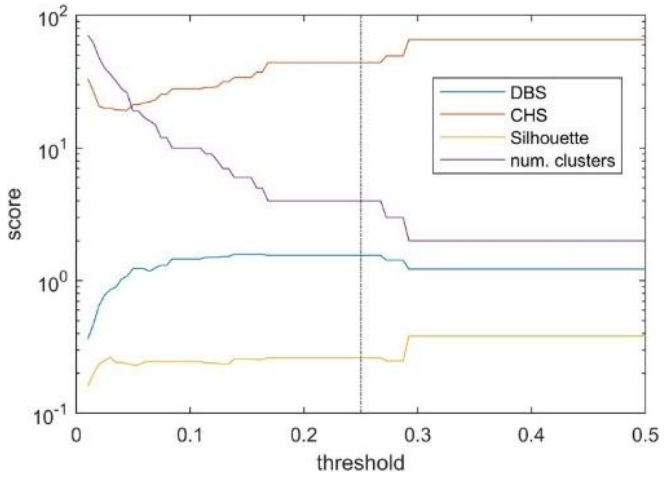

Figure 45. Clustering parameters changing in function of cluster distance metric threshold.

Using the SciPy Python package, a dendrogram representation of the hierarchical clustering was generated and cluster labels were assigned using the distance threshold derived from this structure. To identify the optimal cluster solution, cluster quality was evaluated across a range of dendrogram-cutting thresholds using three established metrics: the Silhouette score, the Calinski-Harabasz Score (CHS) and the Davies-Bouldin Score (DBS). Higher Silhouette and CHS values and lower DBS values indicated better clustering performance. The distance threshold was systematically varied, with these metrics computed at each step and the threshold that provided the best overall balance across the three measures was selected. Figure 45 shows how cluster quality metrics vary as a function of the distance threshold used to cut the dendrogram. Three metrics are plotted: Silhouette score (target: close to 1), Calinski-Harabasz Score (target: high) and Davies-Bouldin Score (target: low). Based on balanced performance across these metrics, distance threshold of 0.25 was selected, which produced four different clusters. The cluster quality metrics at this threshold were: Silhouette score = 0.26, Calinski-Harabasz Score = 44.12, Davies-Bouldin Score = 1.55. While the Silhouette score is modest (indicating clusters show some overlap), the overall pattern suggests meaningful grouping of similar lambda components.

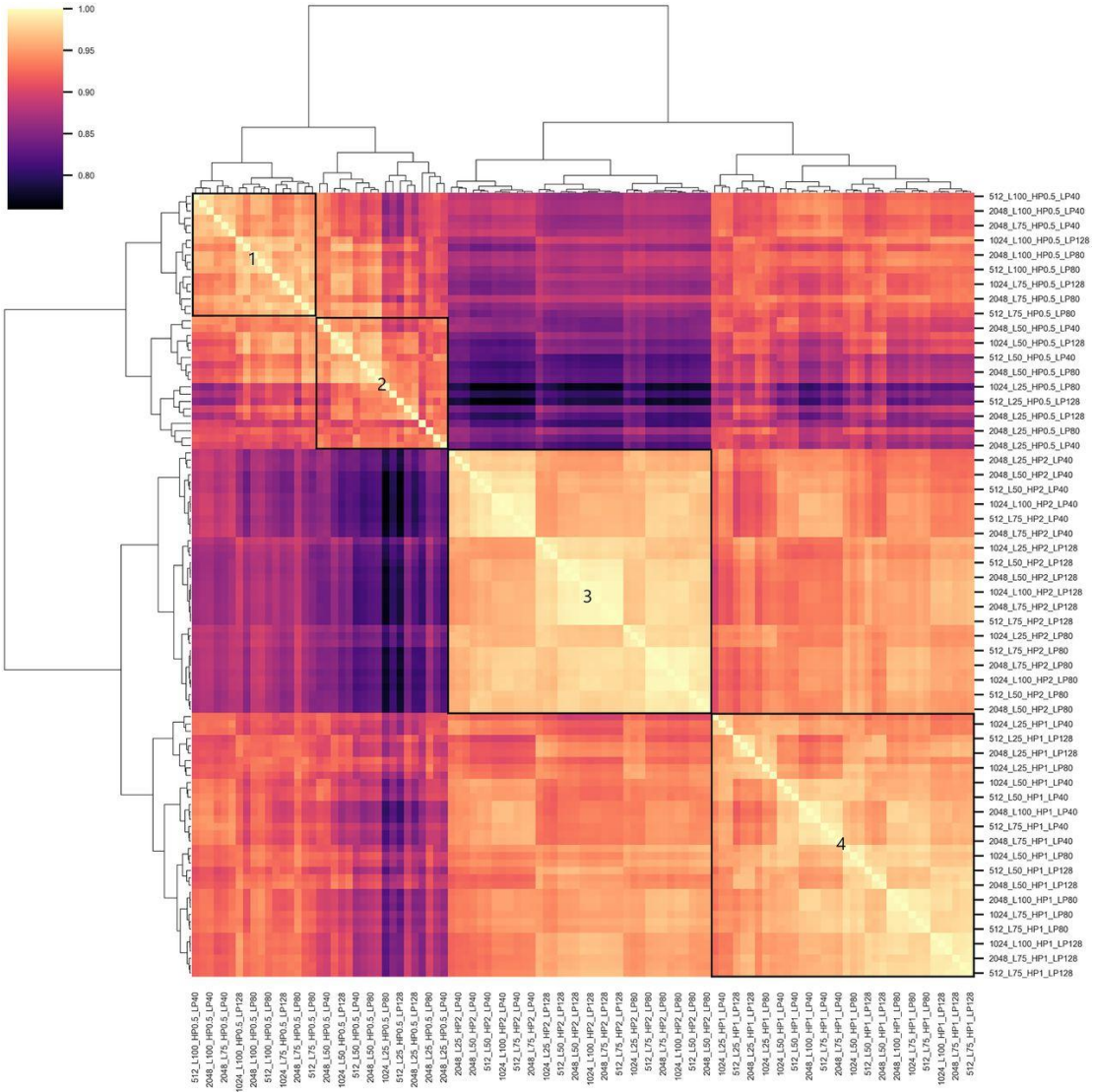

Figure 46. Visual representation of the hierarchical clustering result. Outlined squares numbered 1-4 represent the four clusters. Lighter colours indicate higher similarity between clusters and parameters.

Figure 46 shows which preprocessing settings fall into each cluster, highlighting the parameters that most strongly shape lambda component properties: Cluster 1 includes all pipelines using a 0.5 Hz high-pass filter with more than 50% of the data, whereas Cluster 2 includes all pipelines using the same 0.5 Hz high-pass filter but with 50% or less of the data. Cluster 3 contains all pipelines using a 2 Hz high-pass filter, regardless of data length or any other settings and Cluster 4 contains all pipelines using a 1 Hz high-pass filter, again independent of the remaining parameters. The detailed parameter groupings for each cluster are provided in Table A-1 in Appendix F.

The cluster structure shows a clear hierarchy: the high-pass filter cutoff is the most critical parameter, as it determines whether lambda detection succeeds at all (0.1 Hz fails completely, whereas ≥0.5 Hz succeeds reliably) and drives cluster membership more than any other factor. Data length is the second most important parameter; under 0.5 Hz filtering, longer datasets fall into Cluster 1 and shorter datasets into Cluster 2, but for 1 and 2 Hz filters, all data lengths cluster together, indicating that sufficiently strong high-pass filtering (≥1.0 Hz) makes lambda detection more robust to variations in data quantity. Sampling rate and low-pass filter settings are the least influential, as they do not affect cluster membership. Components with different sampling rates or low-pass filters cluster together as long as they have the same high-pass filter and similar data length. Based on these findings, the recommended setting is to: (1) use a high-

pass filter of at least 0.5 Hz, with 1 or 2 Hz preferred because it consistently forms its own stable cluster; (2) ensure at least 50% of the available data to support reliable lambda detection and (3) treat sampling rate and low-pass filtering as flexible parameters, as rates of 512 Hz or higher and low-pass cutoffs up to 128 Hz are fully sufficient for ICA performance in this context.

4.6 Single-trial lambda detection

Following the validation and preprocessing analysis, the final step was to determine whether the extracted lambda component preserve the temporal precision to support single-trial analysis. Although averaged waveforms confirm the presence of a reliable lambda response, individual saccades can differ in timing and visual input especially in free viewing settings. For this reason, it is important to determine whether ICA-extracted component is precise enough to be detected on single-trials, where natural viewing behaviour happens.

Component identification

After ICA decomposition, each dataset produced approximately 126-128 independent components per participant. To identify which component reflected the lambda response, a semi-automated procedure was applied based on its known spatial and temporal characteristics. Candidate components were first screened for an occipital scalp distribution classified as "brain" by ICLabel. Temporal validation was then applied to these candidates. The lambda component was expected to show a characteristic triangular waveform with a sharp positive peak, to be active during the 8-second painting-viewing periods but relatively quiet during blank response intervals and to exhibit clear consistent positive peaks occurring 60-120 ms after saccade offset. Together, these criteria demonstrated that the selected component reflected physiologically meaningful saccade-related visual activity rather than general occipital fluctuations.

Single-trial peak extraction

Individual lambda peaks were extracted from the identified component time course using a saccade-assisted detection approach. For each saccade offset detected by the eye-tracker, a search window from 40 to 140 ms post-offset was defined, covering the expected latency range for offset-related lambda responses reported in previous research. Within this window, the maximum positive peak in the lambda component's time course was identified using MATLAB's *findpeaks* function and its latency as well as amplitude were recorded. This procedure allows lambda responses to be quantified on a trial-by-trial basis while preserving their temporal alignment with independently measured eye movement events, thus, maintaining physiological validity.

In addition, a prominence-based detection approach was tested for situations where eye-tracking data are unavailable. This method identified peaks directly from the component time course using minimum prominence and inter-peak distance criteria. While this approach allows application to EEG-only datasets, the absence of independent saccade timing limits its ability to verify that detected peaks correspond to true lambda responses.

Detection performance

Using eye-tracking to assist peak detection, mean detection rate of 85.42% (SD = 9.29%) was achieved. This means lambda peaks were detected following approximately 85 out of every 100 saccades which is considered a high rate allowing reliable single-trial analysis. Table 7 summarises the results for each participant, including the number of saccades detected by eye-tracker, number of analysed saccade-offset epochs, number of matched saccade-lambda pairs and the resulting detection rate. For example, participant S7 had 1593 saccades detected but only 1200 matched pairs, resulting in 76.9% detection rate. The remaining saccades not producing detected lambda peaks likely reflect several factors: (1) very small lambda responses following microsaccades that bring minimal new visual information, (2) saccades undetected by eye-tracker, particularly very small saccades below the detection threshold, (3) lambda peaks outside the search window due to unusually early or late responses or (4)

overlapping responses from closely-spaced saccades (<200 ms apart) making individual peak detection difficult.

Table 7. Lambda peak extraction results of the saccade-assisted peak detection

Participant	Num. eye-tracker saccades	Num. saccade offset epochs	Num. detected saccade–lambda pairs (%)
S1	2,210	2,157	1,753 (81.3%)
S2	1,903	1,868	1,481 (79.3%)
S3	2,052	2,013	1,919 (95.3%)
S4	2,034	1,984	1,592 (80.2%)
S5	1,462	1,417	950 (67.0%)
S6	1,660	1,625	1,429 (87.9%)
S7	1,593	1,560	1,200 (76.9%)
S8	1,724	1,688	1,611 (95.4%)
S9	1,540	1,503	1,375 (91.5%)

Table 8 presents results for the prominence-based method applied without eye-tracking information (prominence ≥3.0 and interpeak distance ≥140 ms). This method successfully detected lambda peaks across all participants with patterns generally similar to those obtained using the saccade-assisted method. Its main advantage is that it can be applied to datasets that lack eye-tracking information, making it suitable for archival EEG recordings. However, without saccade timing, it is not possible to independently verify whether each detected peak corresponds to a true saccade-locked lambda response. As a result, this cannot distinguish genuine lambda peaks from other occipital transients and therefore cannot provide the same level of validation as the eye-tracker-assisted approach.

Table 8. Lambda peak extraction results obtained without saccade information

Participant	Num. eye-tracker saccades	Num. detected lambda peaks
S1	2,210	2,718
S2	1,903	2,158
S3	2,052	2,411
S4	2,034	1,469
S5	1,462	1,167
S6	1,660	1,730
S7	1,593	1,906
S8	1,724	2,021
S9	1,540	1,921

The single-trial lambda peak detection for one data segment was illustrated in Figure 47. The lambda component time course (blue) shows detected peaks marked. Saccade onsets (black dashed lines) and offsets (red dashed lines) are superimposed. Most saccade offsets are followed by detected lambda peaks within the expected latency window, showing successful matching. However, three potential lambda peaks could not be matched with saccades as these might represent responses following undetected saccades or spurious peaks. Taken together, these results demonstrate that the ICA-extracted lambda component preserved the temporal structure of the response with sufficient precision to support single-trial measurement during natural viewing.

To contextualise these single-trial dynamics at the scalp level, Figure 48 presents the corresponding lambda-locked ERP topographies. The maps are time-locked to the lambda peak at 0 ms and reveal the expected occipital positivity at peak latency. Pre-lambda activity from -50 ms to -20 ms shows ocular activity consistent with saccade-fixation transitions. Following the peak, the distribution shifts toward frontal-central regions between ~45 ms and 115 ms, suggesting additional processing beyond the primary visual response. From ~120 ms to 165 ms, the activity returns to an occipital pattern, potentially reflecting a subsequent, overlapping lambda component.

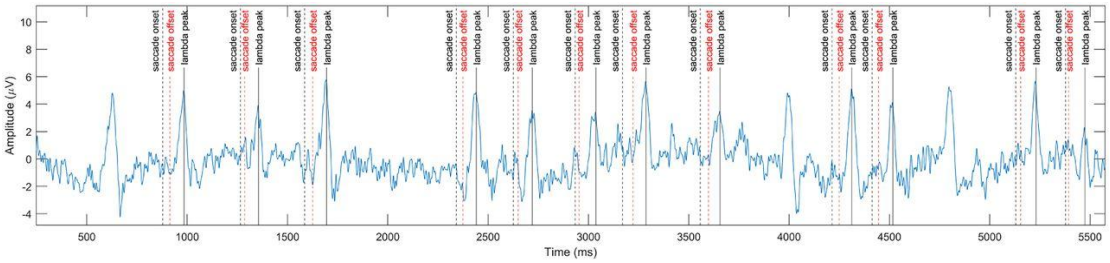

Figure 47. Illustration of the ICA-detected lambda waves (positive-going peaks in blue) with matching saccade onsets and offsets marked by black and red dashed vertical lines, respectively. Three potential lambda peaks could not be matched with saccades as the corresponding saccades were not registered by the eye-tracker.

4.7 Discussion

This study validated ICA for detecting and extracting lambda responses from continuous EEG during naturalistic viewing. The findings establish that ICA reliably identifies lambda components during naturalistic viewing when appropriate preprocessing is used, provide evidence-based parameter recommendations and enable single-trial lambda peak detection. This section interprets these findings, discusses methodological implications, addresses practical applications, acknowledges limitations and bridges to future component-space connectivity research.

4.7.1 ICA reliably detects lambda components with appropriate preprocessing

The most fundamental finding is that ICA successfully detected lambda components in all nine participants when high-pass filtering was set to 0.5 Hz or higher and a 100% detection rate across 108 different preprocessing combinations. This success sharply contrast to the complete failure of all 36 pipelines using 0.1 Hz high-pass filtering, which detected zero lambda components. This outcome on high-pass filter cutoff has important implications [67], [68], [153]. It demonstrates that ICA reliability is not a matter of subtle optimisation or minor parameter tweaking. Rather, there is a critical threshold: inadequate high-pass filtering prevents ICA from working at all, while adequate filtering enables consistent, reliable performance.

ICA identifies independent components by analysing the covariance structure of the data which essentially, it looks for patterns in how different electrodes' signals vary together over time. When slow drifts and DC offsets dominate the data (as occurs with 0.1 Hz filtering), they create strong, artefactual covariance patterns that overwhelm the more subtle patterns reflecting genuine neural sources [54], [67], [152]. ICA attempts to explain these dominant slow variations, producing components that capture drifts rather than neural activity. With adequate high-pass filtering (≥0.5 Hz), these problematic slow variations are removed before ICA, therefore, allowing the algorithm to focus on the covariance patterns reflecting neural sources. The lambda response becomes clearly separable from other activity. Previous research by Winkler et al. (2015) [67] has emphasised the importance of high-pass filtering for ICA, but typically in the context of artefact removal rather than neural component extraction. The findings from this current study thus extend their work by demonstrating that high-pass filtering is critical for extracting neural components of interest, not just for removing artefacts [44], [53], [161].

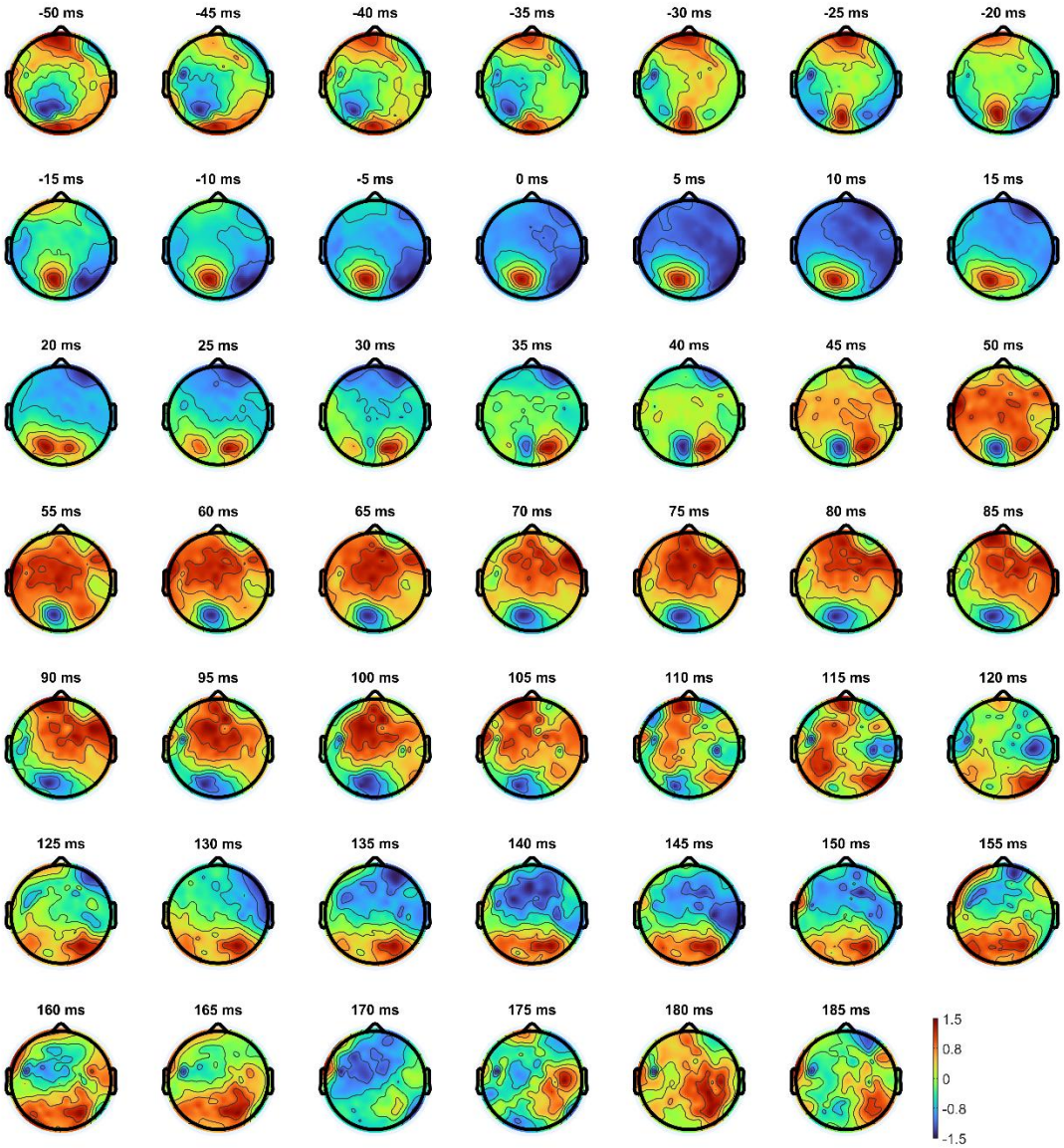

Figure 48. Scalp topographies of lambda-locked ERP activity. Maps are time-locked to the lambda peak at 0 ms. Warmer colours indicate more positive ERP amplitudes and cooler colours indicate negative amplitudes.

Beyond that, the hierarchical clustering of successfully extracted lambda components revealed a clear parameter hierarchy. High-pass filter cutoff was the dominant factor determining cluster membership as all four identified clusters were defined primarily by their high-pass setting (0.5 Hz split by data length, 1 Hz or 2 Hz). Data length was the second important factor, affecting cluster membership within the 0.5 Hz condition but not for 1 or 2 Hz. Sampling rate and low-pass filter had minimal effects, with components clustering together regardless of these settings. This hierarchy provides practical guidance: researchers should prioritise getting the high-pass filter right (use ≥0.5 Hz, preferably 1 Hz), aim for adequate data length (≥50% of the recording) and be flexible about sampling rate and low-pass filter within reasonable ranges. The fact that 1 Hz filtering formed its own distinct cluster suggests this setting may represent an optimal balance. It's aggressive enough to remove problematic slow artefacts but not so aggressive that it begins distorting the lambda responses themselves, which have some low-frequency content. The 2 Hz setting also worked but formed a separate cluster, suggesting it produces slightly different component characteristics.

4.7.2 Multiple validation approaches

Multiple validation approaches were used in this study and all of them pointed to the same conclusion: the ICA-extracted components genuinely represent lambda responses. In the waveform morphology validation, the lambda component waveforms closely matched the well-known triangular lambda pattern described in earlier work [146], [149], [151], [157], [164]. Similarity indices reached 0.97 for peak-locked averages, indicating that the component reflects the same neural activity seen at the sensor level, but with clearer separation from overlapping processes. The sharper and more distinct component waveforms suggest that ICA successfully isolated lambda activity from other neural and artefactual sources. In the timing validation, lambda peak latencies aligned almost exactly with established values in the literature which is around 100-120 ms for onset-related peaks and 60-80 ms for offset-related peaks [146], [151], [164]. This precise match provides strong evidence that the extracted component reflects genuine lambda activity rather than unrelated saccade-locked signals. Ground truth validation using synthetic lambda signals also further confirmed that ICA can extract known lambda-like activity from background EEG. These results also mirrored previous findings that 0.1 Hz high-pass filtering leaves slow drifts that disrupt ICA decomposition, whereas higher cutoffs support stable source separation [67], [68].

The convergence of these three independent validation approaches provides much stronger support than any single method alone. Each approach has limitations, but when all three point to the same conclusion, alternative explanations become highly unlikely.

4.7.3 Single-trial detection enables new research directions

The 85.42% lambda peak detection rate indicates that ICA enables reliable single-trial analysis without the need for signal averaging. Through this capability, several research directions that were previously inaccessible can now be explored. Trial-by-trial variability, which is typically obscured by averaging-based approaches, can now be examined directly. Questions such as whether lambda amplitude varies with attention, whether lambda latency changes with cognitive load, or how lambda responses evolve across time can now be addressed. With 85% single-trial detection accuracy, lambda properties can be correlated with behavioural measures on individual trials, changes across successive saccades can be studied and factors influencing lambda strength can be investigated.

The proposed method can also be useful in visual perception studies analysing individual single-trial lambda peaks without signal averaging that can lead to improved temporal resolution and the extraction of more accurate peak features (amplitude, latency, peak width). It can also be combined with the analysis of other occipito-parietal independent components to understand the correlation between unmixed activation sources during perception.

However, there is a limitation. There were partial saccades that the eye-tracker could not register correctly therefore were not included in the saccade-peak matching process, leaving potential lambda peaks unmatched. In some cases, saccades followed one another quickly producing overlap effects on the lambda peaks.

4.7.4 Implications for visual perception research

Beyond methodological contributions, several implications for the study of visual perception and eye movement control can be drawn from this work. Lambda responses during naturalistic viewing were shown to be reliably detectable during free exploration of complex stimuli, in contrast to most previous lambda research, which relied on controlled laboratory paradigms with fixed targets and uniform backgrounds. By demonstrating reliable detection during genuine aesthetic exploration of art paintings, the methodology is extended to more ecologically valid conditions. This suggests that lambda responses can now be examined in real-world contexts such as reading, scene perception, social interaction and other natural behaviours.

Lambda responses as markers of visual processing are supported by the tight coupling between saccades and lambda peaks, reflected in the 85% detection rate. This coupling indicates that lambda responses reliably mark the arrival and processing of new visual information following each eye movement, making them useful temporal markers for analysing visual

processing dynamics. Potential applications include examining how quickly visual information is processed at different fixation locations, how processing evolves across successive fixations during scene exploration and how lambda responses are modulated by top-down attention or expectations.

An additional implication concerns indirect eye movement information. It was observed that lambda peak detection can provide information about saccade timing even without dedicated eye-tracking. Although eye-tracking was used for validation in this study, the lambda component itself exhibits clear peaks that could be detected in the absence of eye-tracking data. This may be useful for analysing EEG datasets that lack eye-tracking recordings, although eye-tracking remains the gold standard for precise gaze position measurement.

Finally, implications arise for saccade-related artefact handling. For researchers focused on other cognitive processes, lambda responses may act as nuisance artefacts that contaminate signals of interest. The validated methodology presented here offers tools for identifying and removing lambda components when they are unwanted. Alternatively, lambda component activity could be used to regress out saccade-related activity from sensor-level data, improving the interpretability of non-oculomotor EEG signals.

4.7.5 Limitations and future directions

Several limitations should be acknowledged. The study was conducted with a limited participant sample of nine individuals, which is adequate for methodological validation but insufficient for examining individual differences. Larger samples would allow investigation into whether lambda detection reliability varies with factors such as age, visual acuity or oculomotor characteristics. A single experimental paradigm was used, focused on art viewing with free exploration. However, validation across additional paradigms such as reading, scene perception, visual search and controlled saccade tasks, would be valuable for establishing generalisability.

No testing of false detections was performed, because the automated identification method was not evaluated on datasets in which lambda responses are not expected. Future work should assess whether false positives occur under such conditions. Limited saccade parameter analysis was also conducted. Although lambda detection was shown to be independent of saccade amplitude, systematic analyses of relationships between saccade parameters (amplitude, direction, velocity) and lambda properties (amplitude, latency, duration) were not undertaken, leaving a substantial opportunity for future research.

In addition, component-space connectivity was not implemented in this chapter. While ICA was validated for component extraction, the application of component-space connectivity analysis remains a future direction, as discussed in Chapter 5. The present validation provides the necessary foundation, but the full application to aesthetic perception data awaits further development.

Several future directions occur from this work. The validated methodology can be applied to the aesthetic perception dataset from Chapter 3 to identify lambda and other visual components. Systematic investigation of saccade-lambda relationships can be pursued to examine how lambda properties are modulated by saccade parameters and stimulus characteristics. The approach can be extended to component-space connectivity, applying the validated preprocessing and identification methods to connectivity analyses between ICA components. Finally, testing across diverse paradigms and populations will be essential for establishing the generalisability of the methodology.

4.7.6 Moving towards component-space connectivity

The broader motivation for this validation work is to establish a methodological foundation for component-space connectivity analysis, the potential future direction outlined in Chapter 5. The analyses in this chapter provide the groundwork necessary for moving from sensor-level connectivity to a more anatomically interpretable component-level framework.

Sensor-space connectivity, as discussed in Chapter 3, is fundamentally constrained by source mixing [34], [106]. Although metrics such as dwPLI substantially reduce the influence of volume conduction, they cannot fully resolve the fact that each electrode records a mixture

of signals from multiple neural sources. As a result, the connectivity patterns observed between abstract and figurative art reflect meaningful network-level dynamics but cannot be interpreted as precise anatomical interactions. Component-space connectivity offers a potential solution by estimating connectivity between ICA components rather than between electrodes. Because ICA components are maximally independent by construction, connectivity between components is less susceptible to volume conduction and source mixing and therefore has the potential to provide more interpretable understandings into functional interactions.

The validation work in this chapter establishes several essential prerequisites for such an approach. First, it demonstrates that ICA can reliably extract neural components when appropriate preprocessing is applied [67], [153]. This reliability is crucial; without it, any attempt to compute connectivity between components would lack methodological validity. Second, the analyses identify preprocessing parameters such as the optimal high-pass filter cutoff and the minimum data length that can be directly applied to the aesthetic-perception dataset introduced in Chapter 3. Third, the chapter develops and validates automated procedures for identifying components based on their spatial and temporal characteristics. Although applied here to lambda components, the same framework can be adapted to identify components relevant to aesthetic perception, such as those associated with visual processing, attention or evaluative processes. Finally, the chapter establishes a general validation strategy using components with well-defined physiological properties, providing a template for validating other component classes in future work.

Several steps remain before component-space connectivity can be fully implemented. Aesthetic-related components must first be identified in the dataset used in Chapter 3, based on the identification framework developed in this chapter. These components then require validation through experimental manipulations or behavioural correlates to ensure that they reflect genuine cognitive processes. Once validated, connectivity can be computed between components using dwPLI or other robust metrics. The resulting component-space networks can then be compared with the sensor-space connectivity patterns reported in Chapter 3 to determine whether component-level analysis offers additional insight or improved interpretability. Ultimately, these networks can be interpreted in terms of aesthetic processing, linking connectivity patterns to perceptual, attentional and evaluative mechanisms.

This sequence, moving from validating ICA reliability in the present chapter to applying component-level connectivity in future work, reflects a careful and rigorous methodological strategy. By first testing the approach on a component with clear and objective validation criteria, a solid foundation is established for later analyses. This ensures that future applications of ICA-based connectivity methods are both robust and scientifically defensible.

4.8 Conclusion

This chapter demonstrated that ICA can reliably extract physiologically meaningful lambda responses from continuous EEG recorded during naturalistic viewing. By systematically varying preprocessing parameters, I showed that successful lambda recovery depends primarily on adequate high-pass filtering: cutoffs of 0.5 Hz or higher consistently supported stable ICA decomposition, whereas 0.1 Hz filtering failed to isolate the component. High-pass filtering came out as the dominant factor influencing ICA performance, whereas sampling rate and low-pass filtering had comparatively limited effects.

The extracted components exhibited all defining characteristics of the lambda response, including occipito-parietal topographies, fixation-locked timing within the expected physiological range and strong correspondence with sensor-level activity. The automated identification procedure further demonstrated that lambda components can be detected objectively and reproducibly, enabling consistent analysis without manual inspection. Crucially, ICA preserved the temporal precision of the underlying neural source, allowing lambda responses to be detected on a single-trial, fixation-by-fixation basis.

This is important because lambda responses provide a reliable physiological marker of early visual processing at each fixation. During naturalistic viewing, participants make many spontaneous fixations across an extended viewing period and these events occur at

unpredictable times. Traditional stimulus-locked averaging cannot capture this continuous neural activity. By establishing that ICA can isolate lambda responses robustly and at single-trial level, this chapter provides a method for extracting accurate markers of fixation-related processing throughout natural viewing.

However, while ICA enables reliable recovery of fixation-locked components, the broader challenge is to understand how these components and the networks they reflect can contribute to the unfolding of aesthetic perception over the full viewing interval. The next chapter therefore integrates the findings from connectivity analysis, fixation-locked dynamics and preprocessing validation to develop a unified framework for studying naturalistic aesthetic perception and to outline how component-space approaches can advance future research.

5. GENERAL DISCUSSION

5.1 Overview of thesis contributions

This thesis addressed three interconnected methodological and conceptual gaps identified in Chapter 1: (1) the limited application of robust connectivity methods to aesthetic perception, (2) the lack of physiological understanding of fixation-locked neural activity during naturalistic viewing, and (3) the insufficient validation of ICA for extracting cognitive EEG components. Chapters 3 and 4 addressed these gaps through complementary empirical studies that together form a coherent methodological foundation for future EEG connectivity research.

Chapter 3 demonstrated that sensor space connectivity, when analysed at theoretically motivated processing stages, can reveal meaningful differences between abstract and figurative art. Although the analysis did not track continuous dynamic connectivity, the use of discrete time windows which corresponding to early, intermediate and late perceptual stages, thus, allowed a structured investigation on how functional networks reorganise as aesthetic perception unfolds. These findings align with multistage models of aesthetic processing and support the idea that different artistic styles engage distinct perceptual and semantic processes. Importantly, the use of the dwPLI ensured that the observed differences were not driven by volume conduction artefacts, but instead reflected genuine differences in phase based coordination.

Chapter 4 established a validated framework for ICA decomposition using fixation-locked lambda responses as a physiological ground truth. Lambda responses are well-characterised occipital potentials that occur 70-120 ms after fixation onset and reflect early visual processing. Their temporal precision and physiological details make them ideal markers for evaluating decomposition reliability of brain components. By systematically evaluating 144 preprocessing pipelines, Chapter 4 identified high-pass filtering as the key determinant of decomposition quality and demonstrated that ICA can reliably extract physiologically interpretable components when preprocessing is appropriately controlled. The chapter also introduced an automated identification framework and showed that lambda components cluster consistently across participants, providing evidence that ICA produces reproducible functional sources.

Together, these findings address the three research gaps by demonstrating that sensor space connectivity can capture meaningful cognitive differences when robust metrics are used, establishing the lambda response as a reliable fixation locked neural marker in naturalistic viewing, and providing the first systematic validation of ICA for cognitive EEG components. The remainder of this chapter outlines a roadmap for advancing EEG connectivity research, integrating theoretical perspectives, methodological innovations and open issues that remain unresolved.

5.2 Theoretical roadmap for understanding aesthetic perception

Aesthetic perception unfolds through rapid interactions between distributed neural populations, consistent with the multistage architecture described in Chapter 1 and Chapter 3. Theoretical models such as Leder's model of aesthetic appreciation [5], [6] propose that aesthetic experience comes from sequential stages of perceptual analysis, semantic processing and evaluative judgement. From a neural perspective, these stages map onto the communication-through-coherence framework [12], which emphasise that different frequency bands support distinct modes of information exchange across cortical networks. These models predict that aesthetic perception should involve temporally layered and frequency-specific patterns of functional connectivity.

The connectivity findings in Chapter 3 align closely with this theory. Distinct network patterns at early (100 ms), intermediate (300 ms) and late (500 ms) stages, indicated that the brain differentiates between abstract and figurative art from the earliest moments of visual processing and persists through later processing stages. In the early window (around 100 ms), both abstract and figurative art evoke strong occipital connectivity, consistent with initial visual analysis. However, subtle differences emerge even at this early stage, with figurative art showing stronger delta-band connectivity in left occipital and parietal regions, while abstract

art shows more widespread frontal-posterior connectivity. By the intermediate stage (around 300 ms), connectivity patterns diverge more clearly. Figurative art shows increased theta and alpha connectivity in frontoparietal networks, potentially reflecting semantic processing and object recognition. Abstract art shows stronger beta connectivity in occipital and parietal regions, possibly reflecting sustained perceptual analysis and attempts to extract meaning from non-representational forms. In the later stage (around 500 ms), these sustained connectivity differences persist, with figurative art maintaining frontoparietal networks (consistent with semantic integration) and abstract art showing widespread gamma connectivity (potentially reflecting integrative processing across multiple perceptual and cognitive systems). These findings also align with the theoretical models of aesthetic appreciation [5], [6], which proposes that different types of artworks engage processing stages to different degrees. The connectivity patterns suggest that abstract art places greater demands on perceptual processing and requires more widespread network integration, while figurative art facilitates more focused semantic processing through frontoparietal networks.

Moreover, these differences spanned delta through gamma bands and were accompanied by dynamic reorganisation of network hubs, as revealed by node strength analysis. This pattern demonstrates that sensor-space connectivity, when combined with volume conduction-insensitive metrics and high-density EEG, can provide meaningful insights into functional brain networks. Interpreting these patterns within the theoretical framework suggests that representational content modulates the feedforward sweep of visual processing. The feedforward sweep refers to the initial, rapid propagation of visual information from early sensory areas (e.g. V1) to higher-order cortical regions within the first ~100-150 ms after stimulus onset [165].

Taken together, these findings support the view that aesthetic perception is a temporally layered process in which different artistic styles recruit distinct neural mechanisms across multiple timescales. The early style related differences indicates that aesthetic processing begins during the initial feedforward sweep, while the multi frequency nature of these effects aligns with models proposing that aesthetic experience arises from coordinated activity across distributed neural systems.

5.3 Fixation-locked neural dynamics as a mechanism for naturalistic perception

A central contribution of this thesis is the demonstration that fixation-locked neural activity provides a physiologically grounded window into the temporal organisation of naturalistic perception. Unlike traditional ERP paradigms, which rely on stimulus locked averaging, FRPs align neural activity to the onset of each fixation, capturing the rapid perceptual cycles that structure real world viewing. Lambda responses, in particular, reflect early visual processing and have been shown to be sensitive to saccade magnitude, spatial frequency [145] and visual context. Their consistent temporal structure makes them ideal markers for studying perceptual processing during free viewing.

Chapter 4 demonstrated that lambda responses can be reliably extracted during naturalistic art viewing, even in the presence of variable fixation durations and complex visual input. This finding has significant theoretical implications. It suggests that aesthetic perception is not a continuous process, but rather unfolds as a sequence of discrete perceptual cycles, each anchored to a fixation. This aligns with theories of active vision [166], which propose that the visual system samples the environment through rapid, fixation aligned processing episodes. It also provides a physiological anchor for interpreting the connectivity differences observed in Chapter 3. For example, the early connectivity differences between abstract and figurative art may reflect differences in the processing of visual information during the first fixation, while the intermediate and late differences may reflect subsequent cycles of perceptual and semantic processing.

The fixation locked approach also has methodological implications. Because lambda responses have a consistent temporal structure, they provide a rare opportunity to evaluate the reliability of ICA decompositions. Chapter 4 showed that ICA can reliably extract lambda

components when preprocessing is appropriately controlled, and that these components cluster consistently across participants. This provides a foundation for using fixation-locked components as ground truth for validating decomposition methods, including band-pass ICA and component-space connectivity which will be further discussed in the next section.

5.4 Methodological roadmap for future EEG connectivity research

Several methodological advances could strengthen future work, including (1) combining validated ICA with source localisation techniques (e.g. DIPFIT, distributed source modelling) to improve anatomical interpretation, (2) exploring directed connectivity measures (e.g. Granger causality, transfer entropy) at the component level to investigate causal relationships between brain regions, (3) examining time-varying connectivity patterns using sliding-window or adaptive approaches to capture rapid network reconfigurations during aesthetic processing and (4) combining EEG with other modalities, eye-tracking or behavioural measures to provide matching evidence for functional network organisation.

5.4.1 Beyond sensor-space connectivity

Chapter 3 demonstrated that sensor space connectivity, when combined with a robust metric such as the dwPLI, can reveal meaningful differences between conditions. At the same time, several important limitations must be acknowledged. First, sensor-space connectivity cannot provide definitive anatomical localisation. While the observed patterns (e.g. frontal-occipital connectivity in alpha band, widespread delta connectivity) are interpretable in terms of broad functional networks, the precise cortical sources cannot be determined from scalp recordings alone. Second, even robust metrics like dwPLI cannot fully eliminate the influence of source mixing; they reduce but do not completely solve the volume conduction problem. Third, sensor-level analyses mix activity from multiple underlying sources, making it difficult to distinguish whether observed connectivity reflects direct interactions between specific neural populations or indirect coupling through common inputs. These limitations thus motivate a shift toward source-resolved and component-level connectivity.

Importantly, these limitations do not invalidate the findings but rather define their appropriate scope of interpretation. Since both conditions (abstract and figurative paintings) are affected by the same sensor-level constraints, the differences observed between them remain valid. The consistency of connectivity patterns across time points and frequency bands, combined with their alignment with theoretical predictions about aesthetic processing (e.g. increased semantic processing for figurative art, increased perceptual processing for abstract art), suggests that sensor-level analyses capture genuine cognitive phenomena. The significant differences observed provide valid evidence that different artistic styles engage distinct patterns of inter-regional communication, even if the precise anatomical locations cannot be resolved from sensor-level data alone. This represents a valuable contribution to understanding aesthetic perception while acknowledging the constraints of the methodology.

5.4.2 Component-space connectivity as the next step

Chapter 4 established that ICA can reliably extract physiologically meaningful brain components when preprocessing is appropriately controlled. ICA's successful separation of lambda responses from other neural and artefactual sources suggests that it should likewise be capable of decomposing the mixed sensor signals recorded during aesthetic perception (Chapter 3) into distinct neural components. Conducting connectivity analysis at the component level, rather than at the sensor level, would therefore yield estimates that are more spatially interpretable, since components represent independent sources rather than mixtures of overlapping activity.

A key advantage of component-space connectivity is its improved spatial resolution and reduced susceptibility to volume conduction. Because ICA enforces spatial independence, any temporal correlation or phase synchronisation observed between components cannot be explained by both components detecting the same underlying source [44]. This makes connectivity between components more likely to reflect genuine functional interactions rather than spurious correlations created by shared inputs.

To illustrate this, consider the sensor-level scenario where two electrodes record activity from the same neural generator. These electrodes will show high correlation simply because they share the same input. When ICA is applied, this shared activity is captured by a single component, and does not appear as connectivity between multiple components. Connectivity between components therefore reflects relationships between distinct sources. In this sense, ICA offers a practical compromise between raw sensor analysis and full source localisation [53], [167]. Source reconstruction provides the most direct way to address volume conduction but requires individual anatomical MRI scans, involves complex modelling decisions and is computationally intensive [31]. ICA, in contrast, does not require anatomical information, avoids many of these modelling assumptions and is computationally more efficient [52].

However, interpreting component topographies requires caution. Although ICA produces spatially distinct components, the resulting scalp maps do not uniquely determine their cortical generators because the EEG inverse problem allows multiple source configurations to produce the same topography [31]. Anatomical localisation should therefore be conservative. Importantly, ICA components can still be meaningfully characterised at the functional level through their temporal dynamics, frequency and connectivity patterns, which are often the primary variables of interest in studies of perception and aesthetics.

These conceptual advantages make ICA a promising framework for connectivity analysis, but several practical challenges need to be addressed before it can be applied to aesthetic perception. First, unlike lambda responses (which have objective behavioural markers from eye-tracking), aesthetic-related components lack clear ground-truth validation. Identifying which components reflect genuine cognitive processes versus residual noise or artefacts requires careful and different validation approaches. Second, determining the optimal number of components to analyse and selecting appropriate connectivity metrics for component-space analysis requires further methodological development. Third, statistical procedures for comparing component-space connectivity across conditions also need to be established.

5.4.3 Band-pass ICA as a novel approach

A promising extension is band-pass ICA, where ICA is applied to narrow-band filtered data (e.g. theta-ICA, alpha-ICA, gamma-ICA). This approach isolates oscillatory generators more cleanly, enhances frequency-specific component separation and allows direct extraction of phase time series without wavelets. It supports phase-based connectivity (e.g. PLI, PLV) at the component level and may reveal oscillatory microstates or frequency-specific functional units. Because EEG power follows a 1/f distribution, higher frequency activity (e.g. beta-gamma) has lower amplitude and is more easily masked by broadband fluctuations, narrow-band filtering can therefore increase the relative prominence of these oscillations. This will potentially help ICA to separate weak, frequency-specific sources that would otherwise be masked by stronger low frequency structure. Band-pass ICA has been explored in limited contexts [168], but remains underdeveloped and its suitability for cognitive or naturalistic EEG paradigms requires further systematic evaluation.

5.4.4 Component clustering across participants

One of the broader methodological insights that emerged from my work is the value of treating ICs not merely as artefact-free signals, but as meaningful functional units that can be analysed in their own right. Through the clustering of components across participants based on scalp maps, dipole locations and activation time courses, I was able to identify reproducible groups of sources that reflected consistent neural sources. Figure 49 illustrates this clearly. Despite coming from different participants, the independent components in this cluster share a highly similar occipital scalp distribution, forming a coherent lambda-related visual cluster. This scalp-level consistency is further supported by the anatomical localisation shown in Figure 50, where DIPFIT localisations converge on a lateral occipital source. These consistencies demonstrates that ICA can be used not only to clean the data but, it provides access to stable, physiologically interpretable sources that recur across individuals.

Importantly, this opens the door to future analyses that move beyond sensor-space connectivity. Instead of computing synchrony between electrodes, which are mixtures of

multiple sources, connectivity could be assessed directly between component clusters that represent more anatomically and functionally coherent generators. Such an approach would reduce the influence of volume conduction, improve interpretability, and allow us to examine how distinct neural sources interact during aesthetic perception. In this sense, the component-level structure revealed in my data is not only a validation of ICA's reliability but also a foundation for a more source-resolved connectivity framework in future neuroaesthetic research.

The validated ICA preprocessing guidelines from Chapter 4 can be directly applied to the aesthetic perception dataset from Chapter 3. Components can be identified using adaptations of the automated identification framework developed for lambda responses or through component-clustering approaches. Once validated, connectivity can be computed between components using dwPLI or other robust metrics and the resulting component-space networks can be compared with the sensor-space connectivity patterns reported in Chapter 3. This bridging work represents a natural next step that builds directly on the methodological foundations established in this thesis. Aside from that, the validated ICA methodology can also be extended to other cognitive domains beyond aesthetic perception. Visual search, sentence reading, scene perception and memory tasks all involve eye movements and could benefit from lambda component identification and removal. Additionally, the validation framework developed for lambda responses can be adapted to other well-characterised cognitive components (P300, N170, error-related negativity) to establish general guidelines for ICA preprocessing across cognitive paradigms.

5.4.5 Directed connectivity and causal inference

The current connectivity findings remain correlational. They do not reveal directionality, causal flow or cross frequency interactions. Addressing these theoretical questions requires methodological advances that move beyond sensor-space connectivity and incorporate source-resolved and directed connectivity approaches. Phase Slope Index (PSI) estimates directionality based on frequency-dependent phase delays and is robust to instantaneous mixing [33], but still requires source-resolved data for reliable interpretation. Orthogonalised Partial Directed Coherence (oPDC) captures time-varying directional interactions and reduces spurious flows from volume conduction [169]. Similarly, time-varying Granger causality has been applied to combined EEG/MEG data in epilepsy research, showing how multimodal approaches can reveal directed information flow [170]. Envelope-based connectivity [167], [171] captures slow fluctuations in coupling strength and may be particularly relevant for aesthetic evaluation, which unfolds over longer timescales. These methods highlight a theoretical shift from static connectivity to temporally structured, directed and frequency specific models of cognitive processing.

5.4.6 A unified pipeline for future studies

The findings from Chapters 3 and 4 suggest a unified pipeline for future EEG connectivity research. First, preprocessing should use validated ICA parameters, such as a 1 Hz high-pass filter, at least 50% of the available data, and flexible sampling rates and low-pass filter cut-offs. Data can then be band-pass filtered into different frequency bands, followed by running ICA decomposition within each band. Components can then be clustered across participants based on scalp maps, dipoles and time courses. Phase or envelope signals can be extracted from each component and directed connectivity metrics such as PSI, oPDC or Granger causality can be applied. Connectivity networks can then be compared across conditions. This pipeline integrates the validated methods from this thesis with state-of-the-art connectivity approaches, offering a path toward source-resolved, temporally structured and theoretically interpretable connectivity analysis.

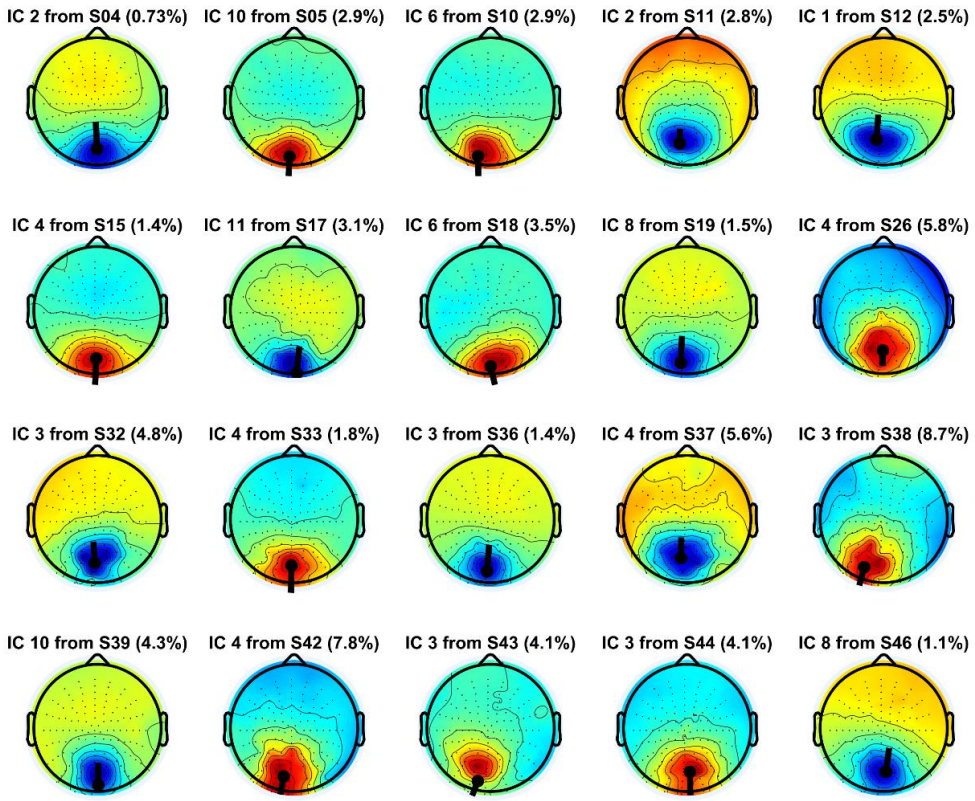

Figure 49. Independent components showing a reproducible occipital cluster corresponding to the lambda-related source across participants.

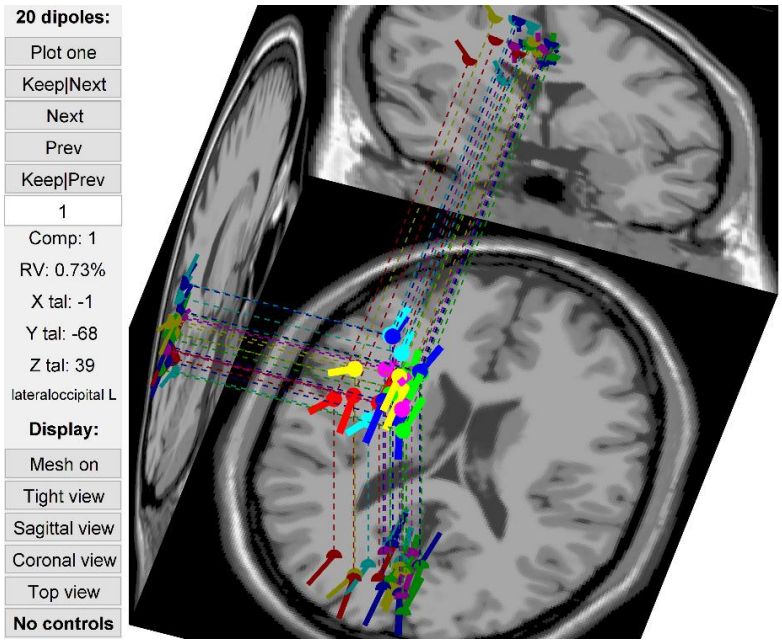

Figure 50. DIPFIT-based anatomical cluster for lambda occipital component.

5.5 Open issues in the field

Despite methodological progress, several challenges in cognitive EEG studies remain unresolved. A central issue is the lack of objective physiological markers for most cognitive components. Outside of well-defined responses such as the lambda component, many ICA components are validated only through indirect criteria such as morphology, spectral content or task modulation [77], [86], making it difficult to determine whether a component reflects a genuine neural process or residual artefact. This problem is compounded by the fact that ICA components are functional units rather than anatomical sources: because of the EEG inverse problem, scalp topographies do not uniquely specify their cortical generators and anatomical interpretations must remain cautious [31], [84]. Even in component space, residual mixing cannot be fully eliminated and some degree of shared variance between components is unavoidable.

A second open issue concerns component identity and stability across individuals. ICA does not guarantee that the same cognitive process will be represented by the same component across participants, even when preprocessing is standardised. Differences in anatomy, noise structure and individual viewing behaviour can lead to different decompositions, complicating group-level analyses and component clustering [54], [152]. Establishing reliable cross-participant correspondences remains a major challenge for component-level connectivity work.

A further open issue concerns the limited evidence available for band-pass ICA. Although the idea of applying ICA to narrow band-filtered data has been mentioned in methodological discussions, there are very few empirical EEG studies that have evaluated this approach [168] and none in cognitive or naturalistic paradigms. As a result, the field lacks consensus on when, or whether, band-pass ICA should be used for cognitive EEG studies and systematic validation is still needed before it can be confidently integrated into naturalistic or neuroaesthetic research pipelines.

Aside from that, effective connectivity methods introduce additional complications. Approaches such as Granger causality or dynamic causal modelling rely on autoregressive models that assume stable lag relationships over time, yet EEG oscillations are highly non-stationary and evolve on timescales that often exceed the temporal resolution of these models [102], [172]. As a result, effective connectivity estimates are sensitive to noise, filtering choices and the specification of temporal model order, and small preprocessing differences can lead to conflicting conclusions. Moreover, little is known about how oscillatory interactions at the component level unfold across frequency bands and cross frequency coupling remains difficult to estimate reliably in naturalistic tasks.

Free-viewing also introduces its own set of challenges. Variability in fixation patterns, saccade amplitudes and moment to moment visual input complicates the interpretation of neural responses, and the absence of trial based structure makes traditional averaging approaches less informative [146]. Preprocessing pipelines also vary widely across laboratories, and differences in filtering, referencing, ICA criteria or artefact rejection can substantially affect connectivity estimates. As a result, component level findings require careful validation across datasets before they can be considered robust markers of aesthetic perception.

5.6 Chapter summary

This chapter brought together the theoretical and methodological contributions of the thesis, showing how the findings from Chapters 3 and 4 address long standing gaps in EEG based neuroaesthetics. Sensor-space connectivity revealed that abstract and figurative paintings engage distinct, frequency-specific networks across early, intermediate and late processing stages, aligning with multistage models of aesthetic perception and communication-through-coherence accounts of cortical information flow. The fixation locked analyses demonstrated that aesthetic perception unfolds through discrete perceptual cycles locked to each fixation, and the validated lambda response provided a rare physiological benchmark for evaluating ICA reliability during naturalistic viewing. Together, these results establish a coherent framework linking theoretical models of aesthetic processing with robust empirical evidence.

Building on this foundation, the chapter outlined a methodological roadmap for advancing EEG connectivity research. Component- and source-resolved connectivity, band-pass ICA, directed connectivity metrics and unified preprocessing pipelines offer promising opportunities for improving spatial interpretability and capturing causal interactions. At the same time, several open issues remain unresolved, including the lack of physiological markers for most cognitive components, instability of component identity across individuals, uncertainties surrounding band-pass ICA, the temporal problem of effective connectivity methods and the variability introduced by free-viewing. Addressing these challenges will require systematic validation, cross-dataset comparisons and methodological standardisation. Overall, the chapter positions the thesis as both a theoretical and methodological contribution, providing a strong foundation for future work on the neural dynamics of aesthetic perception.

6. CONCLUSIONS

This thesis investigated how oscillatory activity is organised during aesthetic perception and evaluated methodological pathways that can support more precise, source-resolved interpretations of EEG data in naturalistic settings. By combining sensor-space connectivity analysis with a systematic validation of ICA, the work addressed both conceptual and technical challenges inherent in studying complex visual experiences such as art viewing. The findings demonstrated that oscillatory networks responded in frequency-specific and stimulus-dependent ways, and that ICA can reliably isolated meaningful neural generators even during long, free-viewing paradigms. Together, these results provide a foundation for integrating large-scale network dynamics with component-level representations of neural activity.

The first major conclusion concerns the nature of oscillatory connectivity during aesthetic perception. Abstract and figurative paintings engage distinct patterns of synchronisation across delta, theta, alpha, beta and gamma bands. These patterns were not uniform across time but evolved across the early stages of viewing, suggesting that aesthetic perception involves dynamic reorganisation of functional networks. While sensor-space connectivity remained affected by volume conduction, the consistent differences observed across conditions indicated that oscillatory interactions played a meaningful role in shaping how viewers processed visual complexity, extracted meaning and formed aesthetic impressions.

The second major conclusion related to the reliability of ICA in naturalistic EEG paradigms. The validation work in Chapter 4 showed that ICA consistently recovered the fixation-related lambda response, a well-established marker of early visual processing. This was demonstrated through multiple complementary approaches: waveform morphology, latency distributions, ground truth comparisons with eye tracking and systematic exploration of preprocessing parameters. The results confirmed that ICA was not only suitable to be used for artefact removal but also capable of isolating physiologically interpretable components that reflected genuine neural activity across multiple preprocessing pipeline combinations. This was particularly important for naturalistic paradigms, where overlapping sources and continuous eye movements can obscure meaningful signals at the scalp level.

A third conclusion concerned the methodological bridge between sensor-space and component-space analyses. While this thesis did not implement full component-space connectivity, it established the necessary groundwork by demonstrating that ICA components were stable, interpretable and suitable for further analysis. This opened the door to applying connectivity metrics directly to independent components, which would reduce the influence of volume conduction and allow for more anatomically grounded interpretations. Such an approach would also enable the use of directed and effective connectivity methods, which require clean, source-resolved signals to produce meaningful results.

Taken together, these conclusions highlighted the value of integrating oscillatory theory, network neuroscience and source-resolved EEG methods to study aesthetic perception. This thesis showed that aesthetic experience was not merely a subjective or psychological phenomenon but was supported by dynamic neural processes that unfold across multiple spatial and temporal scales. It also demonstrated that methodological advances particularly in source separation and connectivity analysis could provide deeper insights into these processes.

At the same time, several limitations must be acknowledged. Sensor-space connectivity remained constrained by the mixing of sources at the scalp and while dwPLI mitigated zero-lag artefacts, it could not fully eliminate the influence of volume conduction. This means that the connectivity differences observed between abstract and figurative paintings cannot be interpreted as direct interactions between specific cortical regions, nor can they be mapped to anatomical pathways. ICA, although powerful, did not provide direct anatomical localisation, and group level interpretations required careful clustering and validation. Moreover, ICA performance depended on data length, filtering choices and sampling rate, and although these factors were systematically tested, the analysis was limited to a specific set of pipelines and may not generalise to all preprocessing strategies used in the literature. Preprocessing choices also influenced ICA outcomes, underscoring the need for standardised pipelines and transparent reporting. In the fixation-locked analysis, the identification of lambda responses relied on

accurate eye-tracker synchronisation and on the assumption that the extracted component reflected a single dominant visual source, more complex or overlapping sources may not be captured by this approach. Finally, while this thesis focused on neural dynamics, future work should integrate behavioural and subjective measures more directly to link network activity with aesthetic experience.

Despite these limitations, this thesis provided a clear and actionable pathway for future research. Component-space connectivity, band-pass ICA, fixation-locked analyses and effective connectivity methods such as PSI, PDC, and oPDC represent promising directions for advancing the field. These approaches could reveal how neural networks reorganised from fixation-to-fixation, how different frequency bands contributed to perceptual processing and how individual differences shaped aesthetic experience. More broadly, the methodological framework developed here can be applied beyond neuroaesthetics to other domains that involve naturalistic cognition, such as scene perception, sentence reading and decision-making tasks.

7. CONTRIBUTION TO SCIENCE

Thesis I. *I proposed a method to identify large-scale neural networks engaged during the viewing of abstract and figurative paintings, and demonstrated that aesthetic perception involves dynamic, frequency- and style-specific patterns of connectivity.*

I used high-density EEG, time-frequency analysis and the debiased weighted Phase-Lag Index (dwPLI) to track how oscillatory interactions evolve across delta, theta, alpha, beta and gamma bands during the viewing of abstract and figurative paintings. By analysing connectivity across multiple time windows, I showed that connectivity patterns change systematically over the course of viewing and differ between stimulus categories, indicating that abstract and figurative artworks engage distinct perceptual and interpretive processes. I further applied graph theory metrics to identify the functional roles of occipital and parietal hubs, demonstrating that aesthetic perception relies on distributed, frequency-specific networks rather than isolated regions. Through this approach, I provided a methodologically rigorous sensor space framework for studying functional connectivity in neuroaesthetics, using metrics specifically designed to minimise the influence of volume conduction and clarifying what can and cannot be inferred from sensor-level connectivity in higher order cognitive tasks.

Publications related to this thesis group are: [J1], [C3], [C4], [C5], [C7].

Related chapter/section: Chapter 3.

Thesis II. *I demonstrated that ICA can reliably extract the lambda response as a fixation-locked neural component during naturalistic art viewing, indicating that perception is based on the sequence of discrete visual processing cycles.*

By combining EEG with eye-tracking, I demonstrated that ICA can isolate fixation-locked neural activity, comprising the lambda response, which can be extracted even under naturalistic conditions despite variability in fixation timing, stimulus complexity and viewing behaviour. The extracted components exhibited consistent timing relative to saccade onset and offset, showed the expected occipital topography and waveform morphology, and remained stable across different artworks and viewing conditions. I validated the temporal precision of these components using saccade aligned information and demonstrated that their characteristics reflect discrete cycles of early visual processing. This work provides systematic evidence that aesthetic perception unfolds through a sequence of fixation-locked neural events, extending findings from controlled paradigms and showing that naturalistic viewing does not exclude the identification of reliable early visual components.

Publications related to this thesis group are: [J2], [C2], [C6].

Related chapter/section: Chapter 4, Section 4.3-4.4.

Thesis III. *I investigated the reliability of ICA for extracting meaningful neural components from free-viewing EEG data by examining how different preprocessing choices affect the stability and reproducibility of ICA decompositions, and identified the conditions under which ICA can consistently isolate meaningful neural signals.*

I developed a multi layered validation framework to assess ICA component quality using waveform morphology, latency distributions, saccade-locked alignment and single-trial detectability. By systematically varying filtering parameters, sampling rate and data length, I identified preprocessing configurations that consistently improve lambda component extraction and demonstrated that some pipelines produce stable, physiologically interpretable components, whereas others produce unstable decompositions. I showed that these differences are systematic rather than random, indicating that preprocessing decisions exert a strong and predictable influence on ICA outcomes. I also demonstrated that ICA can recover meaningful neural activity at the single-trial level, revealing fine-grained visual dynamics that are typically obscured in averaged ERPs. This contribution provides evidence-based guidance for selecting preprocessing strategies that support robust ICA performance and establishes a methodological foundation for future component-space connectivity analyses in naturalistic EEG research.

Publications related to this thesis group are: [J2], [C1].

Related chapter/section: Chapter 4, Section 4.5.

List of author publications

List of journal articles

[J1] **I. S. Suhaili**, Z. Nagy, and Z. Juhász, "Functional Connectivity Differences in the Perception of Abstract and Figurative Paintings," Applied Sciences, vol. 14, no. 20, 2024, doi: 10.3390/app14209284.

[J2] **I. S. binti Suhaili,** B. Tóth, Z. Nagy, and Z. Juhász, "Reliable Single-trial Detection of Saccade-related Lambda Responses with Independent Component Analysis," ENEURO, vol. 12, no. 11, 2025, doi: 10.1523/ENEURO.0270-25.2025.

List of conference publications

[C1] **I. S. Suhaili**, Z. Nagy, and Z. Juhász, "Single-trial detection of lambda responses in free-viewing EEG measurements," in 34th Annual Computational Neuroscience Meeting (CNS*2025), Florence, Italy, Jul. 2025, J. Comput. Neurosci., vol. 54, suppl. 1, p. 315, 2026, doi: 10.1007/s10827-025-00915-4.

[C2] **I. S. Suhaili**, Z. Nagy, and Z. Juhász, "Single-trial source-resolved EEG analysis of a free-viewing neuroaesthetic task with independent component analysis," in International Neuroscience Conference (INC) 2026*,* Budapest, Hungary, Jan. 2026, Abstract Book, Poster PS06.22.

[C3] **I. S. binti Suhaili**, Z. Nagy, and Z. Juhasz, "Comparing Brain Responses to Abstract and Representational Style Paintings: A High-Density EEG Connectivity Study," in The Federation of European Neuroscience Societies (FENS) Forum 2024, Vienna, Austria, Jun. 2024, Poster PS03-27AM-536.

[C4] **I. S. Suhaili**, Z. Juhász, and Z. Nagy, "On the perception of paintings: A high-density EEG study," in IBRO World Congress 2023, Granada, Spain, Sep. 2023, IBRO Neurosci. Rep., vol. 15, pp. S900 – S901, 2023, doi: 10.1016/j.ibneur.2023.08.1888.

[C5] **I. S. Suhaili**, Z. Nagy, and Z. Juhász, "The modulation effect of art painting content on saccade-evoked perceptual processes: A high-density EEG Study," in Annual Meeting of the Hungarian Neuroscience Society, MITT 2025, Debrecen, Hungary, Jan. 2025, Abstract Book, 2025, p. 45.

[C6] **I. S. binti Suhaili** and Z. Juhasz, "Uncovering Neural Saccadic Responses using Electroencephalogram (EEG) during Natural Viewing of Paintings," in 7th Hungarian Neuroscience Doctoral Conference for Undergraduate Students, Graduate Students and Junior Post-Docs (HUNDOC), Pécs, Hungary, Jan. 2024, Abstract Booklet, p. 98.

[C7] **I. S. binti Suhaili**, Z. Juhasz, Z. Wang, F. I. Mohamed, Cs. Borbely, and Z. Nagy, "Aesthetic experiences registered by high density EEG: a functional connectivity study," in XXXV Neumann Colloquium Conference, Szeged, Hungary, Nov. 2022, Az egészségügyi informatika COVID előtt és COVID után - A XXXV. Neumann Kollokvium konferencia kiadványa, pp. 82–89, ISBN 978-615-5036-22-4.

References

[1] S. Zeki, Y. Bao, and E. Pöppel, 'Neuroaesthetics: The art, science, and brain triptych', *PsyCh journal*, vol. 9, pp. 427–428, Aug. 2020, doi: 10.1002/pchj.383.

[2] A. Chatterjee and O. Vartanian, 'Neuroaesthetics', *Trends in Cognitive Sciences*, vol. 18, no. 7, pp. 370–375, Jul. 2014, doi: 10.1016/j.tics.2014.03.003.

[3] M. T. Pearce *et al.*, 'Neuroaesthetics: The Cognitive Neuroscience of Aesthetic Experience', *Perspect Psychol Sci*, vol. 11, no. 2, pp. 265–279, Mar. 2016, doi: 10.1177/1745691615621274.

[4] A. Chatterjee, 'Neuroaesthetics: A Coming of Age Story', *Journal of Cognitive Neuroscience*, vol. 23, no. 1, pp. 53–62, Jan. 2011, doi: 10.1162/jocn.2010.21457.

[5] H. Leder, B. Belke, A. Oeberst, and D. Augustin, 'A model of aesthetic appreciation and aesthetic judgments', *British Journal of Psychology*, vol. 95, no. 4, pp. 489–508, 2004, doi: 10.1348/0007126042369811.

[6] H. Leder and M. Nadal, 'Ten years of a model of aesthetic appreciation and aesthetic judgments : The aesthetic episode - Developments and challenges in empirical aesthetics', *Br J Psychol*, vol. 105, no. 4, pp. 443–464, Nov. 2014, doi: 10.1111/bjop.12084.

[7] M. Nadal, 'The experience of art: insights from neuroimaging', *Prog Brain Res*, vol. 204, pp. 135–158, 2013, doi: 10.1016/B978-0-444-63287-6.00007-5.

[8] M. Nadal, E. Munar, M. Angel Capo, J. Rossello, and C. J. Cela-Conde, 'Towards a framework for the study of the neural correlates of aesthetic preference.', *Spatial vision*, vol. 21, 2008.

[9] G. Buzsáki and A. Draguhn, 'Neuronal Oscillations in Cortical Networks', *Science*, vol. 304, no. 5679, pp. 1926–1929, Jun. 2004, doi: 10.1126/science.1099745.

[10] G. Buzsáki, *Rhythms of the Brain*. Oxford University Press, 2006. doi: 10.1093/acprof:oso/9780195301069.001.0001.

[11] P. Fries, 'A mechanism for cognitive dynamics: neuronal communication through neuronal coherence', *Trends in Cognitive Sciences*, vol. 9, no. 10, pp. 474–480, Oct. 2005, doi: 10.1016/j.tics.2005.08.011.

[12] P. Fries, 'Rhythms for Cognition: Communication through Coherence', *Neuron*, vol. 88, no. 1, pp. 220–235, Oct. 2015, doi: 10.1016/j.neuron.2015.09.034.

[13] O. Jensen and A. Mazaheri, 'Shaping Functional Architecture by Oscillatory Alpha Activity: Gating by Inhibition', *Front. Hum. Neurosci.*, vol. 4, Nov. 2010, doi: 10.3389/fnhum.2010.00186.

[14] J. Lin *et al.*, 'Theta band power increases in the posterior hippocampus predict successful episodic memory encoding in humans', *Hippocampus*, vol. 27, no. 10, pp. 1040–1053, 2017.

[15] G. Buzsáki, 'Theta Oscillations in the Hippocampus', *Neuron*, vol. 33, no. 3, pp. 325–340, Jan. 2002, doi: 10.1016/S0896-6273(02)00586-X.

[16] W. Klimesch, 'Alpha-band oscillations, attention, and controlled access to stored information', *Trends in Cognitive Sciences*, vol. 16, no. 12, pp. 606–617, Dec. 2012, doi: 10.1016/j.tics.2012.10.007.

[17] O. Jensen and A. Mazaheri, 'Shaping functional architecture by oscillatory alpha activity: gating by inhibition', *Frontiers in human neuroscience*, vol. 4, p. 186, 2010.

[18] J. Barone and H. E. Rossiter, 'Understanding the Role of Sensorimotor Beta Oscillations', *Front. Syst. Neurosci.*, vol. 15, May 2021, doi: 10.3389/fnsys.2021.655886.

[19] C. Tallon-Baudry and O. Bertrand, 'Oscillatory gamma activity in humans and its role in object representation', *Trends in Cognitive Sciences*, vol. 3, no. 4, pp. 151–162, Apr. 1999, doi: 10.1016/S1364-6613(99)01299-1.

[20] J. Rodriguez-Larios and K. Alaerts, 'Tracking Transient Changes in the Neural Frequency Architecture: Harmonic Relationships between Theta and Alpha Peaks Facilitate Cognitive Performance', *J. Neurosci.*, vol. 39, no. 32, pp. 6291–6298, Aug. 2019, doi: 10.1523/JNEUROSCI.2919-18.2019.

[21] M. Alavash, S. Tune, and J. Obleser, ‘Dynamic large-scale connectivity of intrinsic cortical oscillations supports adaptive listening in challenging conditions’, *PLOS Biology*, vol. 19, no. 10, p. e3001410, Oct. 2021, doi: 10.1371/journal.pbio.3001410.
[22] C. T. Cripe and A. Delorme, ‘Independent Component Analysis (ICA) With Covariates Strengthens Behavioral Links in Electroencephalography (EEG) Connectivity’, *Cureus*, vol. 17, no. 6, p. e86533, Jun. 2025, doi: 10.7759/cureus.86533.
[23] D. A. Nguyen-Danse, S. Singaravelu, L. A. S. Chauvigné, A. Mottaz, L. Allaman, and A. G. Guggisberg, ‘Feasibility of Reconstructing Source Functional Connectivity with Low-Density EEG’, *Brain Topogr*, vol. 34, no. 6, pp. 709–719, Nov. 2021, doi: 10.1007/s10548-021-00866-w.
[24] S. Phadikar, O. Agcaoglu, and V. D. Calhoun, ‘Group Joint Independent Component Analysis (Group jICA): a Novel Method to Jointly Decompose and Link Simultaneous EEG and fMRI’, in *2025 IEEE International Conference on Image Processing (ICIP)*, Sep. 2025, pp. 2277–2281. doi: 10.1109/ICIP55913.2025.11084549.
[25] R. VanRullen and S. J. Thorpe, ‘The Time Course of Visual Processing: From Early Perception to Decision-Making’, *Journal of Cognitive Neuroscience*, vol. 13, no. 4, pp. 454–461, May 2001, doi: 10.1162/08989290152001880.
[26] S. Marković, ‘Perceptual, Semantic and Affective Dimensions of Experience of Abstract and Representational Paintings’, *Journal of Vision - J VISION*, vol. 10, pp. 1230–1230, Aug. 2010, doi: 10.1167/10.7.1230.
[27] M. Siegel, T. H. Donner, and A. K. Engel, ‘Spectral fingerprints of large-scale neuronal interactions’, *Nat Rev Neurosci*, vol. 13, no. 2, Art. no. 2, Feb. 2012, doi: 10.1038/nrn3137.
[28] J.-M. Schoffelen and J. Gross, ‘Source connectivity analysis with MEG and EEG’, *Human Brain Mapping*, vol. 30, no. 6, pp. 1857–1865, 2009, doi: 10.1002/hbm.20745.
[29] P. L. Nunez and R. Srinivasan, *Electric fields of the brain: the neurophysics of EEG*. Oxford university press, 2006.
[30] C. M. Michel, M. M. Murray, G. Lantz, S. Gonzalez, L. Spinelli, and R. Grave de Peralta, ‘EEG source imaging’, *Clinical Neurophysiology*, vol. 115, no. 10, pp. 2195–2222, Oct. 2004, doi: 10.1016/j.clinph.2004.06.001.
[31] R. Grech *et al.*, ‘Review on solving the inverse problem in EEG source analysis’, *J NeuroEngineering Rehabil*, vol. 5, no. 1, p. 25, Nov. 2008, doi: 10.1186/1743-0003-5-25.
[32] P. L. Nunez *et al.*, ‘EEG coherency: I: statistics, reference electrode, volume conduction, Laplacians, cortical imaging, and interpretation at multiple scales’, *Electroencephalography and Clinical Neurophysiology*, vol. 103, no. 5, pp. 499–515, Nov. 1997, doi: 10.1016/S0013-4694(97)00066-7.
[33] G. Nolte, O. Bai, L. Wheaton, Z. Mari, S. Vorbach, and M. Hallett, ‘Identifying true brain interaction from EEG data using the imaginary part of coherency’, *Clinical Neurophysiology*, vol. 115, no. 10, pp. 2292–2307, Oct. 2004, doi: 10.1016/j.clinph.2004.04.029.
[34] C. J. Stam, G. Nolte, and A. Daffertshofer, ‘Phase lag index: Assessment of functional connectivity from multi channel EEG and MEG with diminished bias from common sources’, *Human Brain Mapping*, vol. 28, no. 11, pp. 1178–1193, 2007, doi: 10.1002/hbm.20346.
[35] K. J. Friston, ‘Functional and effective connectivity in neuroimaging: A synthesis’, *Human Brain Mapping*, vol. 2, no. 1–2, pp. 56–78, Jan. 1994, doi: 10.1002/hbm.460020107.
[36] E. Bullmore and O. Sporns, ‘Complex brain networks: graph theoretical analysis of structural and functional systems’, *Nat Rev Neurosci*, vol. 10, no. 3, pp. 186–198, Mar. 2009, doi: 10.1038/nrn2575.
[37] K. J. Friston, ‘Functional and Effective Connectivity: A Review’, *Brain Connectivity*, vol. 1, no. 1, pp. 13–36, Jan. 2011, doi: 10.1089/brain.2011.0008.

[38] C. J. Cela-Conde *et al.*, ‘Dynamics of brain networks in the aesthetic appreciation’, *Proc. Natl. Acad. Sci. U.S.A.*, vol. 110, no. supplement_2, pp. 10454–10461, Jun. 2013, doi: 10.1073/pnas.1302855110.
[39] E. Munar *et al.*, ‘Aesthetic appreciation: event-related field and time-frequency analyses’, *Front. Hum. Neurosci.*, vol. 5, 2012, doi: 10.3389/fnhum.2011.00185.
[40] C. J. Cela-Conde, L. Agnati, J. P. Huston, F. Mora, and M. Nadal, ‘The neural foundations of aesthetic appreciation’, *Progress in Neurobiology*, vol. 94, no. 1, pp. 39–48, Jun. 2011, doi: 10.1016/j.pneurobio.2011.03.003.
[41] P. Sarasso *et al.*, ‘Beauty in mind: Aesthetic appreciation correlates with perceptual facilitation and attentional amplification’, *Neuropsychologia*, vol. 136, p. 107282, Jan. 2020, doi: 10.1016/j.neuropsychologia.2019.107282.
[42] L. Höfel and T. Jacobsen, ‘Electrophysiological indices of processing aesthetics: Spontaneous or intentional processes?’, *International Journal of Psychophysiology*, vol. 65, no. 1, pp. 20–31, Jul. 2007, doi: 10.1016/j.ijpsycho.2007.02.007.
[43] M. Boccia *et al.*, ‘Where does brain neural activation in aesthetic responses to visual art occur? Meta-analytic evidence from neuroimaging studies’, *Neuroscience & Biobehavioral Reviews*, vol. 60, pp. 65–71, Jan. 2016, doi: 10.1016/j.neubiorev.2015.09.009.
[44] S. Makeig, A. Bell, T.-P. Jung, and T. J. Sejnowski, ‘Independent Component Analysis of Electroencephalographic Data’, in *Advances in Neural Information Processing Systems*, MIT Press, 1995. Accessed: Jan. 04, 2026. [Online]. Available: https://proceedings.neurips.cc/paper_files/paper/1995/hash/754dda4b1ba34c6fa89716b85d68532b-Abstract.html
[45] T.-P. Jung *et al.*, ‘Removing electroencephalographic artifacts by blind source separation’, *Psychophysiology*, vol. 37, no. 2, pp. 163–178, Mar. 2000, doi: 10.1111/1469-8986.3720163.
[46] C. Brunner, M. Billinger, M. Seeber, T. R. Mullen, and S. Makeig, ‘Volume Conduction Influences Scalp-Based Connectivity Estimates’, *Front. Comput. Neurosci.*, vol. 10, Nov. 2016, doi: 10.3389/fncom.2016.00121.
[47] F. Perrin, J. Pernier, O. Bertrand, and J. F. Echallier, ‘Spherical splines for scalp potential and current density mapping’, *Electroencephalography and Clinical Neurophysiology*, vol. 72, no. 2, pp. 184–187, Feb. 1989, doi: 10.1016/0013-4694(89)90180-6.
[48] M. S. Hämäläinen and R. J. Ilmoniemi, ‘Interpreting magnetic fields of the brain: minimum norm estimates’, *Med. Biol. Eng. Comput.*, vol. 32, no. 1, pp. 35–42, Jan. 1994, doi: 10.1007/BF02512476.
[49] B. D. Van Veen, W. Van Drongelen, M. Yuchtman, and A. Suzuki, ‘Localization of brain electrical activity via linearly constrained minimum variance spatial filtering’, *IEEE Trans. Biomed. Eng.*, vol. 44, no. 9, pp. 867–880, Sep. 1997, doi: 10.1109/10.623056.
[50] R. Oostenveld and T. F. Oostendorp, ‘Validating the boundary element method for forward and inverse EEG computations in the presence of a hole in the skull’, *Human Brain Mapping*, vol. 17, no. 3, pp. 179–192, 2002, doi: 10.1002/hbm.10061.
[51] A. Hyvärinen and E. Oja, ‘Independent component analysis: algorithms and applications’, *Neural Networks*, vol. 13, no. 4, pp. 411–430, Jun. 2000, doi: 10.1016/S0893-6080(00)00026-5.
[52] A. Delorme and S. Makeig, ‘EEGLAB: an open source toolbox for analysis of single-trial EEG dynamics including independent component analysis’, *J Neurosci Methods*, vol. 134, no. 1, pp. 9–21, Mar. 2004, doi: 10.1016/j.jneumeth.2003.10.009.
[53] A. Delorme, J. Palmer, J. Onton, R. Oostenveld, and S. Makeig, ‘Independent EEG Sources Are Dipolar’, *PLOS ONE*, vol. 7, no. 2, p. e30135, Feb. 2012, doi: 10.1371/journal.pone.0030135.
[54] L. Pion-Tonachini, K. Kreutz-Delgado, and S. Makeig, ‘ICLabel: An automated electroencephalographic independent component classifier, dataset, and website’,

NeuroImage, vol. 198, pp. 181–197, Sep. 2019, doi: 10.1016/j.neuroimage.2019.05.026.
[55] F. Artoni, D. Menicucci, A. Delorme, S. Makeig, and S. Micera, 'RELICA: A method for estimating the reliability of independent components', *NeuroImage*, vol. 103, pp. 391–400, Dec. 2014, doi: 10.1016/j.neuroimage.2014.09.010.
[56] H. Berger, 'Über das elektroenkephalogramm des menschen', *Archiv für psychiatrie und nervenkrankheiten*, vol. 87, no. 1, pp. 527–570, 1929.
[57] E. Niedermeyer and F. H. L. da Silva, *Electroencephalography: Basic Principles, Clinical Applications, and Related Fields*. Lippincott Williams & Wilkins, 2005.
[58] W. Singer, 'Neuronal Synchrony: A Versatile Code for the Definition of Relations?', *Neuron*, vol. 24, no. 1, pp. 49–65, Sep. 1999, doi: 10.1016/S0896-6273(00)80821-1.
[59] F. Varela, J.-P. Lachaux, E. Rodriguez, and J. Martinerie, 'The Brainweb: Phase Synchronization and Large-Scale Integration', *Nature reviews. Neuroscience*, vol. 2, pp. 229–39, May 2001, doi: 10.1038/35067550.
[60] O. Sporns, 'Structure and function of complex brain networks', *Dialogues in Clinical Neuroscience*, vol. 15, no. 3, pp. 247–262, Sep. 2013, doi: 10.31887/DCNS.2013.15.3/osporns.
[61] D. S. Bassett and O. Sporns, 'Network neuroscience', *Nat Neurosci*, vol. 20, no. 3, pp. 353–364, Mar. 2017, doi: 10.1038/nn.4502.
[62] R. M. Hutchison *et al.*, 'Dynamic functional connectivity: Promise, issues, and interpretations', *NeuroImage*, vol. 80, pp. 360–378, Oct. 2013, doi: 10.1016/j.neuroimage.2013.05.079.
[63] D. Vidaurre *et al.*, 'Discovering dynamic brain networks from big data in rest and task', *NeuroImage*, vol. 180, pp. 646–656, Oct. 2018, doi: 10.1016/j.neuroimage.2017.06.077.
[64] S. Palva and J. M. Palva, 'Discovering oscillatory interaction networks with M/EEG: challenges and breakthroughs', *Trends in Cognitive Sciences*, vol. 16, no. 4, pp. 219–230, Apr. 2012, doi: 10.1016/j.tics.2012.02.004.
[65] K. Kontson *et al.*, '"Your Brain on Art": Emergent cortical dynamics during aesthetic experiences', *Frontiers in Human Neuroscience*, vol. 9, 2015, Accessed: Oct. 10, 2022. [Online]. Available: https://www.frontiersin.org/articles/10.3389/fnhum.2015.00626
[66] M. Vinck, R. Oostenveld, M. van Wingerden, F. Battaglia, and C. M. A. Pennartz, 'An improved index of phase-synchronization for electrophysiological data in the presence of volume-conduction, noise and sample-size bias', *NeuroImage*, vol. 55, no. 4, pp. 1548–1565, Apr. 2011, doi: 10.1016/j.neuroimage.2011.01.055.
[67] I. Winkler, S. Debener, K.-R. Müller, and M. Tangermann, 'On the influence of high-pass filtering on ICA-based artifact reduction in EEG-ERP', in *2015 37th Annual International Conference of the IEEE Engineering in Medicine and Biology Society (EMBC)*, Aug. 2015, pp. 4101–4105. doi: 10.1109/EMBC.2015.7319296.
[68] M. Klug and K. Gramann, 'Identifying key factors for improving ICA-based decomposition of EEG data in mobile and stationary experiments', *European Journal of Neuroscience*, vol. 54, no. 12, pp. 8406–8420, 2021, doi: 10.1111/ejn.14992.
[69] F. L. da Silva, 'EEG and MEG: relevance to neuroscience', *Neuron*, vol. 80, no. 5, pp. 1112–1128, 2013.
[70] R. B. Buxton, 'The physics of functional magnetic resonance imaging (fMRI)', *Rep. Prog. Phys.*, vol. 76, no. 9, p. 096601, Sep. 2013, doi: 10.1088/0034-4885/76/9/096601.
[71] N. K. Logothetis, 'What we can do and what we cannot do with fMRI', *Nature*, vol. 453, no. 7197, pp. 869–878, Jun. 2008, doi: 10.1038/nature06976.
[72] R. Hari and R. Salmelin, 'Magnetoencephalography: From SQUIDs to neuroscience: Neuroimage 20th Anniversary Special Edition', *NeuroImage*, vol. 61, no. 2, pp. 386–396, Jun. 2012, doi: 10.1016/j.neuroimage.2011.11.074.
[73] R. Hari and A. Puce, *MEG-EEG Primer*. Oxford University Press, 2023.

[74] G. Buzsáki, C. A. Anastassiou, and C. Koch, 'The origin of extracellular fields and currents — EEG, ECoG, LFP and spikes', *Nat Rev Neurosci*, vol. 13, no. 6, pp. 407–420, Jun. 2012, doi: 10.1038/nrn3241.
[75] M. Teplan, 'FUNDAMENTALS OF EEG MEASUREMENT', *MEASUREMENT SCIENCE REVIEW*, vol. 2, 2002.
[76] E.-J. Speckmann, 'Introduction of the neurophysiological basis of the EEG and DC potentials', *Electroencephalography: Basic principles, clinical applications, and related fields*, pp. 15–26, 1993.
[77] S. J. Luck, *An introduction to the event-related potential technique*. MIT press, 2014.
[78] B. J. Thio and W. M. Grill, 'Relative contributions of different neural sources to the EEG', *NeuroImage*, vol. 275, p. 120179, Jul. 2023, doi: 10.1016/j.neuroimage.2023.120179.
[79] M. F. Bear, B. W. Connors, and M. A. Paradiso, *Neuroscience: Exploring the Brain*. Wolters Kluwer, 2015.
[80] R. D. Pascual-Marqui, 'Discrete, 3D distributed, linear imaging methods of electric neuronal activity. Part 1: exact, zero error localization', Oct. 18, 2007, *arXiv*: arXiv:0710.3341. doi: 10.48550/arXiv.0710.3341.
[81] C. M. Michel and D. Brunet, 'EEG Source Imaging: A Practical Review of the Analysis Steps', *Front. Neurol.*, vol. 10, Apr. 2019, doi: 10.3389/fneur.2019.00325.
[82] S. J. Luck and E. S. Kappenman, *The Oxford handbook of event-related potential components*. Oxford university press, 2011.
[83] D. Purves *et al.*, *Principles of cognitive neuroscience*, vol. 83, no. 3. Sinauer Associates Sunderland, 2013.
[84] S. Makeig, S. Debener, J. Onton, and A. Delorme, 'Mining event-related brain dynamics', *Trends in cognitive sciences*, vol. 8, no. 5, pp. 204–210, 2004.
[85] G. Pfurtscheller and F. H. Lopes da Silva, 'Event-related EEG/MEG synchronization and desynchronization: basic principles', *Clinical Neurophysiology*, vol. 110, no. 11, pp. 1842–1857, Nov. 1999, doi: 10.1016/S1388-2457(99)00141-8.
[86] M. X. Cohen, *Analyzing Neural Time Series Data: Theory and Practice*. MIT Press, 2014.
[87] J. Fell *et al.*, 'Neural Bases of Cognitive ERPs: More than Phase Reset', *Journal of Cognitive Neuroscience*, vol. 16, no. 9, pp. 1595–1604, Nov. 2004, doi: 10.1162/0898929042568514.
[88] P. Sauseng, W. Klimesch, W. R. Gruber, S. Hanslmayr, R. Freunberger, and M. Doppelmayr, 'Are event-related potential components generated by phase resetting of brain oscillations? A critical discussion', *Neuroscience*, vol. 146, no. 4, pp. 1435–1444, Jun. 2007, doi: 10.1016/j.neuroscience.2007.03.014.
[89] O. Bertrand, C. Tallon-Baudry, and J. Pernier, 'Time-Frequency Analysis of Oscillatory Gamma-Band Activity: Wavelet Approach and Phase-Locking Estimation', in *Biomag 96*, C. J. Aine, G. Stroink, C. C. Wood, Y. Okada, and S. J. Swithenby, Eds, New York, NY: Springer, 2000, pp. 919–922. doi: 10.1007/978-1-4612-1260-7_224.
[90] A. Grossmann, R. Kronland-Martinet, and J. Morlet, 'Reading and Understanding Continuous Wavelet Transforms', in *Wavelets*, J.-M. Combes, A. Grossmann, and P. Tchamitchian, Eds, Berlin, Heidelberg: Springer, 1990, pp. 2–20. doi: 10.1007/978-3-642-75988-8_1.
[91] T. Harmony, 'The functional significance of delta oscillations in cognitive processing', *Front. Integr. Neurosci.*, vol. 7, Dec. 2013, doi: 10.3389/fnint.2013.00083.
[92] M. J. Kahana, D. Seelig, and J. R. Madsen, 'Theta returns', *Current Opinion in Neurobiology*, vol. 11, no. 6, pp. 739–744, Dec. 2001, doi: 10.1016/S0959-4388(01)00278-1.
[93] J. E. Lisman and O. Jensen, 'The Theta-Gamma Neural Code', *Neuron*, vol. 77, no. 6, pp. 1002–1016, Mar. 2013, doi: 10.1016/j.neuron.2013.03.007.

[94] O. Jensen and C. D. Tesche, ‘Frontal theta activity in humans increases with memory load in a working memory task’, *European journal of Neuroscience*, vol. 15, no. 8, pp. 1395–1399, 2002.
[95] W. Klimesch, ‘EEG alpha and theta oscillations reflect cognitive and memory performance: a review and analysis’, *Brain research reviews*, vol. 29, no. 2–3, pp. 169–195, 1999.
[96] S. Palva and J. M. Palva, ‘New vistas for α-frequency band oscillations’, *Trends in Neurosciences*, vol. 30, no. 4, pp. 150–158, Apr. 2007, doi: 10.1016/j.tins.2007.02.001.
[97] A. K. Engel and P. Fries, ‘Beta-band oscillations — signalling the status quo?’, *Current Opinion in Neurobiology*, vol. 20, no. 2, pp. 156–165, Apr. 2010, doi: 10.1016/j.conb.2010.02.015.
[98] M. Siegel, T. H. Donner, and A. K. Engel, ‘Spectral fingerprints of large-scale neuronal interactions’, *Nat Rev Neurosci*, vol. 13, no. 2, pp. 121–134, Feb. 2012, doi: 10.1038/nrn3137.
[99] P. Fries, ‘Neuronal Gamma-Band Synchronization as a Fundamental Process in Cortical Computation’, *Annual Review of Neuroscience*, vol. 32, no. Volume 32, 2009, pp. 209–224, Jul. 2009, doi: 10.1146/annurev.neuro.051508.135603.
[100] R. T. Canolty and R. T. Knight, ‘The functional role of cross-frequency coupling’, *Trends in Cognitive Sciences*, vol. 14, no. 11, pp. 506–515, Nov. 2010, doi: 10.1016/j.tics.2010.09.001.
[101] M. Craddock, J. Martinovic, and M. M. Müller, ‘Accounting for microsaccadic artifacts in the EEG using independent component analysis and beamforming’, *Psychophysiology*, vol. 53, no. 4, pp. 553–565, Apr. 2016, doi: 10.1111/psyp.12593.
[102] A. M. Bastos and J.-M. Schoffelen, ‘A Tutorial Review of Functional Connectivity Analysis Methods and Their Interpretational Pitfalls’, *Front. Syst. Neurosci.*, vol. 9, Jan. 2016, doi: 10.3389/fnsys.2015.00175.
[103] J.-P. Lachaux, E. Rodriguez, J. Martinerie, and F. J. Varela, ‘Measuring phase synchrony in brain signals’, *Hum. Brain Mapp.*, vol. 8, no. 4, pp. 194–208, 1999, doi: 10.1002/(SICI)1097-0193(1999)8:4<194::AID-HBM4>3.0.CO;2-C.
[104] S. Baillet, J. C. Mosher, and R. M. Leahy, ‘Electromagnetic brain mapping’, *IEEE Signal processing magazine*, vol. 18, no. 6, pp. 14–30, 2002.
[105] J. M. Palva *et al.*, ‘Ghost interactions in MEG/EEG source space: A note of caution on inter-areal coupling measures’, *NeuroImage*, vol. 173, pp. 632–643, Jun. 2018, doi: 10.1016/j.neuroimage.2018.02.032.
[106] S. Haufe, V. V. Nikulin, K.-R. Müller, and G. Nolte, ‘A critical assessment of connectivity measures for EEG data: A simulation study’, *NeuroImage*, vol. 64, pp. 120–133, Jan. 2013, doi: 10.1016/j.neuroimage.2012.09.036.
[107] R. Bruña, F. Maestú, and E. Pereda, ‘Phase locking value revisited: teaching new tricks to an old dog’, *J. Neural Eng.*, vol. 15, no. 5, p. 056011, Jul. 2018, doi: 10.1088/1741-2552/aacfe4.
[108] R. Bruña, F. Maestú, and E. Pereda, ‘Phase locking value revisited: teaching new tricks to an old dog’, *J. Neural Eng.*, vol. 15, no. 5, p. 056011, Oct. 2018, doi: 10.1088/1741-2552/aacfe4.
[109] K. Yoshinaga *et al.*, ‘Comparison of Phase Synchronization Measures for Identifying Stimulus-Induced Functional Connectivity in Human Magnetoencephalographic and Simulated Data’, *Front. Neurosci.*, vol. 14, Jun. 2020, doi: 10.3389/fnins.2020.00648.
[110] G. Chiarion, L. Sparacino, Y. Antonacci, L. Faes, and L. Mesin, ‘Connectivity Analysis in EEG Data: A Tutorial Review of the State of the Art and Emerging Trends’, *Bioengineering (Basel)*, vol. 10, no. 3, p. 372, Mar. 2023, doi: 10.3390/bioengineering10030372.
[111] M. Rubinov and O. Sporns, ‘Complex network measures of brain connectivity: Uses and interpretations’, *NeuroImage*, vol. 52, no. 3, pp. 1059–1069, Sep. 2010, doi: 10.1016/j.neuroimage.2009.10.003.

[112] D. J. Watts and S. H. Strogatz, ‘Collective dynamics of “small-world” networks’, *Nature*, vol. 393, no. 6684, pp. 440–442, Jun. 1998, doi: 10.1038/30918.
[113] L. C. Freeman, ‘A Set of Measures of Centrality Based on Betweenness’, *Sociometry*, vol. 40, no. 1, pp. 35–41, 1977, doi: 10.2307/3033543.
[114] M. E. J. Newman, ‘Modularity and community structure in networks’, *Proceedings of the National Academy of Sciences*, vol. 103, no. 23, pp. 8577–8582, Jun. 2006, doi: 10.1073/pnas.0601602103.
[115] S. Makeig and J. Onton, ‘ERP features and EEG dynamics: an ICA perspective’, *Oxford handbook of event-related potential components*, pp. 51–86, 2011.
[116] A. J. Bell and T. J. Sejnowski, ‘An information-maximization approach to blind separation and blind deconvolution’, *Neural computation*, vol. 7, no. 6, pp. 1129–1159, 1995.
[117] J.-F. Cardoso, ‘High-Order Contrasts for Independent Component Analysis’, *Neural Computation*, vol. 11, no. 1, pp. 157–192, Jan. 1999, doi: 10.1162/089976699300016863.
[118] T.-W. Lee, M. Girolami, and T. J. Sejnowski, ‘Independent Component Analysis Using an Extended Infomax Algorithm for Mixed Subgaussian and Supergaussian Sources’, *Neural Computation*, vol. 11, no. 2, pp. 417–441, Feb. 1999, doi: 10.1162/089976699300016719.
[119] A. Hyvarinen, ‘Fast and robust fixed-point algorithms for independent component analysis’, *IEEE Transactions on Neural Networks*, vol. 10, no. 3, pp. 626–634, May 1999, doi: 10.1109/72.761722.
[120] C. Gil Ávila *et al.*, ‘DISCOVER-EEG: an open, fully automated EEG pipeline for biomarker discovery in clinical neuroscience’, *Sci Data*, vol. 10, no. 1, p. 613, Sep. 2023, doi: 10.1038/s41597-023-02525-0.
[121] R. Oostenveld, P. Fries, E. Maris, and J.-M. Schoffelen, ‘FieldTrip: Open Source Software for Advanced Analysis of MEG, EEG, and Invasive Electrophysiological Data’, *Computational Intelligence and Neuroscience*, vol. 2011, no. 1, p. 156869, 2011, doi: 10.1155/2011/156869.
[122] A. Delorme *et al.*, ‘EEGLAB, SIFT, NFT, BCILAB, and ERICA: New Tools for Advanced EEG Processing’, *Computational Intelligence and Neuroscience*, vol. 2011, no. 1, p. 130714, 2011, doi: 10.1155/2011/130714.
[123] E. Maris and R. Oostenveld, ‘Nonparametric statistical testing of EEG- and MEG-data’, *Journal of Neuroscience Methods*, vol. 164, no. 1, pp. 177–190, Aug. 2007, doi: 10.1016/j.jneumeth.2007.03.024.
[124] M. Aubert *et al.*, ‘Palaeolithic cave art in Borneo’, *Nature*, vol. 564, no. 7735, pp. 254–257, 2018.
[125] E. Pihko *et al.*, ‘Experiencing Art: The Influence of Expertise and Painting Abstraction Level’, *Frontiers in Human Neuroscience*, vol. 5, 2011, Accessed: Oct. 19, 2023. [Online]. Available: https://www.frontiersin.org/articles/10.3389/fnhum.2011.00094
[126] E. A. Vessel and N. Rubin, ‘Beauty and the beholder: Highly individual taste for abstract, but not real-world images’, *Journal of Vision*, vol. 10, no. 2, p. 18, Feb. 2010, doi: 10.1167/10.2.18.
[127] U. Kirk, M. Skov, M. S. Christensen, and N. Nygaard, ‘Brain correlates of aesthetic expertise: a parametric fMRI study’, *Brain Cogn*, vol. 69, no. 2, pp. 306–315, Mar. 2009, doi: 10.1016/j.bandc.2008.08.004.
[128] V. S. Ramachandran and W. Hirstein, ‘The science of art: a neurological theory of aesthetic experience’, *Journal of Consciousness Studies*, vol. 6, no. 6–7, pp. 15–51, Jun. 1999.
[129] J. van Paasschen, F. Bacci, and D. P. Melcher, ‘The Influence of Art Expertise and Training on Emotion and Preference Ratings for Representational and Abstract Artworks’, *PLOS ONE*, vol. 10, no. 8, p. e0134241, Aug. 2015, doi: 10.1371/journal.pone.0134241.
[130] O. Vartanian and V. Goel, ‘Neuroanatomical correlates of aesthetic preference for paintings’, *NeuroReport*, vol. 15, no. 5, p. 893, Apr. 2004.

[131] T. Jacobsen and L. Höfel, ‘Descriptive and evaluative judgment processes: Behavioral and electrophysiological indices of processing symmetry and aesthetics’, *Cognitive, Affective, & Behavioral Neuroscience*, vol. 3, no. 4, pp. 289–299, Dec. 2003, doi: 10.3758/CABN.3.4.289.
[132] J. Bhattacharya and H. Petsche, ‘Shadows of artistry: cortical synchrony during perception and imagery of visual art’, *Cognitive Brain Research*, vol. 13, no. 2, pp. 179–186, Apr. 2002, doi: 10.1016/S0926-6410(01)00110-0.
[133] B. Sbriscia-Fioretti, C. Berchio, D. Freedberg, V. Gallese, and M. A. Umiltà, ‘ERP Modulation during Observation of Abstract Paintings by Franz Kline’, *PLOS ONE*, vol. 8, no. 10, p. e75241, Oct. 2013, doi: 10.1371/journal.pone.0075241.
[134] S. Righi, G. Gronchi, G. Pierguidi, S. Messina, and M. P. Viggiano, ‘Aesthetic shapes our perception of every-day objects: An ERP study’, *New Ideas in Psychology*, vol. 47, pp. 103–112, Dec. 2017, doi: 10.1016/j.newideapsych.2017.03.007.
[135] J. E. Else, J. Ellis, and E. Orme, ‘Art expertise modulates the emotional response to modern art, especially abstract: an ERP investigation’, *Frontiers in Human Neuroscience*, vol. 9, 2015, Accessed: Oct. 19, 2023. [Online]. Available: https://www.frontiersin.org/articles/10.3389/fnhum.2015.00525
[136] R. C. Oldfield, ‘The assessment and analysis of handedness: The Edinburgh inventory’, *Neuropsychologia*, vol. 9, no. 1, pp. 97–113, Mar. 1971, doi: 10.1016/0028-3932(71)90067-4.
[137] J. Dawson, ‘Visceral and Behavioural Responses to Modern Art: Influence of Expertise, Type of Art and Context - ProQuest’. Accessed: Nov. 09, 2022. [Online]. Available: https://www.proquest.com/openview/fd5cc5523eec3be61533ebb006c591ed/1?cbl=51922&pq-origsite=gscholar&parentSessionId=7PYtHgqSpk8Mdgc%2FjlfhRguHxZTXFYvMEV3RdFLchD4%3D
[138] J. van Paasschen, F. Bacci, and D. P. Melcher, ‘The Influence of Art Expertise and Training on Emotion and Preference Ratings for Representational and Abstract Artworks’, *PLOS ONE*, vol. 10, no. 8, p. e0134241, Aug. 2015, doi: 10.1371/journal.pone.0134241.
[139] J. R. Crawford and J. D. Henry, ‘The Positive and Negative Affect Schedule (PANAS): Construct validity, measurement properties and normative data in a large non-clinical sample’, *British Journal of Clinical Psychology*, vol. 43, no. 3, pp. 245–265, 2004, doi: 10.1348/0144665031752934.
[140] ‘Headcap, Headcaps’. Accessed: Jan. 14, 2026. [Online]. Available: https://www.biosemi.com/headcap.htm
[141] M. MATLAB, ‘Version 23.2.0 (R2023b)’, 2023.
[142] S. Makeig, ‘Auditory event-related dynamics of the EEG spectrum and effects of exposure to tones’, *Electroencephalography and Clinical Neurophysiology*, vol. 86, no. 4, pp. 283–293, Apr. 1993, doi: 10.1016/0013-4694(93)90110-H.
[143] R. Grandchamp and A. Delorme, ‘Single-Trial Normalization for Event-Related Spectral Decomposition Reduces Sensitivity to Noisy Trials’, *Front. Psychol.*, vol. 2, Sep. 2011, doi: 10.3389/fpsyg.2011.00236.
[144] R. Batt, M. Palmiero, C. Nakatani, and C. van Leeuwen, ‘Style and spectral power: processing of abstract and representational art in artists and non-artists’, *Perception*, vol. 39, no. 12, pp. 1659–1671, 2010, doi: 10.1068/p6747.
[145] A. J. Ries, D. Slayback, and J. Touryan, ‘The fixation-related lambda response: Effects of saccade magnitude, spatial frequency, and ocular artifact removal’, *International Journal of Psychophysiology*, vol. 134, pp. 1–8, Dec. 2018, doi: 10.1016/j.ijpsycho.2018.09.004.
[146] O. Dimigen, W. Sommer, A. Hohlfeld, A. M. Jacobs, and R. Kliegl, ‘Coregistration of eye movements and EEG in natural reading: Analyses and review’, *Journal of Experimental Psychology: General*, vol. 140, no. 4, pp. 552–572, 2011, doi: 10.1037/a0023885.

[147] A. Madison, C. Callahan-Flintoft, S. M. Thurman, R. A. C. Hoffing, J. Touryan, and A. J. Ries, 'Fixation-related potentials during a virtual navigation task: The influence of image statistics on early cortical processing', *Atten Percept Psychophys*, vol. 87, no. 1, pp. 261–283, Jan. 2025, doi: 10.3758/s13414-024-03002-5.
[148] A. Yagi, 'Averaged cortical potentials (lambda responses) time-locked to onset and offset of saccades', *Psychobiology*, vol. 9, no. 3, pp. 318–320, Sep. 1981, doi: 10.3758/BF03326985.
[149] A. Yagi, 'Lambda waves associated with offset of saccades: A subject with large lambda waves', *Biological Psychology*, vol. 8, no. 3, pp. 235–238, May 1979, doi: 10.1016/0301-0511(79)90051-6.
[150] C. C. Evans, 'Spontaneous excitation of the visual cortex and association areas — Lambda waves', *Electroencephalography and Clinical Neurophysiology*, vol. 5, no. 1, pp. 69–74, Feb. 1953, doi: 10.1016/0013-4694(53)90054-6.
[151] G. W. Thickbroom, W. Knezevicˇ, W. M. Carroll, and F. L. Mastaglia, 'Saccade onset and offset lambda waves: relation to pattern movement visually evoked potentials', *Brain Research*, vol. 551, no. 1, pp. 150–156, Jun. 1991, doi: 10.1016/0006-8993(91)90927-N.
[152] A. Delorme and S. Makeig, 'EEGLAB: an open source toolbox for analysis of single-trial EEG dynamics including independent component analysis', *Journal of Neuroscience Methods*, vol. 134, no. 1, pp. 9–21, Mar. 2004, doi: 10.1016/j.jneumeth.2003.10.009.
[153] O. Dimigen, 'Optimizing the ICA-based removal of ocular EEG artifacts from free viewing experiments', *NeuroImage*, vol. 207, p. 116117, Feb. 2020, doi: 10.1016/j.neuroimage.2019.116117.
[154] M. Mennes, H. Wouters, B. Vanrumste, L. Lagae, and P. Stiers, 'Validation of ICA as a tool to remove eye movement artifacts from EEG/ERP', *Psychophysiology*, vol. 47, no. 6, pp. 1142–1150, 2010, doi: 10.1111/j.1469-8986.2010.01015.x.
[155] A. Olsen, 'The Tobii I-VT fixation filter', *Tobii Technology*, vol. 21, no. 4–19, p. 5, 2012.
[156] A. Yagi, 'Lambda response as an index of visual perception research', *Jpn. Psychol. Res*, vol. 24, no. 2, pp. 106–110, 1982, doi: 10.4992/psycholres1954.24.106.
[157] L. Vigon, R. Saatchi, J. E. W. Mayhew, N. A. Taroyan, and J. P. Frisby, 'Effect of signal length on the performance of independent component analysis when extracting the lambda wave', *Med Bio Eng Comput*, vol. 40, no. 2, pp. 260–268, Mar. 2002, doi: 10.1007/bf02348134.
[158] I. S. binti Suhaili, B. Toth, Z. Nagy, and Z. Juhasz, 'Reliable Single-Trial Detection of Saccade-Related Lambda Responses with Independent Component Analysis', *eNeuro*, vol. 12, no. 11, Nov. 2025, doi: 10.1523/ENEURO.0270-25.2025.
[159] Z. Zakeri, S. Assecondi, A. P. Bagshaw, and T. N. Arvanitis, 'Influence of Signal Preprocessing on ICA-Based EEG Decomposition', in *XIII Mediterranean Conference on Medical and Biological Engineering and Computing 2013*, L. M. Roa Romero, Ed., Cham: Springer International Publishing, 2014, pp. 734–737. doi: 10.1007/978-3-319-00846-2_182.
[160] H. Kim, J. Luo, S. Chu, C. Cannard, S. Hoffmann, and M. Miyakoshi, 'ICA's bug: How ghost ICs emerge from effective rank deficiency caused by EEG electrode interpolation and incorrect re-referencing', *Front. Signal Process.*, vol. 3, Apr. 2023, doi: 10.3389/frsip.2023.1064138.
[161] J. Onton, M. Westerfield, J. Townsend, and S. Makeig, 'Imaging human EEG dynamics using independent component analysis', *Neuroscience & Biobehavioral Reviews*, vol. 30, no. 6, pp. 808–822, Jan. 2006, doi: 10.1016/j.neubiorev.2006.06.007.
[162] F. Murtagh and P. Contreras, 'Algorithms for hierarchical clustering: an overview', *Wiley interdisciplinary reviews: data mining and knowledge discovery*, vol. 2, no. 1, pp. 86–97, 2012.

[163] J. H. Ward Jr, ‘Hierarchical grouping to optimize an objective function’, *Journal of the American statistical association*, vol. 58, no. 301, pp. 236–244, 1963.
[164] K. Kazai and A. Yagi, ‘Comparison between the lambda response of eye-fixation-related potentials and the P100 component of pattern-reversal visual evoked potentials’, *Cognitive, Affective, & Behavioral Neuroscience*, vol. 3, no. 1, pp. 46–56, Mar. 2003, doi: 10.3758/CABN.3.1.46.
[165] S. Thorpe, D. Fize, and C. Marlot, ‘Speed of processing in the human visual system’, *Nature*, vol. 381, no. 6582, pp. 520–522, Jun. 1996, doi: 10.1038/381520a0.
[166] J. Findlay and I. Gilchrist, ‘Active Vision: The Psychology of Looking and Seeing’, *Journal of Neuro-ophthalmology - J NEURO-OPHTHALMOL*, vol. 26, Aug. 2003, doi: 10.1093/acprof:oso/9780198524793.001.0001.
[167] J. F. Hipp, D. J. Hawellek, M. Corbetta, M. Siegel, and A. K. Engel, ‘Large-scale cortical correlation structure of spontaneous oscillatory activity’, *Nat Neurosci*, vol. 15, no. 6, p. 10.1038/nn.3101, Jun. 2012, doi: 10.1038/nn.3101.
[168] B. Wang and S. Omatu, ‘Acoustic signal separation of mechanical devices using ICA with band-pass filters’, *Artif Life Robotics*, vol. 9, no. 1, pp. 46–50, Apr. 2005, doi: 10.1007/s10015-004-0320-x.
[169] A. Omidvarnia, G. Azemi, B. Boashash, J. M. O. Toole, and S. Vanhatalo, ‘Measuring time-varying information flow for scalp EEG signals: orthogonalized partial directed coherence’, *MEASURING TIME*.
[170] M. Antonakakis, S. Rampp, M. Zervakis, J. Wellmer, and C. Wolters, *Dynamic effective connectivity of combined EEG/MEG sources in pharmacoresistant epilepsy*. 2021.
[171] C. Duclos *et al.*, ‘Differential classification of states of consciousness using envelope- and phase-based functional connectivity’, *NeuroImage*, vol. 237, p. 118171, Aug. 2021, doi: 10.1016/j.neuroimage.2021.118171.
[172] A. K. Seth, A. B. Barrett, and L. Barnett, ‘Granger Causality Analysis in Neuroscience and Neuroimaging’, *J. Neurosci.*, vol. 35, no. 8, pp. 3293–3297, Feb. 2015, doi: 10.1523/JNEUROSCI.4399-14.2015.

Appendix A

Initial Assessment

Sex	*Age*	*Are you a visual artist?*	*Do you have prior formal art education?*	*Do you wear glasses or contact lenses to correct your vision?*	*Are you colour blind, or have any other conditions which may affect your vision?*	*Which hand do you most prefer/use?*	*Have you ever suffered either a traumatic or acquired brain injury?*	*Do you have any history of neurological disorders?*
Female	28	No	No	No	No	Right	No	No
Male	22	No	No	Yes	No	Right	No	No
Male	26	No	No	Yes	Yes	Right	No	No
Male	20	No	No	No	No	Right	No	No
Female	36	No	No	Yes	No	Right	No	No
Female	37	No	No	No	No	Right	No	No
Male	30	No	No	Yes	Yes	Right	No	No
Female	22	No	No	Yes	No	Right	No	No
Male	34	No	No	No	No	Right	No	No
Male	26	No	No	Yes	No	Right	Yes	No
Male	18	No	No	No	No	Right	No	No
Male	22	No	No	Yes	No	Right	No	No
Female	20	Yes	No	Yes	No	Right	No	Yes
Female	22	No	No	Yes	No	Right	No	No
Female	22	No	No	No	No	Right	No	No
Female	26	No	No	No	No	Right	No	No
Male	22	No	No	No	No	Right	No	No
Female	26	No	No	Yes	No	Right	No	No
Male	35	No	No	No	No	Right	No	No
Female	24	No	No	No	No	Right	No	No
Male	35	No	No	Yes	No	Right	No	No
Female	25	No	No	Yes	No	Right	No	No
Female	25	No	No	Yes	No	Right	No	No
Female	26	No	No	No	No	Right	No	No

Appendix B

Art Expertise Assessment

On average, how many times do you visit art galleries?	*On average, how many times do you visit art museums?*	*In the average week how many hours each week do you spend looking at visual art?*	*In the average week how many hours each week do you spend reading about visual art (publication/ online/digital)?*	*In the average week how many hours do you spend making visual art?*	*How many years have you studied fine art after the age of 16?*	*How many years have you studied art history after the age of 16?*
Every 6 months	Every 6 months	1	0	1	0	0
Almost Never	Yearly	1	2	0	0	0
Almost Never	Yearly	0	0	0	0	0
Yearly	Yearly	1	0	0	0	0
Almost Never	Almost Never	0	0		0	0
Almost Never	Almost Never	1	0	0	0	0
Yearly	Every 6 months	1	0	0	0	0
Almost Never	Almost Never	0	0	0	0	0
Almost Never	Almost Never	2	0	0	0	0
Almost Never	Yearly	1	0	0	0	0
Yearly	Yearly	4	1	1	0	1
Almost Never	Almost Never	1	0	0	0	0
Almost Never	Almost Never	5	1	4	0	0
Every 6 months	Every 6 months	1	0	1	0	0
Almost Never	Almost Never	2	1	0	0	0
Almost Never	Every 6 months	3	0	0	0	0
Almost Never	Almost Never	1	0	0	0	0
Almost Never	Yearly	3	4	1	2	2
Yearly	Yearly	1	1	1	0	0
Almost Never	Almost Never	0	0	0	0	0
Yearly	Yearly	3	3	3	2	2
Yearly	Yearly	3	3	0	0	0
Every 6 months	Every 2 months	1	0	0	0	0
Every 2 months	Monthly	3	1	5	5	4

Appendix C

Handedness Questionnaire

Handedness Questionnaire

Instructions

For each of the activities below, please indicate:

Which hand you prefer for that activity?
Do you ever use the other hand for the activity?

Which hand do you prefer to use when:		no pref		Do you ever use the other hand?
Writing:	Left ○	○	○ Right	☐ Yes
Drawing:	Left ○	○	○ Right	☐ Yes
Throwing:	Left ○	○	○ Right	☐ Yes
Using Scissors:	Left ○	○	○ Right	☐ Yes
Using a Toothbrush:	Left ○	○	○ Right	☐ Yes
Using a Knife (without a fork):	Left ○	○	○ Right	☐ Yes
Using a Spoon:	Left ○	○	○ Right	☐ Yes
Using a broom (upper hand):	Left ○	○	○ Right	☐ Yes
Striking a Match:	Left ○	○	○ Right	☐ Yes
Opening a Box (holding the lid):	Left ○	○	○ Right	☐ Yes
items below are not on the standard inventory:				
Holding a Computer Mouse:	Left ○	○	○ Right	☐ Yes
Using a Key to Unlock a Door:	Left ○	○	○ Right	☐ Yes
Holding a Hammer:	Left ○	○	○ Right	☐ Yes
Holding a Brush or Comb:	Left ○	○	○ Right	☐ Yes
Holding a Cup while Drinking	Left ○	○	○ Right	☐ Yes

Evaluate

Appendix D

PANAS Questionnaire

ID:_____ Age:_____ Date:_____

PANAS Questionnaire

This scale consists of a number of words that describe different feelings and emotions. Read each item and then list the number from the scale below next to each word. Indicate to what extent you feel this way right now, that is, the present moment.

		Very slightly or Not at all	A little	Moderately	Quite a bit	Extremely
1	Interested	1	2	3	4	5
2	Distressed	1	2	3	4	5
3	Excited	1	2	3	4	5
4	Upset	1	2	3	4	5
5	Strong	1	2	3	4	5
6	Guilty	1	2	3	4	5
7	Scared	1	2	3	4	5
8	Hostile	1	2	3	4	5
9	Enthusiastic	1	2	3	4	5
10	Proud	1	2	3	4	5
11	Irritable	1	2	3	4	5
12	Alert	1	2	3	4	5
13	Ashamed	1	2	3	4	5
14	Inspired	1	2	3	4	5
15	Nervous	1	2	3	4	5
16	Determined	1	2	3	4	5
17	Attentive	1	2	3	4	5
18	Jittery	1	2	3	4	5
19	Active	1	2	3	4	5
20	Afraid	1	2	3	4	5

Appendix E

Subject Information and Informed Consent Form

STUDY ON FINE ART PERCEPTION DETECTED BY HIGH DENSITY EEG

Name of Participant :

SUBJECT INFORMATION

INTRODUCTION

You are invited to take part voluntarily in this research study on fine art perception to understand the underlying brain processes at time of looking at a painting. We use a high density EEG to study brain events related bioelectric activity. This is a non-invasive and harmless technique.

Before signing the consent to participate in this research study, it is important that you read and understand this form. If you agree to participate, you will receive a copy of this form to keep for your records. You are expected to make a visit once for the experiment throughout this research study.

The EEG data collected in this study will analyse your brain functions. The EEG record will be used only for scientific purposes in anonymised manner.

STUDY PROCEDURES

You are expected to attend one experiment session throughout the research study. Prior to your visit, you are assessed for qualifying assessment, art expertise assessment, handedness assessment and mood assessment. You will be given an identification number to ensure your confidentiality.

After passing all the assessments and signing the consent form, the experiment will start. 128-channel BioSemi ActiveTwo EEG (Biosemi Inc., Heerlen, Netherlands) will be placed on your head for data acquisition.

During the experiment, you will view a series of paintings and press a button after each painting to indicate whether you 'like' or 'dislike' the painting. The experiment is expected to last about 30 minutes.

RISKS

EEG examination is a non-invasive diagnostic, or research technology. It is a safe procedure. If any important new information detected by EEG on your health condition, further medical assistance will be provided by a neurologist, professor Zoltan Nagy, the advisor in this project.

CONFIDENTIALITY

Your information will be kept confidential by the researchers and will not be made publicly available unless disclosure is required by law. Data obtained from this study that does not identify you individually will be used only for research purposes and in scientific publications.

Your data may be reviewed by researchers of our group, may be held, and processed on our computers but it will never be made available to the third parties.

By signing the informed consent form, you authorize the record review, information storage and data transfer as described above.

PARTICIPATION IN THE STUDY

Your participation in this study is entirely voluntary. You may refuse to take part in the study, or you may stop participation in the study anytime, without penalty or loss of benefits in which you are otherwise entitled.

POSSIBLE BENEFITS [Benefits to Individual, Community, University]

Study procedures will be provided at no cost to you and there is no reimbursement for participating in this research study. You may receive information about your result done in this study. We hope that the result and information regarding this research will benefit future study.

QUESTIONS

If you have any questions about this study, please contact the researcher, Iffah Syafiqah binti Suhaili at ssiffah@gmail.com or +362021 38826.

INFORMED CONSENT FORM

CONFIRMATION STATEMENT

Participant's Name :

ID :

Researcher's Name :

By signing this, I am confirming the following:

- I have read and understood all the information in this Subject Information and Informed Consent Form.
- All my questions have been answered to my satisfaction.
- I voluntarily agree and express my readiness to participate in this EEG-based research study and to follow the study procedures.
- I am aware that there is no reimbursement for participating in this study.
- I can withdraw my consent at any time without consequences.
- I have received a copy of this Subject Information and Informed Consent Form to keep for myself.

Date :

Participant's Name :

_____

Participant's Signature

Name of Researcher Conducting Consent Discussion :

Date :

_____

Signature of Researcher Conducting Consent Discussion

Appendix F

Supplementary Figures

Figure A-1. The set of 40 figurative paintings presented as stimuli in the experiment.

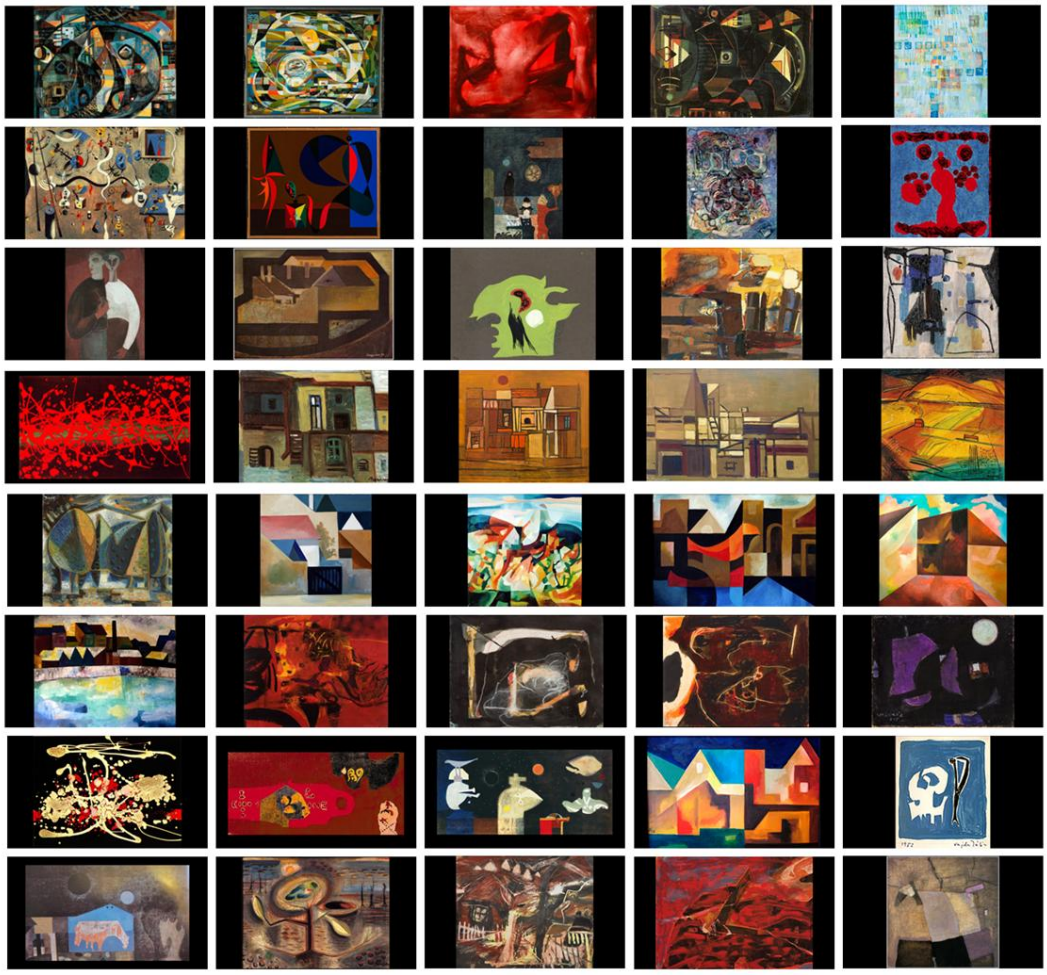

Figure A-2. The set of 40 abstract paintings presented as stimuli in the experiment.

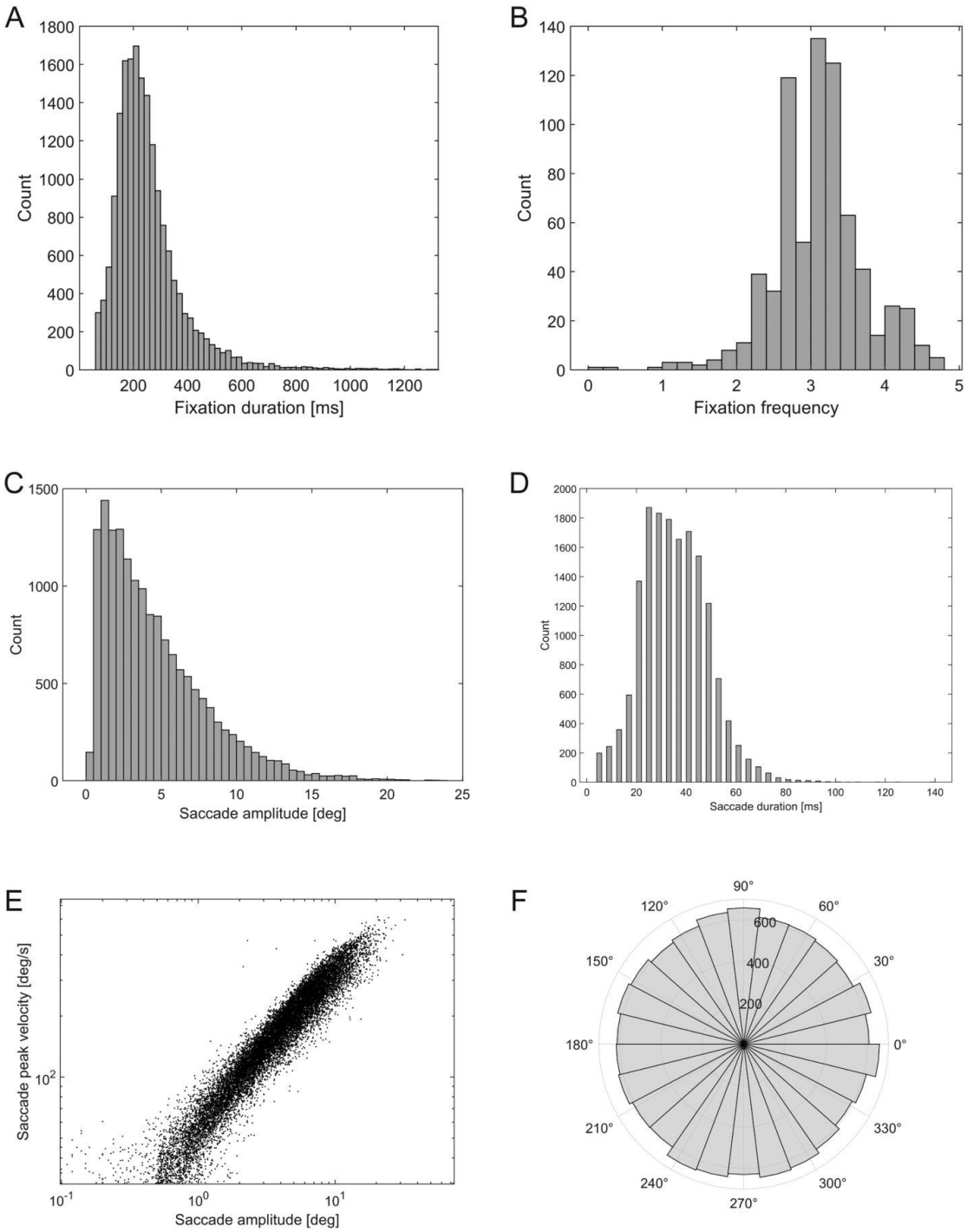

Figure A-3. Eye movement data combined from all participants. a) Distribution of the fixation duration. b) Distribution of the fixation frequency. c) Distribution of the saccade amplitude. d) Distribution of the saccade duration. e) Saccade main sequence. f) Saccade angular histogram.

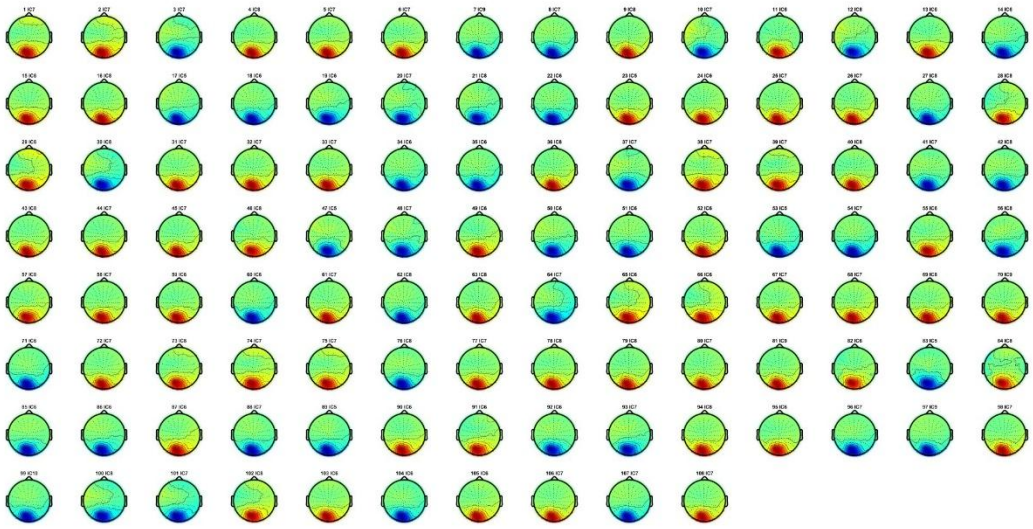

Figure A-4. Projected scalp maps of the lambda components extracted from all 108 preprocessing pipelines with high-pass filtering ≥0.5 Hz. Each map shows the ICA-projected scalp distribution of the automatically identified lambda component for one preprocessing configuration. Despite differences in sampling rate, low-pass cutoff and data length, all components exhibit a consistent occipito-parietal focus characteristic of the lambda response, demonstrating the robustness of component topography across preprocessing settings.

Supplementary Table

Table A-1. Clustering of preprocessing parameter combinations into four groups based on correlation similarity.

	Cluster 1	Cluster 2	Cluster 3	Cluster 4
1	1024_L100_HP0.5_LP128	1024_L25_HP0.5_LP128	1024_L100_HP2_LP128	1024_L100_HP1_LP128
2	1024_L100_HP0.5_LP40	1024_L25_HP0.5_LP40	1024_L100_HP2_LP40	1024_L100_HP1_LP40
3	1024_L100_HP0.5_LP80	1024_L25_HP0.5_LP80	1024_L100_HP2_LP80	1024_L100_HP1_LP80
4	1024_L75_HP0.5_LP128	1024_L50_HP0.5_LP128	1024_L25_HP2_LP128	1024_L25_HP1_LP128
5	1024_L75_HP0.5_LP40	1024_L50_HP0.5_LP40	1024_L25_HP2_LP40	1024_L25_HP1_LP40
6	1024_L75_HP0.5_LP80	1024_L50_HP0.5_LP80	1024_L25_HP2_LP80	1024_L25_HP1_LP80
7	2048_L100_HP0.5_LP128	2048_L25_HP0.5_LP128	1024_L50_HP2_LP128	1024_L50_HP1_LP128
8	2048_L100_HP0.5_LP40	2048_L25_HP0.5_LP40	1024_L50_HP2_LP40	1024_L50_HP1_LP40
9	2048_L100_HP0.5_LP80	2048_L25_HP0.5_LP80	1024_L50_HP2_LP80	1024_L50_HP1_LP80
10	2048_L75_HP0.5_LP128	2048_L50_HP0.5_LP128	1024_L75_HP2_LP128	1024_L75_HP1_LP128
11	2048_L75_HP0.5_LP40	2048_L50_HP0.5_LP40	1024_L75_HP2_LP40	1024_L75_HP1_LP40
12	2048_L75_HP0.5_LP80	2048_L50_HP0.5_LP80	1024_L75_HP2_LP80	1024_L75_HP1_LP80
13	512_L100_HP0.5_LP128	512_L25_HP0.5_LP128	2048_L100_HP2_LP128	2048_L100_HP1_LP128
14	512_L100_HP0.5_LP40	512_L25_HP0.5_LP40	2048_L100_HP2_LP40	2048_L100_HP1_LP40
15	512_L100_HP0.5_LP80	512_L25_HP0.5_LP80	2048_L100_HP2_LP80	2048_L100_HP1_LP80
16	512_L75_HP0.5_LP128	512_L50_HP0.5_LP128	2048_L25_HP2_LP128	2048_L25_HP1_LP128
17	512_L75_HP0.5_LP40	512_L50_HP0.5_LP40	2048_L25_HP2_LP40	2048_L25_HP1_LP40
18	512_L75_HP0.5_LP80	512_L50_HP0.5_LP80	2048_L25_HP2_LP80	2048_L25_HP1_LP80
19			2048_L50_HP2_LP128	2048_L50_HP1_LP128
20			2048_L50_HP2_LP40	2048_L50_HP1_LP40
21			2048_L50_HP2_LP80	2048_L50_HP1_LP80
22			2048_L75_HP2_LP128	2048_L75_HP1_LP128
23			2048_L75_HP2_LP40	2048_L75_HP1_LP40
24			2048_L75_HP2_LP80	2048_L75_HP1_LP80
25			512_L100_HP2_LP128	512_L100_HP1_LP128
26			512_L100_HP2_LP40	512_L100_HP1_LP40
27			512_L100_HP2_LP80	512_L100_HP1_LP80
28			512_L25_HP2_LP128	512_L25_HP1_LP128
29			512_L25_HP2_LP40	512_L25_HP1_LP40
30			512_L25_HP2_LP80	512_L25_HP1_LP80
31			512_L50_HP2_LP128	512_L50_HP1_LP128
32			512_L50_HP2_LP40	512_L50_HP1_LP40
33			512_L50_HP2_LP80	512_L50_HP1_LP80
34			512_L75_HP2_LP128	512_L75_HP1_LP128
35			512_L75_HP2_LP40	512_L75_HP1_LP40
36			512_L75_HP2_LP80	512_L75_HP1_LP80